Forschungszentrum Karlsruhe

Technik und Umwelt

Wissenschaftliche Berichte

FZK 6047

Study for the Intercomparison between the Global Fit and the Optimal Estimation Methods in Case of the Limb Radiance Measurements

V. S. Kostsov*, A. V. Polyakov*, Yu. M. Timofeyev*, T. v. Clarmann, G. P. Stiller

Institut für Meteorologie und Klimaforschung

***Sankt Petersburg State University**
Research Institute of Physics

Forschungszentrum Karlsruhe GmbH, Karlsruhe
1997

ABRISS

Studie über den Vergleich zwischen Global Fit- und Optimal- Estimation Methoden für die Anwendung auf Horizontsondierungsmessungen

Die "Global Fit" (GF) und "Optimal Estimation" (OE) Inversionsmethoden wurden auf der Basis simulierter Strahldichtespektren, wie ein hochauflösendes Interferometer sie im Horizontsondierungsmodus messen würde, verglichen. Es wurde ein Meßszenario gewählt, das dem des MIPAS Experiments entspricht, welches auf der polaren Plattform ENVISAT-1 als Weltraumexperiment geplant ist. Die Vorteile beider Methoden hinsichtlich der Datenauswertung wurden theoretisch und numerisch mit Hilfe von Testrechnungen untersucht. Der Vergleich wurde für verschiedene Atmosphärenmodelle durchgeführt, die alle zu einem Ensemble aus Druck-, Temperatur, Ozon- und Wasserdampfprofilen gehören. Das Ensemble der Profile wurde auf Basis der TIGR Datenbank sowie atmosphärischen Parametern aus dem ATMOS Datensatz erstellt. Die Horizontsondierungsspektren wurden für kleine spektrale Bereiche, sog. Microwindows, in den CO_2, O_3, und H_2O Banden modelliert. Der Einfluss folgender Parameter und Faktoren auf Retrievalfehler von Druck, Temperatur, Ozon und Wasserdampf wurde abgeschätzt: spektrales Rauschen, Startwert, a priori Statistik, Konvergenzkriterien, aktuelle atmosphärische Bedingungen, Feinstruktur der Profile, sowie das endliche Gesichtsfeld des Messgerätes. Empfehlungen für die Anwendung des Global Fit und Optimal Estimation Algorithmus wurden ausgearbeitet.

Es folgen die wichtigsten Ergebnisse und Schlussfolgerungen der Studie:
Bei Messungen mit einem hochauflösenden Horizontsondierungsgerät wie MIPAS sind die Fehler der abgeleiteten Druck- und Temperaturprofile für beide Methoden (GF und OE) fast gleich groß. Im Höhenbereich zwischen 25 und 60 km sind sie mit Werten kleiner 1% bzw. 1K - oft sogar noch weniger - typischerweise klein. Der Höhenbereich zwischen 8 und 25 km ist für die pT-Ableitung am problematischsten. Es wurde gezeigt, dass die geringe erreichbare Genauigkeit in diesem Bereich durch die Einflüsse von Ozon- und Wasserdampflinien verursacht wird, wobei die Konzentrationen dieser beiden Gase als unsicher angenommen werden müssen. Mit "Einflüssen" sind Flügel von Spektrallinien gemeint, die vom untersuchten Microwindow weit entfernt sind. Aufgrund des hohen Informationsgehalts der Messungen in den ausgewählten Microwindows sind die Ergebnisse der Testrechnungen unabhängig davon, welches Profil innerhalb des statistischen Ensembles betrachtet wird. Obwohl die GF Methode in Höhen über 60 km aufgrund ihrer Fehlerfortpflanzungscharakteristik grössere Fehler als OE produziert, ist die folgende Schlussfolgerung zulässig: Aufgrund des hohen Informationsgehalts der Horizontsondierungsmessungen in den vorgeschlagenen pT-Microwindows unterscheiden sich die Ergebnisse der Global Fit und Optimal Estimation Methoden nicht signifikant voneinander (Fehlerabschätzungen auf Basis der Fehlermatrixmethode bestätigen diese Schlußfolgerung).

Für die Ozontestfälle wurde gezeigt dass:

- die Retrievals für beide (GF und OE) Methoden im Höhenbereich zwischen 25 und 50 km mit Fehlern kleiner 2% sehr gut sind;
- beide Methoden unterhalb 25 km und oberhalb 50 km größere Fehler produzieren.
- außerhalb des unproblematischen Höhenbereichs von 25 bis 50 km die Global Fit Methode größere Fehler liefert als Optimal Estimation.
- die Global Fit Methode langsamer konvergiert.

Es wurde gezeigt, dass große Fehler in den unteren Schichten durch Unsicherheiten der Druck-, Temperatur- und Wasserdampfprofile erklärt werden können.

In den oberen Schichten wird die verminderte Genauigkeit durch eine Abnahme des Signal/Rauschverhältnisses, und im Falle der Global Fit Methode durch Fehlerfortpflanzungs-effekte, verursacht.
Für die Auswertung von Ozon ist die Optimal Estimation Methode der Global Fit Methode in den Höhenbereichen 8-20 km und 50-65 km überlegen; zwischen 20 und 50 km sind beide

Methoden praktisch gleichwertig. Diese Schlußfolgerung wird durch Testrechnungen und die Analyse der Fehlermatrix belegt. Ein weiterer Vorteil der Optimal Estimation Methode ist die schnellere Konvergenz.

Mit beiden Methoden gelangen Wasserdampfretrievals mit bester Genauigkeit im Höhenbereich von 25 bis 45 km; die Fehler lagen hier meist unter 5 %. Dennoch lieferte die Optimal Estimation Methode die glatteren Profile.

Im Höhenbereich von 45-65 km nahmen für beide Methoden die Fehler aufgrund des verminderten Signal/Rausch-Verhältnisses zu. Zusätzlich spielte bei der Global Fit Methode die Fehlerfortpflanzung eine Rolle; in einigen Fällen verursachte Global Fit Fehler von über 50 % in größeren Höhen.

Es zeigte sich, dass die Wasserdampfretrievals sehr empfindlich auf Unsicherheiten der Druck-, Temperatur- und Ozonprofile in der oberen Troposphäre und unteren Stratosphäre sind. Aus diesen Gründen divergierte die Iteration für die meisten Testfälle in 8 km Höhe. Folglich ist der Höhenbereich 8-25 km für beide Methoden durch grosse Fehler - bis zu einigen Dutzend Prozent - charakterisiert.

Die Hauptschlußfolgerung für das Wasserdampfretrieval kann folgendermaßen formuliert werden: a) Unsicherheit anderer Parameter beeinflusst das Ergebnis erheblich und macht das Wasserdampfretrieval in der Umgebung von 8 km unmöglich. b) Bis zu einer Höhe von 45 km erhält man mit Global Fit und Onion Peeling praktisch die gleichen Ergebnisse, während weiter oben Optimal Estimation überlegen ist.

Allgemein ist für Druck-, Temperatur-, Ozon- und Wasserdampfretrievals festzustellen:

1) Eine Erhöhung der Genauigkeit im Bereich von 8-25 km sollte verstärkt angestrebt werden. Im Rahmen des Microwindow-Konzepts kann dieses Problem leicht gelöst werden, indem man die Beiträge weit entfernter Linien ausserhalb des Microwindows als lokal wellenzahlunabhängiges "Hintergrundkontinuum" parametrisiert. In dieser Studie wurde ein solches "Hintergrundkontinuum" nicht berücksichtigt. Ein solcher Ansatz wird jedoch im Rahmen anderer Studien am Institut für Meteorologie und Klimaforschung entwickelt. Diese Studien behandeln außerdem Korrelationen des spektralen Rauschens und Unsicherheiten der Sichtlinienkenntnis in Elevation in angemessenerer Form.

2) Weiterhin verdient das Problem der Konvergenzbeschleunigung des iterativen Prozesses Aufmerksamkeit. Die Vorauswahl des Startprofils durch einen Preprozessor stellt eine Lösungsmöglichkeit dar.

ABSTRACT

The global fit (GF) and the optimal estimation (OE) methods have been compared on the basis of simulations of limb radiance measurements by a high resolution interferometer. The simulations were close to the scenarios of the MIPAS measurements scheduled for the space mission on board the ENVISAT-1 polar platform. The advantages of the applicability of each of the mentioned methods to the interpretation of data have been investigated theoretically and on the basis of numerically simulated test retrievals. The intercomparisons have been carried out for the set of models belonging to the ensemble of atmospheric profiles of pressure, temperature, and concentrations of ozone and water vapor. The ensemble of profiles has been created on the basis of the TIGR database and atmospheric parameters retrieved from the ATMOS data. The limb radiance measurements have been modeled in the microwindows located in the CO_2, O_3, and H_2O absorption bands. The influence of the following parameters and factors on the errors of the retrieval of pressure, temperature, ozone and water vapor profiles has been estimated: random measurement noise, initial guess, a priori statistics, convergence criteria, atmospheric conditions, fine structure of profiles, finite angular resolution of measurements. The recommendations have been worked out for the utilization of the global fit and optimal estimation algorithms in the case of the MIPAS data processing.

The main results and conclusions derived in the course of the study are the following:

In case of the high spectral resolution limb radiance measurements by an instrument like MIPAS the retrieval errors for pressure and temperature profiles for both GF and OE methods are nearly identical and small in the altitude range 25-60 km and are characterized by the values less than 1% and 1 K correspondingly (in some cases the errors were even smaller). The altitude range 8-25 km is the most problematic for p-T retrieval. It was shown that the low accuracy of the temperature and pressure retrievals in these layers is stipulated by the interference from the uncertainties of the ozone and water vapor profiles. By the term “interference” the far-wing contributions by transitions situated far off the target microwindows are designated. The results of the retrievals do not depend upon the specific profile in the statistical ensemble due to the high information content of measurements in the preselected microwindows. Despite the fact that at altitudes greater than 60 km the GF method produced larger errors than the OE method due to the effect of error propagation from the higher layers which is characteristic for the GF method, the following main conclusion can be made: due to the high information content of limb radiance measurements in the microwindows preselected for p-T retrieval the global fit and the optimal estimation methods produce the results which do not differ significantly (the error estimations made on the basis of error matrix calculations confirm this conclusion).

The ozone retrieval test cases showed that:

- the retrievals are very good for both GF and OE methods in the altitude range 25-50 km (the errors are less than 2%);
- both methods deliver larger errors below 25 km and above 50 km;
- the errors of the GF methods are considerably larger than the errors of the OE method (excluding the region of high accuracy retrievals 25-50 km);
- the convergence of the iterative process is slower for the GF method.

It was shown that the increase of errors in the lower layers is explained by the interference from the uncertainties in the pressure, temperature and water vapor profiles.

In the upper layers the decrease of accuracy is caused by the decrease of signal-to-noise ratio for both methods and additionally by error propagation effect for the GF method.

So, in the ozone retrieval problem the optimal estimation method is more preferable than the global fit method in the altitude ranges 8-20 km and 50-65 km and there is practically no difference between the methods in the altitude range 20-50 km. This conclusion is confirmed by the test retrievals and by the error estimations on the basis of error matrix calculations. Another advantage of the optimal estimation method is its faster convergence.

For the water vapor retrieval task the most accurate retrievals were observed in the altitude range 25-45 km for both methods where the errors were mainly less than 5%. However in this region the OE method delivered more smooth solution.

In the region 45-65 km the errors increased due to the decrease of signal-to-noise ratio for both methods. Additionally for the GF method the error propagation effect was another error source and in some cases the GF method caused errors more than 50% at the upper altitudes.

The water vapor retrieval problem appeared to be very sensitive to the interference from the uncertainties of pressure, temperature and ozone profiles in the upper troposphere and lower stratosphere. In most of test retrievals the iterative process diverged at the altitude of 8 km. It was shown that the divergence was the consequence of the interference from the uncertainties in the pressure, temperature and ozone profiles. As a consequence the region 8-25 km was characterized by the large retrieval errors for both methods reaching dozens of percent.

The main conclusions for the water vapor retrieval task may be formulated as follows: a) the interference of other parameters dramatically influences the results and in most cases makes the determination of water vapor profile in the vicinity of 8 km impossible ; b) the GF and the OE methods deliver practically the same results up to the altitude of 45 km, in the higher layers the OE method is much more preferable.

General consideration of the p-T, ozone and water vapor retrieval problems indicated that:

1) Special attention should be paid to the increasing of the retrieval accuracy in the altitude range 8-25 km. In the frame of the microwindow concept this problem could be easily solved by approximating far-wing contributions by transitions which are far off the target microwindows by a locally wavenumber-independent “background continuum”. In the present study the retrieval of the “background continuum” was not included but is already being developed in the course of other studies at the Institut für Meteorologie und Klimaforschung, Forschungszentrum Karlsruhe. Furthermore, these studies also more adequately treat the noise correlations and uncertainties in the tangent altitude pointing.

2) The problem of speeding up the convergence of the iterative process also requires attention. The possible solution is the selection of the initial guess by special high performance algorithm.

Table of contents

Abbreviations

CLAES	**C**ryogenic **L**imb **A**rray **E**talon **S**pectrometer
FIS	**F**itting **I**ndex for **S**pectra
FOV	**F**ield **o**f **V**iew
GF	**G**lobal **F**it (method)
ILS	**I**nstrumental **L**ine **S**hape
ISAMS	**I**mproved **S**tratospheric and **M**esospheric **S**ounder
LIMS	**L**imb **I**nfrared **M**onitor of the **S**tratosphere
LOS	**L**ine-**o**f-**S**ight
LTE	**L**ocal **T**hermodynamic **E**quilibrium
MIPAS	**M**ichelson **I**nterferometer for **P**assive **A**tmospheric **S**ounding
NESR	**N**oise **E**quivalent **S**pectral **R**adiance
OE	**O**ptimal **E**stimation (method)
rms	**r**oot **m**ean **s**quare (error)
SNR	**S**ignal-to-**N**oise **R**atio
SPIRT-NLC	**S**imulation **P**rogram for **I**nfrared **R**adiative **T**ransfer - **N**on-**L**TE **C**ode
SSA	**S**hift of **S**olution at iteration step (**A**bsolute)
SSR	**S**hift of **S**olution at iteration step (**R**elative)

1. Introduction

Modern satellite methods of environmental sensing give the possibility to provide global information on spatial-temporal variations of different parameters of physical state of the atmosphere and underlying surface - temperature, gaseous content, optical and microphysical characteristics of aerosols and clouds, etc. [*Kondratyev and Timofeyev*, 1970; *Houghton et al*., 1984; *Timofeyev*, 1986]. Limb observation geometry is commonly used for sounding the middle atmosphere due to a number of the advantages - high informativity, relatively high vertical resolution, absence of the surface interfering [*Gille and House*, 1971]. In the last years, this measurement geometry has been successfully used in satellite experiments. In the coming years, new satellite experiments are planned with the MIPAS and other instruments.

The Michelson Interferometer for Passive Atmospheric Sounding - MIPAS will operate on the ENVISAT-1 polar platform and will measure the infrared emissions of atmospheric species in the stratosphere, mesosphere, and lower thermosphere. The primary goal will be the retrieval of the vertical profiles of pressure, temperature, and several target species: O_3, H_2O, CH_4, N_2O, and HNO_3. Since the MIPAS interferometer is designed for measuring the atmospheric limb radiation in the wide spectral range with high spectral resolution and low error level, high instrument informativity relative to various atmospheric parameters is expected [*Fischer and Oelhaf*, 1996]. Several studies have been carried out [*Oelhaf and Fischer*, 1983; *Clarmann et al*., 1991; *Echle et al*., 1992; *Clarmann et al*., 1993a; *Clarmann et al*., 1993b; *Echle et al*., 1994; *Echle et al.*, 1995; *Clarmann et al.*, 1995] in which the information content of the MIPAS measurements, the accuracy of determining different atmospheric parameters and a number of theoretical problems of data interpretation were investigated.

Remote methods of atmospheric sensing can be considered in a general way as the combination of a measuring device, various *a priori* information (radiative transfer model, characteristics of radiation-media interaction, boundary conditions, observation geometry) and an algorithm of processing the measurement information. All these components determine, to specific extent, the quality of remote sensing results.

Numerous works have been dedicated to analysis of the influence of various factors on the accuracy of atmospheric remote sounding by limb emission measurements. The errors of retrieving the vertical profiles of the atmospheric temperature, the H_2O, O_3, HNO_3 and NO_2 contents from the LIMS measurements were estimated in a number of papers, published in *Journal of Geophysical Research* [**89,** No. D4, 1984]. The details of the operational processing of the LIMS measurements are described by *Bailey and Gille* [1986]. In this paper, in particular, the errors of retrieving the atmospheric temperature, pressure and ozone content caused by radiative transfer model and the retrieval algorithm are estimated. It was shown that these errors may be important.

Abbas et al. [1985] analyzed the influence of angular aperture of satellite instrument on the accuracy of retrieving the temperature and gaseous content characteristics. The calculations at various angular resolutions (from 0 to 1 degree) demonstrated increasing of the width of weighting functions (the kernels of integral equations) and the upward shifting of the peak level when the resolution is degraded. Neglecting finite angular resolution results in additional systematic errors in the retrieved temperature but has very small influence on the ozone content retrieval. *Rodgers et al*. [1993] proposed to take the angular aperture influence into account during the prior stage of data processing by solving a corresponding integral equation.

A specific algorithm of solving the inverse problem of pressure, temperature and ozone content retrievals was proposed by *Kumer and Mergenthaler* [1991]. At a later time, this algorithm was used to interpret the measurement data of the CLAES satellite instrument [*Gille et al*., 1996].

In the past years, different methods and algorithms of solving the inverse problems were proposed and justified. These methods can be classified according to the amount and type of an *a priori* information used and according to the ways of stabilizing the inverse operator of the problem [*Kondratyev and Timofeyev*, 1970; *Houghton et al*., 1984]. An application of one or

another specific algorithm of solving the inverse problem influences, to some extent, the quality of the results. This fact was verified in numerical experiments on comparing various interpretation procedures in the problem of thermal sounding by nadir measurements [*Kondratyev and Timofeyev*, 1978], and by slant path measurements [*Carlotti*, 1988; *Clarmann et al*., 1991]. In the paper by *Carlotti* [1988], the global fit method was applied to retrieving the vertical profiles of atmospheric gases from the slant path measurements by balloon-borne spectrometer. The comparison of this method with the onion peeling method showed (the ozone profile retrieval was taken as an example) smaller error-bars for the global fit method than for the onion peeling analysis. *Clarmann et al*. [1991] analyzed the influence of different atmospheric stratification schemes used in approximation of an integral form of the radiative transfer equation on the accuracy of retrieving the CO_2 vertical profile. It was shown that oscillations of solution corresponding to the "level model" were larger than those corresponding to the "layer model".

Various aspects of solving the inverse problem of retrieving the gaseous content characteristics were discussed by *Marks and Rodgers* [1993] (relevant to the interpretation of the ISAMS measurement data). In this paper, the examples of numerical experiments on retrieving the O_3, CO and CH_4 vertical profiles by optimal estimation method are given. Extensive treatment of solving different inverse problems by optimal estimation method has been done by *Rodgers* [1990]. Numerous examples of applying this method are cited in the studies devoted to the interpretation of the experiments with different instruments onboard UARS satellite [*J. Geoph. Res*., **101**, No. D6, 1996].

The optimal estimation method (OE) [*Turchin et al*., 1970; *Pokrovsky and Timofeyev*, 1972; *Rodgers*, 1976] and the global fit method (GF) [*Carlotti*, 1988] are the ones which are commonly used for solving the inverse problems of atmospheric limb remote sensing. The present study deals with the intercomparison between these two methods. The investigations were stipulated by the necessity to investigate and test the methods which can be suitable for the MIPAS data processing. As it was mentioned above, the quality of the retrieval of atmospheric parameters may be quite different for different retrieval methods and schemes.

In the present study the inverse problems of pressure-temperature (p-T), ozone and water vapor retrieval from the limb radiance measurements are considered. The measurement scenario has been selected close to that of the future MIPAS mission. Each problem (task) is solved by the global fit and the optimal estimation methods and the results are compared. It should be noted, that a description of the general optimal estimation algorithm was presented in the report by *Kostsov et al*. [1996] where the first results of applying this method to the problem of joint retrieval of the vertical profiles of temperature and pressure are given. In the study [*Kostsov et al*., 1996] the wavenumber range was used which comprised the CO_2 microwindows preselected by *Clarmann et al*. [1994].

The comparison of GF and OE methods was carried out by means of numerical experiments based on a closed-loop scheme and was performed for various atmospheric conditions (atmospheric models). The basis for the physics-mathematical model of the satellite experiment with the MIPAS interferometer was a well-known integral form of thermal radiation transfer equation (under conditions of LTE and neglecting the scattering effects) [*Kondratyev and Timofeyev*, 1978; *Houghton et al*., 1984].

The present report is structured as follows:

Section 2 contains a brief theoretical comparative analysis of the optimal estimation and global fit algorithms. An overview of the planned MIPAS experiment, the characteristics of the MIPAS instrument, and the peculiarities of the measurement scenario are given in Section 3. Atmospheric models used for the test retrievals are described in Section 4. General descriptions of numerical experiments are given in Section 5 as well as the peculiar features of test retrievals in specific cases. Section 6 contains the description and analysis of the test retrievals for 3 above mentioned tasks (p-T, ozone and water vapor determination). The influence of random measurement noise, initial guess, finite FOV of an instrument on the results of the retrievals are discussed also in Section 6. Special subsection is devoted to the discussion of the possibility to retrieve fine structure of profiles and to the analysis of the influence of atmospheric conditions

on the retrieval accuracy. The principal results and recommendations for further studies are given in Section 7.

2. The mathematical basis of the Global Fit and Optimal Estimation algorithms

In the last three decades, various approaches to solving the inverse problems of atmospheric optics have been developed and well described in literature. We will take advantage of the approach of Rodgers [*Rodgers*, 1990; *Marks and Rodgers*, 1993] in outlining the mathematical basis of retrieval methods. Following the terminology used in these papers, let us introduce the terms and notations.

The "state vector" **x** is a vector of unknowns to be estimated from the measurements, describing the state of the atmosphere. Usually, it will be a profile of some quantity, given at a finite number *n* of levels, where *n* is large enough to represent the possible atmospheric variations adequately. However, it may in principle comprise any set of relevant variables, such as coefficients for a representation of the profile. We will consider the joint vector, combining the profiles of several parameters of the atmosphere state, as **x** vector. For example, it may be the vector composed from the vectors of temperature and pressure corresponding to specific atmospheric levels.

The "measurement" **y** is vector of *m* measured quantities. Measurements are made to a finite accuracy, with measurement error ε assumed to be normally distributed with mean zero and known covariance $\mathbf{S}_\mathbf{y}$. In general case, the measurement error has the complex structure and contains both systematic and random noise components. As the methods of eliminating the systematic errors are not the theme of our study, let us consider only the noise error component.

The "forward model" *F* characterizes the measurement **y**, describing how it depends on the state vector **x**. In our case, it was implemented as a computer code, intended for simulations of the limb radiance measurement values and errors. Following *Rodgers* [1990],

$$\mathbf{y} = F(\mathbf{x}, \mathbf{b}) + \varepsilon_\mathbf{y}, \tag{2.1}$$

where **b** is a vector of model parameters (such as spectral line data, calibration parameters, etc.) which are not perfectly known. In case when it is possible to neglect the influence of the forward model errors, equation (2.1) may be introduced in a simplified form (2.1a):

$$\mathbf{y} = F(\mathbf{x}) + \varepsilon_\mathbf{y} \tag{2.1a}$$

Equation (2.1a) is a mathematical model of the measurement process allowing to derive the solution of inverse problem by mathematical methods, in particular by the global fit (GF) and optimal estimation (OE) methods. The GF method represents one of the simplest approaches (see, for example, the work of *Carlotti* [1988]) referred usually as Least Squares Fit (LSF): the solution is derived by minimizing with respect to **x** the scalar

$$\Phi_{GF} = \left(\mathbf{y} - F(\mathbf{x})\right)^T \mathbf{S}_\mathbf{y}^{-1} \left(\mathbf{y} - F(\mathbf{x})\right). \tag{2.2}$$

Superscript "*T*" denotes the transposition. Function $\mathbf{\Phi}_{\mathrm{GF}}$ is proportional to the standard deviation of measured values from the values, calculated for the atmospheric state **x**, and vector $\hat{\mathbf{x}}$, delivering the minimum to this deviation, is reasonably assumed to be the sought solution.

It is worth noting, that in many cases the task of determining the minimum of the function $\mathbf{\Phi}_{\mathrm{GF}}$ is the ill-posed one, therefore the obtained solution may appear to be strongly oscillating and the iterative process may be unstable. The concept of incorrect or ill-posed problems and the basic principles of their regularization have been formulated by *Tichonov and Arsenin* [1977]. Undoubtedly, other successful methods of treating specific ill-posed problems

have been proposed previously, but A.N.Tichonov created the basis of general mathematical approach.

The basic idea of the regularization is the application of additional information on the solution satisfying the physical nature of the problem and limiting the number of possible solutions in order to obtain the unique estimate. In the process of solving the inverse problems of atmospheric optics, the statistical information on variability of the sought parameters of atmospheric state is most commonly used as the additional (*a priori*) information. In this case, the ensemble of profiles which is used for the derivation of the solution is assumed to be characterized completely by the mean value $\mathbf{x}_a$, and the covariance $\mathbf{S}_a$. The nature of the *a priori* information of that kind leads to so-called "optimal estimation" (OE) method. In the 1960s, this method for linear problems was proposed practically simultaneously by three independent scientific teams [*Turchin et al*., 1968; *Rodgers*, 1971; *Strand and Westwater,* 1968].

Let us consider the fundamental formulae describing this method. Taking the *a priori* statistical information into account and assuming that the solution is part of a Gaussian distribution characterized by $\mathbf{S}_a$, the additional term, characterizing the probability of belonging of solution $\mathbf{x}$ to the *a priori* ensemble, should be introduced in (2.2):

$$\Phi_{OE} = \left(\mathbf{y} - F(\mathbf{x})\right)^T \mathbf{S}_\mathrm{y}^{-1} \left(\mathbf{y} - F(\mathbf{x})\right) + \left(\mathbf{x} - \mathbf{x}_a\right)^T \mathbf{S}_a \left(\mathbf{x} - \mathbf{x}_a\right) \tag{2.3}$$

The solution is found by minimizing the scalar $\mathbf{\Phi}_{\mathrm{OE}}$ with respect to $\mathbf{x}$.

Obviously, the difference between the GF and OE methods is defined by the difference between relationships (2.2) and (2.3). For deriving the extremum points of the $\mathbf{\Phi}_{\mathrm{OE}}$ and $\mathbf{\Phi}_{\mathrm{GF}}$ functions, one can use similar mathematical methods. Theoretically, it is unessential which namely method of minimization is used. But because of the fact that the inverse problems of atmospheric optics require extensive computing, it is recommended to use the algorithms which are developed specially for the tasks of this kind. The well-known algorithm of minimizing the function $\mathbf{\Phi}_{\mathrm{OE}}$, which is very convenient for practical use is described, for example by *Marks and Rodgers* [1993] and *Polyakov and Rozanov* [1989]. It represents an expansion of the "classical" statistical regularization method (developed for linear tasks) to the nonlinear case. Relevant iterative process is described by the following recurrence relation:

$$\mathbf{x}^{i+1} = \mathbf{x}_a + \left(\mathbf{K}^{i\,T} \mathbf{S}_\mathrm{y}^{-1} \mathbf{K}^i + \mathbf{S}_a^{-1}\right)^{-1} \left(\mathbf{K}^{i\,T} \mathbf{S}_\mathrm{y}^{-1} \left(\mathbf{y} - F\left(\mathbf{x}^i\right) + \mathbf{K}^i \left(\mathbf{x}^i - \mathbf{x}_a\right)\right)\right), \tag{2.4}$$

here and below $\mathbf{x}^i$ and $\mathbf{x}^{i+1}$ are solution estimates at consecutive iteration steps, $\mathbf{K}^i$ is the matrix of derivatives of operator F with respect to the components of state vector calculated for the $\mathbf{x}^i$ estimate:

$$\mathbf{K}^i = \frac{\partial F}{\partial \mathbf{x}}\left(\mathbf{x}^i\right)$$

The algorithm can be expressed in several other forms which are mathematically equivalent.

It is necessary to note, that the theory does not guarantee the convergence of iterative process (2.4) for arbitrary operator F. In case of considerable nonlinearity of relationships (such situation may occur for the problems of the gaseous content retrieval with or without specific constraints on the sought variables) the algorithm does not necessarily converge. In order to improve the algorithm convergence, *Marks and Rodgers* [1993] proposed to use the Marquardt algorithm that leads to the following recurrence relation:

$$\mathbf{x}^{i+1} = \mathbf{x}^i + \left(\mathbf{K}^{i\,T} \mathbf{S}_\mathrm{y}^{-1} \mathbf{K}^i + \mathbf{S}_a^{-1} + c\mathbf{I}\right)^{-1} \left(\mathbf{K}^{i\,T} \mathbf{S}_\mathrm{y}^{-1} \left(\mathbf{y} - F\left(\mathbf{x}^i\right)\right) + \mathbf{S}_a^{-1} \left(\mathbf{x}_a - \mathbf{x}^i\right)\right). \tag{2.5}$$

Here $\mathbf{I}$ is a unity matrix, c is a constant. It should be noted that inclusion $c\mathbf{I}$ does not influence the solution but only the path along which the solution is found.

Polyakov [1996] proposed a simple modification of relation (2.4), which has a clear physical meaning and gives the iterative algorithm, which differs from (2.5). Recurrence relation of this algorithm may be written in several equivalent forms, for example:

$$\mathbf{x}^{i+1} = \mathbf{x}^i + \left(\mathbf{K}^{i\,T}\mathbf{S}_\mathbf{y}^{-1}\mathbf{K}^i + \mathbf{S}_a^{-1} + \mathbf{L}^{-1}\right)^{-1}\left(\mathbf{K}^{i\,T}\mathbf{S}_\mathbf{y}^{-1}\left(\mathbf{y} - F\left(\mathbf{x}^i\right)\right) + \mathbf{S}_a^{-1}\left(\mathbf{x}_a - \mathbf{x}^i\right)\right), \quad (2.6.1)$$

$$\mathbf{x}^{i+1} = \mathbf{x}_a + \left(\mathbf{K}^{i\,T}\mathbf{S}_\mathbf{y}^{-1}\mathbf{K}^i + \mathbf{S}_a^{-1} + \mathbf{L}^{-1}\right)^{-1}\left(\mathbf{K}^{i\,T}\mathbf{S}_\mathbf{y}^{-1}\left(\mathbf{y} - F\left(\mathbf{x}^i\right) + \mathbf{K}^i\left(\mathbf{x}^i - \mathbf{x}_a\right)\right) + \mathbf{L}^{-1}\left(\mathbf{x} - \mathbf{x}_a\right)\right) \quad (2.6.2)$$

In (2.6.1) and (2.6.2), **L** is any positively defined matrix. Practically, it can be recommended to use the diagonal matrix with elements, limiting the variations of the components of the vector $\mathbf{x}=\{x_i\}$ at any iterative step. These elements are chosen in such a way that the functional *F* is assumed to be linear at iterative step. The advantage of this algorithm is a possibility of better adaptation to the nonlinearity of initial operator.

The GF version of these algorithms may be easily obtained by passing to the limit at $\mathbf{S}^{-1} \to 0$ i.e. by assuming the absence of *a priori* constraints on the solution. In this case, the recurrence relations (2.5) and (2.6.1) become:

$$\mathbf{x}^{i+1} = \mathbf{x}^i + \left(\mathbf{K}^{i\,T}\mathbf{S}_\mathbf{y}^{-1}\mathbf{K}^i + c\mathbf{I}\right)^{-1}\mathbf{K}^{i\,T}\mathbf{S}_\mathbf{y}^{-1}\left(\mathbf{y} - F\left(\mathbf{x}^i\right)\right) \quad (2.7.1)$$

$$\mathbf{x}^{i+1} = \mathbf{x}^i + \left(\mathbf{K}^{i\,T}\mathbf{S}_y^{-1}\mathbf{K}^i + \mathbf{L}^{-1}\right)^{-1}\mathbf{K}^{i\,T}\mathbf{S}_\mathbf{y}^{-1}\left(\mathbf{y} - F\left(\mathbf{x}^i\right)\right) \quad (2.7.2)$$

It should be stressed that the direct use of the Marquardt algorithm for minimizing the function $\mathbf{\Phi}_{GF}$ also brings to (2.7.1).

Analysis of solution errors in the inverse problem

Let us estimate the errors of solutions produced by the GF and OE methods. For convenience of parallel consideration, the similar formulae will be marked by the same numbers with subscripts relevant to the method.

If $\tilde{\mathbf{x}}$ is the true vector, the task is to estimate the errors of its retrieval by the GF and OE methods. If $\hat{\mathbf{x}}$ is the solution estimate, corresponding to one of examined methods, it must deliver (as follows from (2.1a), (2.2) and (2.3)) the minimum of $\mathbf{\Phi}_{GF}$ or $\mathbf{\Phi}_{OE}$ respectively:

$$\hat{\Phi}_{OE} = \left(F(\tilde{\mathbf{x}}) + \varepsilon - F(\hat{\mathbf{x}})\right)^T\mathbf{S}_\mathbf{y}^{-1}\left(F(\tilde{\mathbf{x}}) + \varepsilon - F(\hat{\mathbf{x}})\right) + \left(\hat{\mathbf{x}} - \mathbf{x}_a\right)^T\mathbf{S}_a^{-1}\left(\hat{\mathbf{x}} - \mathbf{x}_a\right), \quad (2.8_{OE})$$

$$\hat{\Phi}_{GF} = \left(F(\tilde{\mathbf{x}}) + \varepsilon - F(\hat{\mathbf{x}})\right)^T\mathbf{S}_\mathbf{y}^{-1}\left(F(\tilde{\mathbf{x}}) + \varepsilon - F(\hat{\mathbf{x}})\right). \quad (2.8_{GF})$$

Let us assume that $\tilde{\mathbf{x}}$ and $\hat{\mathbf{x}}$ agree closely, and the operator *F* is well described by a linear expansion about a reference state $\breve{\mathbf{x}}$:

$$F(\hat{\mathbf{x}}) \approx F(\breve{\mathbf{x}}) + \mathbf{K}_{\breve{\mathbf{x}}}\left(\hat{\mathbf{x}} - \breve{\mathbf{x}}\right),$$

here $\mathbf{K}_{\breve{\mathbf{x}}}$ is the matrix of derivatives of operator *F* with respect to argument coordinates at the point $\breve{\mathbf{x}}$. Then (2.8_{OE}) and (2.8_{GF}) may be brought to:

$$\hat{\Phi}_{OE} = \left(\varepsilon - \mathbf{K}_{\breve{\mathbf{x}}}(\hat{\mathbf{x}} - \breve{\mathbf{x}})\right)^T\mathbf{S}_\mathbf{y}^{-1}\left(\varepsilon - \mathbf{K}_{\breve{\mathbf{x}}}(\hat{\mathbf{x}} - \breve{\mathbf{x}})\right) + \left(\hat{\mathbf{x}} - \mathbf{x}_a\right)^T\mathbf{S}_a^{-1}\left(\hat{\mathbf{x}} - \mathbf{x}_a\right), \quad (2.9_{OE})$$

$$\hat{\Phi}_{GF} = \left(\varepsilon - \mathbf{K}_{\breve{\mathbf{x}}}(\hat{\mathbf{x}} - \breve{\mathbf{x}})\right)^T\mathbf{S}_\mathbf{y}^{-1}\left(\varepsilon - \mathbf{K}_{\breve{\mathbf{x}}}(\hat{\mathbf{x}} - \breve{\mathbf{x}})\right). \quad (2.9_{GF})$$

As $\hat{\mathbf{x}}$ is the estimate, it provides the minimum of (2.9). Then after differentiating and equating the derivatives to zero, we can write the estimate error $\hat{\mathbf{x}} - \tilde{\mathbf{x}}$ as:

$$\hat{\mathbf{x}} - \tilde{\mathbf{x}} = \left(\mathbf{K}_{\tilde{\mathbf{x}}}{}^{T}\mathbf{S}_{\mathbf{y}}{}^{-1}\mathbf{K}_{\tilde{\mathbf{x}}} + \mathbf{S}_{a}{}^{-1}\right)^{-1}\left(\mathbf{K}_{\tilde{\mathbf{x}}}{}^{T}\mathbf{S}_{\mathbf{y}}{}^{-1}\boldsymbol{\varepsilon} + \mathbf{S}_{a}{}^{-1}\left(\tilde{\mathbf{x}} - \mathbf{x}_{a}\right)\right), \qquad (2.10_{\mathrm{OE}})$$

$$\hat{\mathbf{x}} - \tilde{\mathbf{x}} = \left(\mathbf{K}_{\tilde{\mathbf{x}}}{}^{T}\mathbf{S}_{\mathbf{y}}{}^{-1}\mathbf{K}_{\tilde{\mathbf{x}}}\right)^{-1}\mathbf{K}_{\tilde{\mathbf{x}}}{}^{T}\mathbf{S}_{\mathbf{y}}{}^{-1}\boldsymbol{\varepsilon}. \qquad (2.10_{\mathrm{GF}})$$

The error of profile retrieval, as a random value, is characterized by the mean vector $\overline{\hat{\mathbf{x}}}$ and variability covariance $\mathbf{S}_{\mathrm{M}}$:

$$\overline{\hat{\mathbf{x}}} = E(\hat{\mathbf{x}} - \tilde{\mathbf{x}}) \qquad \mathbf{S}_{M} = E((\hat{\mathbf{x}} - \tilde{\mathbf{x}}) - \overline{\hat{\mathbf{x}}})((\hat{\mathbf{x}} - \tilde{\mathbf{x}}) - \overline{\hat{\mathbf{x}}})^{T},$$

where E is the mathematical expectation symbol.

As a result of transforming (2.10), one can obtain the following formulae for the vector of mean (or constant) error (so-called Null-Space or smoothing Error) (2.11) and for the error covariance (2.12):

$$\overline{\hat{\mathbf{x}}} = \left(\mathbf{K}_{\tilde{\mathbf{x}}}{}^{T}\mathbf{S}_{\mathbf{y}}{}^{-1}\mathbf{K}_{\tilde{\mathbf{x}}} + \mathbf{S}_{a}{}^{-1}\right)^{-1}\mathbf{S}_{a}{}^{-1}\left(\tilde{\mathbf{x}} - \mathbf{x}_{a}\right), \qquad (2.11_{\mathrm{OE}})$$

$$\overline{\hat{\mathbf{x}}} = 0, \qquad (2.11_{\mathrm{GF}})$$

$$\mathbf{S}_{M} = \left(\mathbf{K}_{\tilde{\mathbf{x}}}{}^{T}\mathbf{S}_{\mathbf{y}}{}^{-1}\mathbf{K}_{\tilde{\mathbf{x}}} + \mathbf{S}_{a}{}^{-1}\right)^{-1}\mathbf{K}_{\tilde{\mathbf{x}}}{}^{T}\mathbf{S}_{\mathbf{y}}{}^{-1}\mathbf{K}_{\tilde{\mathbf{x}}}\left(\mathbf{K}_{\tilde{\mathbf{x}}}{}^{T}\mathbf{S}_{\mathbf{y}}{}^{-1}\mathbf{K}_{\tilde{\mathbf{x}}} + \mathbf{S}_{a}{}^{-1}\right)^{-1}, \qquad (2.12_{\mathrm{OE}})$$

$$\mathbf{S}_{M} = \left(\mathbf{K}_{\tilde{\mathbf{x}}}{}^{T}\mathbf{S}_{\mathbf{y}}{}^{-1}\mathbf{K}_{\tilde{\mathbf{x}}}\right)^{-1}. \qquad (2.12_{\mathrm{GF}})$$

The null-space (smoothing) error related to the discrete vector space of retrieval parameters is equal to zero for GF or LSF method. It is obvious that (2.11_{OE}) and (2.12_{OE}) , are transformed into the relationships for GF method at $\mathbf{S}_{a}{}^{-1} \to 0$ (this is the case when the *a priori* information is missing).

Here we supposed that the linear approach well describes the F behavior in the range of the difference between the state vector and estimate. If more strong assumption is valid and $\mathbf{K}_{\mathbf{x}} = \mathbf{K}$, i.e. the covariance of derivatives is constant in all range of *a priori* variability of vector $\mathbf{x}$, the estimate error averaged over *a priori* statistics may be obtained. In this case, total error matrix of retrieval $\hat{\mathbf{S}}_{\mathbf{x}}$ may be treated as the sum of null-space error matrix $\mathbf{S}_{\mathrm{N}}$ and the component due to measurement noise $\mathbf{S}_{\mathrm{M}}$:

$$\hat{\mathbf{S}}_{\mathbf{x}} = \left(\mathbf{S}_{a}{}^{-1} + \mathbf{K}^{T}\mathbf{S}_{\mathbf{y}}{}^{-1}\mathbf{K}\right)^{-1} = \mathbf{S}_{N} + \mathbf{S}_{M}, \qquad (2.13_{\mathrm{OE}})$$

For the GF method:

$$\hat{\mathbf{S}}_{\mathbf{x}} = \left(\mathbf{K}^{T}\mathbf{S}_{\mathbf{y}}{}^{-1}\mathbf{K}\right)^{-1} = \mathbf{S}_{M}, \qquad (2.13_{\mathrm{GF}})$$

as the smoothing error is equal to zero.

The smoothing error covariance for OE method is

$$\mathbf{S}_{N} = \left(\mathbf{S}_{a}{}^{-1} + \mathbf{K}^{T}\mathbf{S}_{\mathbf{y}}{}^{-1}\mathbf{K}\right)^{-1}\mathbf{S}_{a}{}^{-1}\left(\mathbf{S}_{a}{}^{-1} + \mathbf{K}^{T}\mathbf{S}_{\mathbf{y}}{}^{-1}\mathbf{K}\right)^{-1} \qquad (2.14)$$

Although the determinant of noise error covariance $\mathbf{S}_{\mathrm{M}}$ for the GF method is greater than for the OE method, it seems, at first sight, that the zero smoothing error in the GF method is very attractive. But as it was mentioned above, in some cases the application of the GF method encounters serious difficulties associated with the fact that the inverse problem is ill-posed.

Incorrectness of the inverse problems of atmospheric optics and their reduction to finite-dimensional space.

Let us analyze the mathematical operation of the transfer from continuous radiating medium, which is the atmosphere, to the finite-dimensional representation of its parameters, commonly used in solving the inverse problems of atmospheric optics.

Description of radiative transfer processes demands the assignment of atmospheric parameters, influencing the radiative transfer, as continuous functions of the medium. When the model of spherically symmetrical atmosphere is used, the atmospheric state parameters are assumed to be constant at fixed altitude, and it is necessary to know the atmospheric parameters as a continuous function of altitude. Although the theory allows to consider the inverse problems of atmospheric optics for the case of continuous functions of altitude, a practical implementation of algorithms leads necessarily to discretizing the problem and to searching for a solution in finite-dimensional space.

When reducing a continuous, in physical sense, task to a discrete finite-dimensional space, we have to define uniquely what is just meant by the parameters - vector components, and what is the procedure (algorithm), permitting to obtain a value of atmospheric state parameter at any altitude from finite-dimensional vector. Surprisingly, in many studies of the inverse problems, this step of mathematical formulation of the task is not examined in detail.

There are many various approaches to discretization of such problems, but only two are commonly used (see for example [*Clarmann et al*., 1991]). The first assumes the assignment of atmospheric state parameters at discrete altitudes and specific procedure of interpolation - for example, linear interpolating the temperature and gas mixing ratio and exponential interpolating the pressure along the altitude. The second approach assumes that some atmospheric parameters are fixed in given layers (for example, the temperature or gas mixing ratio) or vary in these layers as a simple function of altitude (for example, the pressure and gaseous content - according to the barometric formula). The second approach seems more preferable, as *de facto* any optical (in a broad sense) measurement of radiation, transformed by atmosphere, does not contain the information on a value of any atmospheric parameter at specific altitude, i.e. in an infinitely thin layer. The radiation is transformed by a gaseous volume of a finite size. In addition, a relatively poor spatial resolution is characteristic for the inverse problems of atmospheric optics, and it has the influence on the retrieval errors [*Backus and Gilbert*, 1970]. From the above it follows, that during remote optical measurements, one actually deals with some values spatial-averaged but not with the parameter value at a space point or at specific altitude. As this takes place, the atmospheric stratification has to be quite detailed to describe the typical variability scales of atmospheric parameters examined or influencing the measurements. In addition, the layer thicknesses of atmospheric stratification are to be small as compared with that of weighting functions; otherwise the weighting functions will be distorted and the use of mathematical methods of studying the problem, in particular, for analysis of retrieval errors, will not be valid.

To summarize briefly, the atmospheric stratification should be detailed enough to describe the main properties of initial, essentially continuous, task. It is known, that one of these properties is that the problem is ill-posed. It follows from the common considerations that, under condition of detailed atmospheric stratification, the ill-posed character of these continuous tasks remains. Let us pass further to the problem of regularization of ill-posed tasks.

Any inverse problem of remote sensing may be described by relation (2.2). The principal mathematical problem, arising in the process of solving such ill-posed tasks, is the fact that there is a non-trivial set of estimates, complying with (2.2), and this set is unstable with respect to a representation of measurement noise error.

Before the concept of incorrectness and the regularization procedures have been developed and have become widely used in practice, some attempts of treating the ill-posed problems were successful when they included implicitly a regularization process (constraints for the solution). One of the simplest empirical approaches is a reduction of task dimension. Such reduction of the space of sought parameters has various physical meanings, depending on

the way of discretizing the initial task, but always imposes the essential constraints on the set of sought estimates.

Reduction of the task on rather rarefied altitude grid implies the condition of interpolation links for close values, disposed between two grid levels or of their constancy inside the layer. Actually, this demand is similar to imposing the strong correlation relations between the values, closely located in altitude, but the structure and character of these corellations do not simulate the physical processes really observed in atmosphere.

At the cost of possible bias of the solution in case of too hard a priori constraint, the OE method offers essential advantages over the above approach as it considers real correlations between atmospheric parameters or empirical links, having clear physical sense. This additional information gives a possibility to use a fairly detailed grid of stratification. When using the OE method, one encounters the problem of lacking (or incompleteness) the required *a priori* information. In most cases, systematical direct measurements (with needed characteristics) of required atmospheric parameters are not carried out. Instead of these data, empirical information based on available measurements and on our knowledge of real atmospheric processes may be used. For example, it is usually assumed that due to mixing processes, the values of any atmospheric parameter at neighboring altitudes are similar to a high degree of probability. Then after estimating the relevant correlations, one may construct a model covariance. In this approach, all *a priori* information, inherent in the solving algorithm, is given in explicit form and has clear physical meaning. This approach was used, in particular, for the interpretation of the CLAES data [*Dudhin and Livesey*, 1996].

As shown, for example, by *Backus and Gilbert* [1970], the profiles of atmospheric parameters, retrieved at detailed altitude grid, are obviously characterized by relatively large errors. But the functionals of those, required by the scientific community, can be obtained with the errors, calculated easily on the basis of *a posteriori* covariance [*Conrath*, 1972]. Such functionals are, for example, the same atmospheric parameters averaged over some atmospheric layers up to the total gaseous content accompanied by real estimate of retrieval error.

As the prime object of the present study is a comparison of the GF and OE methods on the basis of simulations of the typical spectral radiation measurements (as expected to be performed e.g. by the MIPAS instrument), we were forced to use rather rough atmospheric stratification to provide the stability of the GF solving algorithm. The choice of the layer thickness equal to 3 km is caused by measurement scenario and instrument vertical resolution. In the problem of comparing two methods, a relatively large altitude step is not too critical as both methods are examined under equal conditions. Use of any regularizing retrieval method, such as OE, would of course allow a finer atmospheric stratification.

3. Overview of the input data: instrument characteristics and measurement scenario

The comparison of the GF and the OE retrieval algorithms in case of high spectral resolution limb radiance measurements was done in the present study on the basis of simulations (however with certain simplifications) of the future MIPAS (Michelson Interferometer for Passive Atmospheric Sounding) measurements.

MIPAS is a Fourier-Transform spectrometer which will be one of the payload instruments on-board the Envisat environmental satellite. The Envisat satellite will fly in a sun-synchronous orbit of 800 km height providing the complete polar coverage. Launch is planned by mid 1999.

The overview of the current critical instrument and subsystem requirements and the MIPAS design is given in the paper by *Endemann et al.* [1996]. Here only the main features are presented which concern the problem of the computer simulation of the MIPAS measurements. Table 3.1 presents the summary of MIPAS performance requirements as reported by *Endemann et al.* [1996].

The distance between instrument and tangent point is about 3300 km. Thus, in order to measure at a predetermined limb height, the pointing of instrument and satellite in elevation

Table 3.1 Requirements to the MIPAS performance

Observation Geometry	
Instantaneous Field-of-View	3 x 30 km^2 (height x width)
elevation pointing	5...250 km above earth limb
azimuth pointing	35^o rearwards, 30^o sideways
Spectral Coverage	
spectral range	685...2410 cm^{-1} (14.6 .. 4.15 μm)
spectral resolution	0.035 cm^{-1}
	total 50000 spectral samples per spectrum at full spectral resolution
spectral resolution modes	reduced to 1/10 full spectral resolution for special measurements
Radiometric Requirements	
radiometric sensitivity NESR	50 ... 4.2 nW/(cm^2 sr cm^{-1})
absolute radiometric accuracy	1% (at 14.6 μm) ... 3% (at 4.15 μm) of input radiance
Measurement Duration	
time per spectrum	4.6 s (full spectral resolution)
	1.0 s (1/10 spectral resolution)
time per elevation scan	75 s (500 km ground trace)
spectral per elevation scan	16 (full spectral resolution)
	75 (1/10 spectral resolution)

direction must be excellent. It is a goal to determine the geometric limb height by pointing information from the spacecraft with a standard deviation below 600 m. Thus a LOS pointing knowledge with respect to nadir of better than 0.01 deg (1 σ) will be required. The LOS calibration is based on the observation of stars moving through the instrumental FOV with the short wavelength channels.

A typical elevation scan will start at about 50-65 km limb height and descent in 3 km steps to 8 km. However MIPAS will be sufficiently flexible to perform any elevation scan sequence within the range of 5 to 150 km limb height, even with variable step sizes.

The Noise Equivalent Spectral Radiance (NESR) characterizes the instrument noise in terms of incident radiance. The noise is assumed uncorrelated if the spectral grid spacing is set to 0.025 cm^{-1} and no nominal apodization is applied (for highest resolution, the nominal case). Self-apodization has no effect on the noise spectrum. The dependence of NESR on the wavenumber region is listed in the Table 3.2.

Table 3.2 The MIPAS NESR values.

Wavenumber range [cm^{-1}]	NESR [nW/(cm^2 sr cm^{-1})]
685 - 970	50
1020 - 1170	40
1215 - 1500	20
1570 - 1750	6
1820 - 2410	4.2

Radiometric calibration consists of:

- offset calibration, by observation of cold space to determine the internal emission of MIPAS (which will be the major source for offset in the spectra);
- gain calibration, by observation of the internal calibration blackbody source to calibrate the instrument response throughout the spectral bands.

The radiometric accuracy for each spectral grid point can be expressed as:

$$r_a = 2 \cdot \text{NESR} + 2\% \text{ of [true source spectral radiance]} \quad (3.1)$$

This formula is valid for all 5 bands using the respective NESR values. 'True source spectral radiance' will be the radiance at a given grid point as would be measured with an "ideal" radiometer, i.e. with no radiometric errors and the same ILS as MIPAS. One more remark should be given: if the source radiance is constant within a given spectral interval then the radiometric accuracy in that interval is the sum of the uncorrelated NESR value and a fully correlated contribution equal to NESR plus 2% of the true source spectral radiance.

In the present study the offset and gain calibration errors were not taken into account and modeled due to the following reasons:

- the offset and gain calibration errors will cause the considerable decreasing of the retrieval accuracy for all atmospheric parameters stipulated by the additional systematic errors. That will make difficult the comparison of the results delivered by two considered methods (GF and OE);
- in reality the correlation of offset errors may be difficult to characterize [*Nett*, 1997, private communication].

The processing of the interferograms is planned to be performed using the Norton-Beer strong apodization function which considerably suppresses the sidelobes [*Norton and Beer*, 1976]. In this case the apodized spectral resolution is expected to be 0.055 cm^{-1}. The resulting instrument line shape (ILS) is shown in Fig. 3.1. For reasons of simplicity noise correlations by apodization have been ignored.

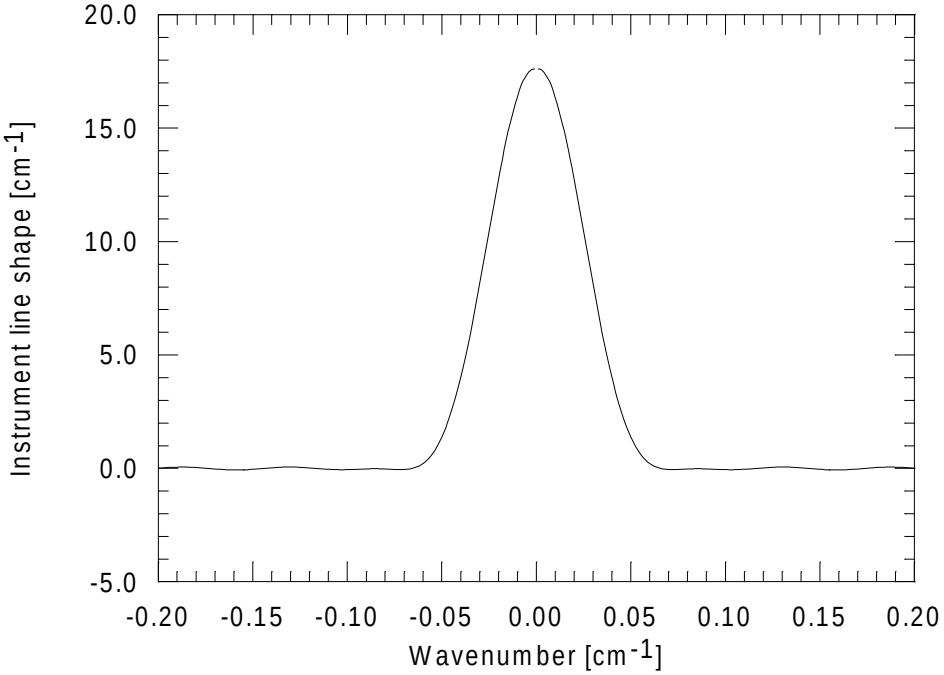

Fig. 3.1 The instrument line shape (ILS) corresponding to the Norton-Beer strong apodization. Spectral resolution 0.055 cm^{-1}.

4. Atmospheric models

The input data for simulation of the spectral limb radiance measurements and performing numerical experiments include set (ensemble) of atmospheric parameters' profiles describing different atmospheric situations. The requirements to such ensemble of profiles are the following:

- Each subset of profiles (which will be referred further as “atmospheric model”) should describe all parameters under investigation, i.e. pressure, temperature, ozone and water vapor.
- Atmospheric parameters should be bounded to the specific altitude grid which is determined by the tangent altitudes of measurements.
- The altitude range should correspond to the altitude range of the MIPAS measurements.
- Profiles in the models should be realistic.
- The ensemble, taken as a whole, should adequately describe the variability of parameters and their covariances.
- The ensemble should contain a number of models which will be sufficient for statistical investigations.

In order to satisfy the above mentioned requirements it was necessary to make special compilation of atmospheric models using available data. The data from the well-known ensemble TIGR and the results of ATMOS measurements have been selected as the basis for such compilation. The TIGR data set contains about 1700 atmospheric models. Every model consists of the vertical profiles of temperature, water vapor and ozone bounded to the pressure grid which is the same for all models. Preliminary analysis showed that the real water vapor profiles are given only for the altitudes below 100-70 mb level. Above this level the profiles were complimented by the profile which does not correspond to modern knowledge about the water vapor distribution in the middle and upper atmosphere. Real ozone profiles which correspond to the temperature profiles are given only for the first 46 atmospheric states. For the other models these profiles are repeated. The upper boundary of the atmosphere in the TIGR database corresponds to the altitude of 65 km. The MIPAS measurements are planned to be carried out also up to this altitude, however it is evident that the limb radiance is transformed also by the above lying layers which should be taken into account in the simulations.

Therefore, only 46 first atmospheric models from the TIGR database were taken as the basis for the compilation excluding water vapor profiles above 100 mb level. For these 46 atmospheric states the altitude levels were calculated in accordance with the pressure grid. Afterwards, all atmospheric parameters were bounded to the common altitude grid with the help of spline interpolation technique. The obtained atmospheric models were complemented by the water vapor profiles above 100 mb level taken from the ATMOS data. The last step was the expanding of profiles to the altitude of 80 km. Below the procedure is described in detail.

The transfer from the pressure grid to the altitude grid.

The dependence pressure-altitude in the atmosphere is described by the well-known hydrostatic equation which is written in the differential form as follows:

$$dp = -\rho(z)g(z)dz \tag{4.1}$$

where p is pressure, ρ is air density, g is the acceleration due to gravity, z denotes altitude. The transfer to the integral values requires the application of the boundary condition. Both air density and the acceleration due to gravity are altitude dependent (for example, the g value at the altitude of 100 km is about 2% less than the value at sea level). The altitude dependence of g is given by the expression:

$$g(z) = g_0\left(\frac{R_0}{R_0 + z}\right)^2 \tag{4.2}$$

where g_0 is the value at the distance R_0 from the Earth center, z is the altitude over R_0. Air density may be expressed as:

$$\rho = \frac{m}{V} = \frac{p\,\mu}{R\,T} \tag{4.4}$$

where m is the molecular mass (for the dry air the value 28.964 can be taken), R is the universal gas constant, T is temperature. The mean molecular mass of the humid air can be calculated as:

$$\mu_{humid} = \mu_{dry}\cdot\frac{1}{1+q_{H_2O}} + \mu_{H_2O}\cdot\frac{q_{H_2O}}{1+q_{H_2O}} \tag{4.5}$$

where q_{H2O} is the water vapor vmr which is the ratio of the water vapor volume to the volume of the dry air.

Let us consider 2 levels in the atmosphere with pressure values p_0 and p_1 ($p_0 > p_1$) and temperature values T_0 and T_1 and assume that the altitude of the level p_0 is known. Assuming also that the initial grid is detailed enough to apply linear interpolation procedure for temperature, we obtain:

$$T(z) = a + bz = T_0 + \frac{\Delta T}{\Delta z} z\,, \qquad \Delta T = T_1 - T_0 \tag{4.6}$$

where Δz is the layer thickness which is to be determined. Taking water vapor vmr constant within the layer and accounting for the fact that the influence of water vapor on the mean molecular mass of air is noticeable only in the thin ground layer the equation (4.1) is transformed to:

$$\frac{dp}{p} = -\frac{\mu_{humid} g_0 R_0^{\,2}}{R(R_0 + z)^2 (T_0 + \frac{\Delta T}{\Delta z} z)} dz \tag{4.7}$$

After integration we obtain:

$$\ln(\frac{p_1}{p_0}) = -\frac{\mu g_0 R_0^{\,2} \Delta z}{R(R_0 \Delta T - T_0 \Delta z)} \cdot \cdot \left(\frac{1}{R_0 + \Delta z} - \frac{1}{R_0} + \frac{\Delta T}{R_0 \Delta T - T_0 \Delta z} \ln\left(\frac{(T_0 + \Delta T) R_0}{T_0 (R_0 + z)} \right) \right) \tag{4.8}$$

After solving this equation with respect to Δz it is possible to get the required z value.

On the basis of the equation (4.8) the altitude grid was calculated for the first 46 models of the TIGR database. The sea level was assigned to pressure value 1000 mb.

Complementation of the ensemble by water vapor and ozone profiles in the higher layers.

As it was mentioned, the water vapor profiles of TIGR database are unrealistic above 100 mb level. Besides, the data for the levels higher than 65 km was missing. We had at our disposal the ATMOS measurements' database which contained profiles of different atmospheric parameters retrieved from the occultation measurements. These data were used for the complementation of the ensemble in the following way:

1) The ATMOS data were transferred to the desired altitude grid.

2) The mean profiles were calculated and also the covariance matrix was calculated which corresponded to the joint vector of atmospheric parameters including pressure, temperature, ozone and water vapor. As a consequence the covariances of the parameters were taken into account.

3) For each of the 46 basic atmospheric models all ATMOS data were analyzed and the most appropriate profiles were used as the complementation. The criterion for the most appropriate profile was the minimum of the following functional:

$$\left\| (x - \bar{x}) \right\|_{D^{-1}} = (x - \bar{x})^T D^{-1} (x - \bar{x}) \tag{4.9}$$

Since the information in the ATMOS database was also incomplete, several water vapor values at 77 km and 80 km altitude remained undefined and 30% of the total number of ozone profiles higher than 65 km remained undefined too. Missing values were added on the empirical basis.

Overview of the ensemble.

The calculated mean profiles of atmospheric parameters and the variability "corridors" are shown in Figures 4.1 and 4.2. The variability corridors correspond to the root-mean-square deviations. For the sake of comparison, the mean profiles from the well-known AFGL-86 database [*Anderson*, 1986] are presented also which correspond to the models "midlatitudes, summer" and "subarctica, winter".

One can see that the variability for temperature is not high and reaches 10 K only at the altitude of 60 km. Unfortunately, we do not have the information on the method used for creating TIGR database. On the basis of the analysis of temperature and ozone data we can come to the conclusion that the ensemble describes most probably local statistics which is usually obtained for one or another geographic region during specific season.

The mean profiles of the ensemble differ noticeably from the mean profiles of AFGL-86 models. However these differences are in accordance with the variability of the profiles in the ensemble. It should be mentioned that the variability of ozone in the upper layers (higher than 65 km) appeared to be much higher than the differences between the mean profiles and the AFGL-86 profiles. It is caused probably by the small amount of data for these altitudes. Nevertheless, since the study deals with the 8-65 km altitude region, the peculiarities of ozone profiles in the upper layers can be considered not important.

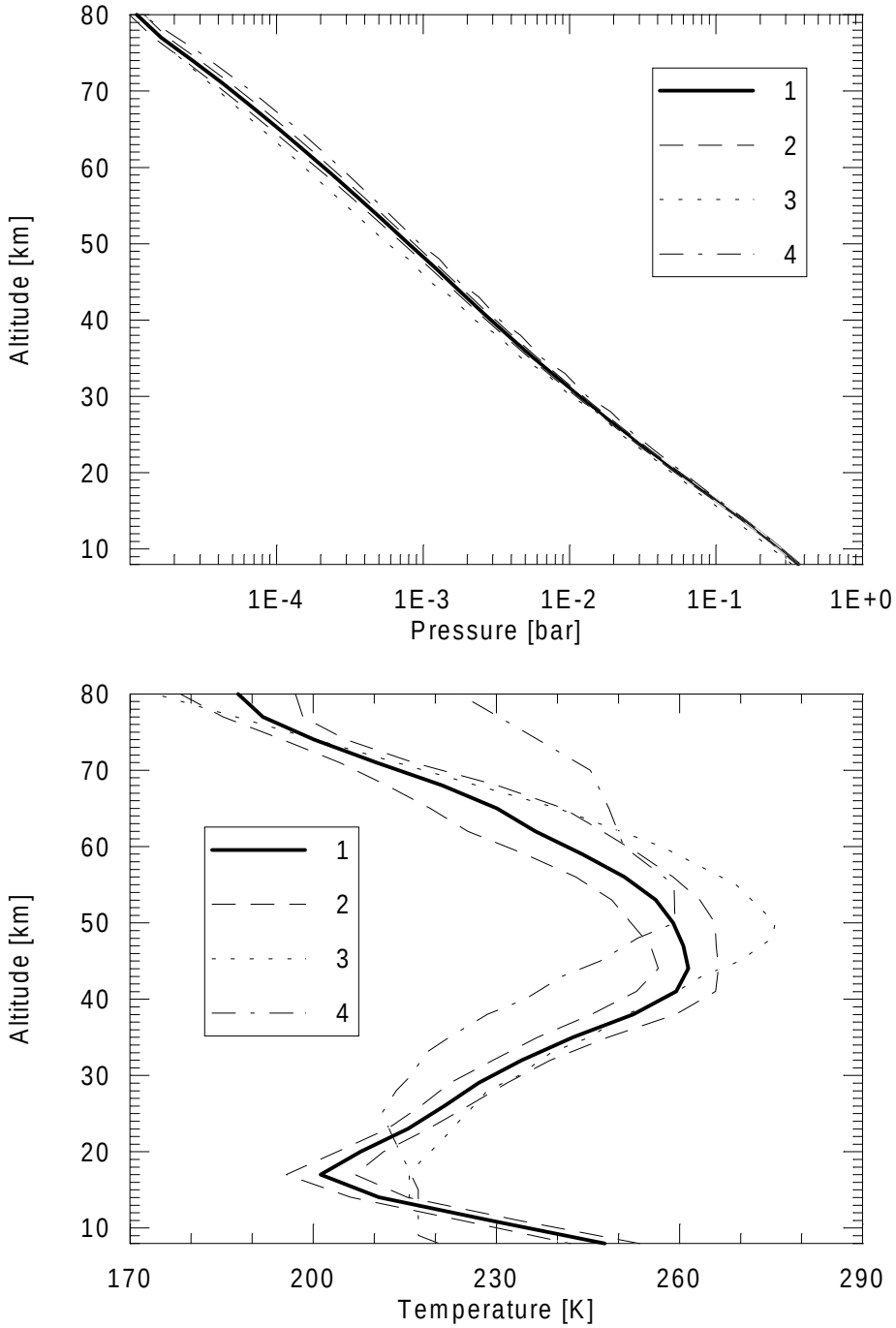

Fig. 4.1 Characteristics of the ensemble of atmospheric models. Upper panel - pressure, lower panel - temperature. 1 - mean profile, 2 - lines showing the "corridor" of variability. Additionally 2 profiles are shown for comparison: 3 - subarctica, winter, 4 - midlatitude, summer.

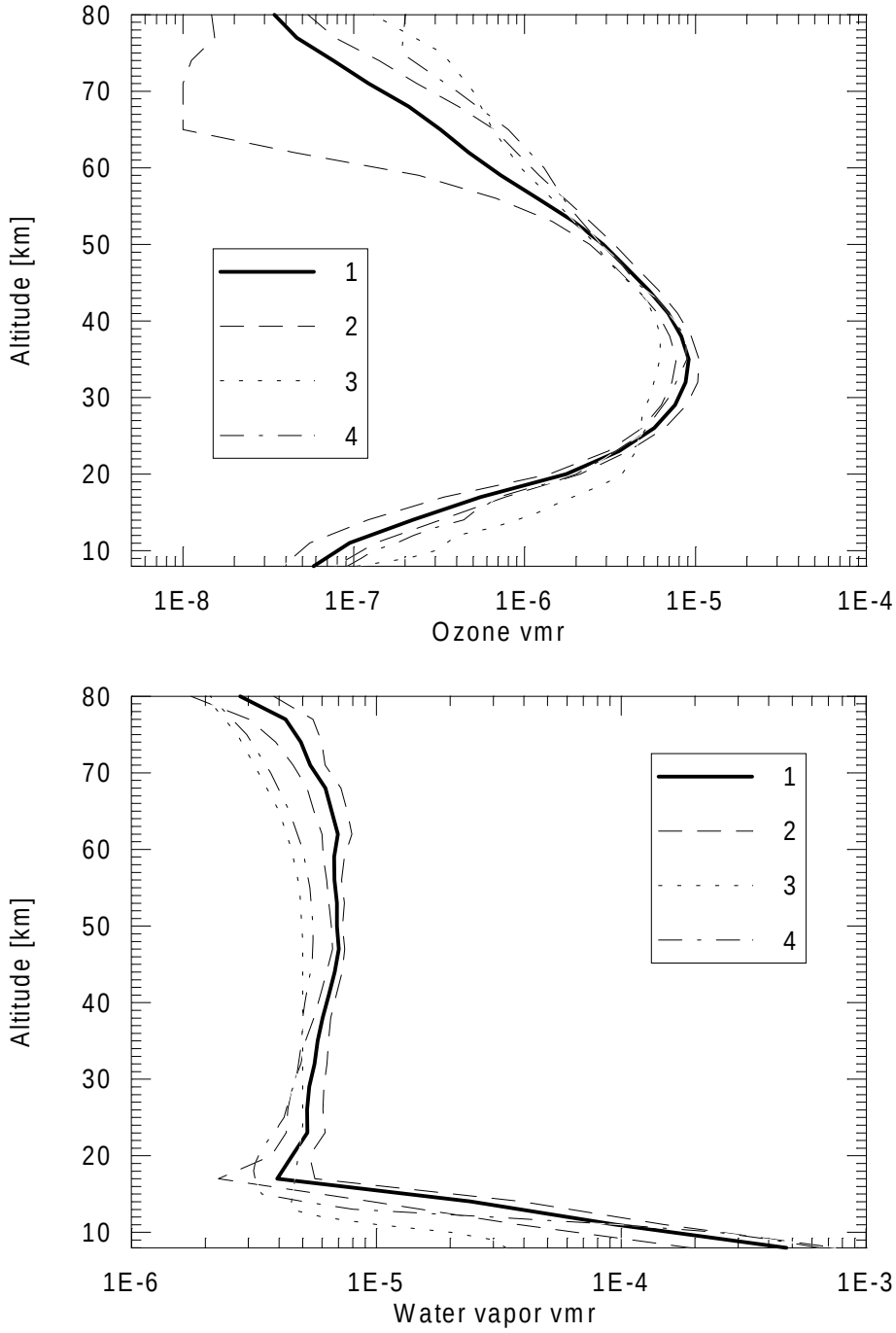

Fig. 4.2 Characteristics of the ensemble of atmospheric models. Upper panel - ozone, lower panel - water vapor. 1 - mean profile, 2 - lines showing the "corridor" of variability. Additionally, 2 profiles are shown for comparison: 3 - subarctica, winter, 4 - midlatitude, summer.

5. Description of the numerical experiments

The microwindows preselected for the pressure-temperature retrieval, water vapor retrieval and ozone retrieval were taken from the results of different studies performed in the Institut für Meteorologie und Klimaforschung, Forschungszentrum Karlsruhe. The description of the method of microwindow selection and the corresponding results can be found in [*Clarmann et al*., 1994] (p-T retrieval) and in subsequent studies [Echle et al., 1995]. The MIPAS research group in IMK is constantly improving the microwindow selection. We used the results (microwindow database) of the latest update with respect to October 1996. Original database contains the sets of microwindows (spectral intervals) sorted by the tangent altitudes. Microwindows were selected so that the specific microwindow could be best suitable for the retrieval of the atmospheric parameter at the specific tangent altitude. For the sake of utilization of the data by the software used in the present study, the microwindows from the database were sorted by the increasing wavenumber. The overlapping microwindows were combined. As the result, the modified database was created where the specific microwindow is characterized by the set of tangent altitudes. Within each microwindow the wavenumber step of measurements was taken equal to 0.025 cm^{-1} which corresponds to the wavenumber step with the uncorrelated random noise.

The set for the p-T retrieval task comprised 123 microwindows with the total wavenumber coverage of about 47 cm^{-1}. The number of microwindows for the water vapor retrievals was 83, however the total wavenumber coverage was considerably larger than for the p-T task and was about 110 cm^{-1}. The number of microwindows for the ozone retrieval task was 90 with the total wavenumber coverage of about 80 cm^{-1}.

The computer code SPIRT-NLC described in the study by *Hollweg et al*. [1995] was used as a main computational tool for the limb radiance line-by-line calculations. The spectral line data were taken from the HITRAN database, 1992 edition. In the limb radiance calculations only the major optically active atmospheric components were considered: water vapor, carbon dioxide, and ozone. For the water vapor the continuum absorption was also taken into account on the basis of the approximating formula. The spectral line shape function was calculated by the Humlicek algorithm [*Humlicek*, 1982]. The instrument line shape function was taken equal to the one of MIPAS with the spectral resolution 0.055 cm^{-1} (see Section 3). Non-LTE and line-mixing effects were not considered. In order to minimize the consumption of computer-time, the infinitesimal angular resolution of measurements was assumed, unless mentioned explicitly.

In the numerical experiments the random noise was simulated for every measurement. By the term “measurement” we denote here the limb radiance value at a given wavenumber and tangent altitude calculated for the selected model plus random noise. The random number generator was used with the gaussian distribution and standard deviation equal to NESR of MIPAS in the correspondent passband. After accounting for the apodization the random noise was assumed to be as indicated in the Table 5.1.

Table 5.1 The MIPAS NESR values (apodized) used in the numerical experiments.

Wavenumber range [cm^{-1}]	NESR [$nW/(cm^2\ sr\ cm^{-1})$]
685 - 970	32
1020 - 1170	26
1215 - 1500	13
1570 - 1750	4
1820 - 2410	3

For all models and retrievals the same random sequence was used (other cases will be mentioned specially).

The retrievals of atmospheric parameters were performed in the iteration process in order to eliminate the errors stipulated by the linearization of the radiative transfer equation. Mean profiles of pressure, temperature, ozone and water vapor were chosen as initial guesses for the retrievals. After every iteration step the following characteristics of convergence of the iterative process were considered:

- FIS: fitting index for spectra;
- SSA: shift of solution (absolute);
- SSR: shift of solution (relative).

Fitting index for spectra was calculated as follows:

$$FIS = \sqrt{\frac{\sum_{m,k}\left(\frac{I_{m,k} - J_{m,k}}{\varepsilon_m}\right)^2}{N}} \tag{5.2}$$

where $I_{m,k}$ is simulated limb radiance value containing random noise for the wavenumber m and tangent altitude k (all tangent altitudes are taken into account), $J_{m,k}$ is the limb radiance value calculated for the retrieved profiles of atmospheric parameters, ε_m is the NESR value for the wavenumber m, N is total number of processed limb radiance values. The physical meaning of the fitting index is the spectral residual expressed in relative units and estimated over all wavenumbers and tangent altitudes.

Absolute and relative shift of solution were calculated using the formulae:

$$SSA = \max_i\left(x_j(z_i) - x_{j-1}(z_i)\right) \tag{5.3}$$

$$SSR = \max_i\left(\frac{x_j(z_i) - x_{j-1}(z_i)}{x_{j-1}(z_i)}\right)\cdot 100\% \tag{5.4}$$

where z is the altitude level, j is the iteration number, and x is the atmospheric parameter value retrieved at the corresponding iteration step. The shift of solution is estimated in the whole altitude range 8-80 km for both methods.

The FIS value characterizes the quality of fitting spectra in the process of solving the inverse problem. Obviously, FIS value should be about 1 in the case when spectra are fitted well (accounting for the presence of noise). However the iteration procedure should be continued until the stabilization of the solution is reached - in this case the errors caused by the nonlinearity of the problem will be minimized. In the numerical experiments we stopped iterations using the criterion based on the SSR value estimation: the procedure was terminated when the condition SSR < 0.1% was satisfied for all retrieved parameters. (For temperature this criterion corresponds to the absolute shift of solution about 0.3 K.) The values of the shift of solution for the termination of the iterative process were chosen on the basis of physical considerations and were to a certain extent arbitrary. The additional investigations seem to be necessary of the problem of optimal selection of these values in order to increase the retrieval accuracy and to speed up the retrieval procedure. Two points should be noticed:

- In the process of p-T retrieval the values of CO_2 number density were controlled and corrected on the basis of the retrieved pressure and temperature assuming constant CO_2 volume mixing ratio. In this case shift of solution for the CO_2 number density was also taken into account (termination criterion 0.1% of RSS) and considered during convergence check.
- In the numerical experiments the limit was set to the total number of iteration steps: 10. That was done in order to avoid the possible situation when the iteration process diverges and therefore can not be controlled.

In the numerical experiments performed with the GF method the temperature, ozone, and water vapor profiles were set equal to the mean values higher than 65 km. That was done in order to avoid underdetermination of the system of equations which is solved, since there were

no simulated measurements higher than 65 km. The altitude range of the pressure profile was 8-80 km (not limited) in order to avoid direct contradiction between the hydrostatic approximation for the retrieved profile and the mean profile (mean pressure and temperature profiles do not satisfy the hydrostatic approximation).

Due to the fact that test retrievals in the iterative process are very computer-time consuming, the numerical experiments were not performed for all models. Instead, 8 most representative models have been selected on the basis of the calculations of probabilities of specific profiles in the statistical ensemble. The probability density function for a multi-dimensional statistical ensemble described by the Gaussian distribution can be expressed by the following formula:

$$P_d(\mathbf{x}) = \frac{1}{(2\pi)^{m/2}|D|^{1/2}} \cdot \exp\left[-\frac{1}{2}\left(\mathbf{x}, D^{-1}\mathbf{x}\right)\right] \tag{5.5}$$

where **x** is the m-dimensional vector which identifies a point in a multi-dimensional space, D is the covariance matrix, $(\mathbf{x},D^{-1}\mathbf{x})$ denotes the scalar product. One can calculate the value of the probability density function for specific pressure profile, for example, if **x** is taken equal to the deviation of this profile from the mean profile and D is the pressure covariance matrix. In the same way it is possible to treat profiles of other parameters.

In the present study we have calculated the probability density for each of 46 profiles of pressure, temperature, water vapor and ozone in the ensemble by the formula:

$$P_d(\mathbf{x}) = \exp\left[-\frac{1}{2}\left(\mathbf{x}, D^{-1}\mathbf{x}\right)\right] \tag{5.6}$$

which is the probability density normalized by the value for **x**=0.

The results are summarized in the Appendix 2. For the test retrievals 8 models were selected using the following criterion: the probability density function values should represent the total range of the values for pressure and temperature profiles. The background of such selection was the assumption that the problem of p-T retrieval was the basic problem since it must be solved before the retrieval of gas profiles. The probability density values for the profiles belonging to selected 8 models are given in the Table 5.2. One can see that $P_d(\mathbf{x})$ values for pressure, temperature water vapor and ozone cover the ranges correspondingly 10^{-2}-10^{-8}, 10^{-2}-10^{-9}, 10^{-3}-10^{-8}, 10^{-2}-10^{-8}. Thus, test retrievals for only 8 models can be used for estimations of the high probability atmospheric situations and "exotic" ones as well.

Table 5.2 Probability density function values for the profiles belonging to models selected for test retrievals.

Model	Pressure	Temperature	Water vapor	Ozone
M33	$0.74\cdot10^{-2}$	$0.16\cdot10^{-2}$	$0.53\cdot10^{-3}$	$0.18\cdot10^{-5}$
M9	$0.58\cdot10^{-3}$	$0.28\cdot10^{-3}$	$0.17\cdot10^{-4}$	$0.32\cdot10^{-2}$
M39	$0.76\cdot10^{-4}$	$0.82\cdot10^{-4}$	$0.63\cdot10^{-4}$	$0.45\cdot10^{-5}$
M26	$0.72\cdot10^{-5}$	$0.24\cdot10^{-5}$	$0.49\cdot10^{-5}$	$0.15\cdot10^{-3}$
M44	$0.60\cdot10^{-6}$	$0.30\cdot10^{-6}$	$0.69\cdot10^{-8}$	$0.15\cdot10^{-8}$
M31	$0.19\cdot10^{-6}$	$0.67\cdot10^{-7}$	$0.18\cdot10^{-4}$	$0.10\cdot10^{-6}$
M46	$0.15\cdot10^{-6}$	$0.74\cdot10^{-8}$	$0.72\cdot10^{-5}$	$0.10\cdot10^{-8}$
M36	$0.48\cdot10^{-8}$	$0.47\cdot10^{-9}$	$0.11\cdot10^{-4}$	$0.30\cdot10^{-7}$

Following the approach to the processing of the MIPAS data developed in IMK [*Clarmann et al.*, 1994] the numerical experiments were performed for the so-called separate retrieval problems (tasks) with reduced number of parameters: p-T (pressure-temperature) retrieval, ozone retrieval and water vapor retrieval. The most attention was paid to the p-T retrieval problem since the results of pressure and temperature determination are necessary input for other problems.

It should be mentioned, however, that we did not follow the retrieval scheme which completely utilizes the advantages of the microwindow concept., i.e. contrary to the basic approach of the MIPAS study team [Echle et al. 1995], we did not determine the non-selective "continuum" contribution in the numerical experiments. That was done because in the present study the aerosol extinction was assumed to be known, and the continuum absorption by water vapor was modeled by an approximating formula and was retrieved implicitly by determination of the water vapor profile. So only the contribution of the lines of the interfering species located outside the microwindows remained the only one component of the "wavenumber - independent" background. Since the main objective of the study was to compare the GF and the OE methods, but not to estimate the retrieval accuracy for real measurements (which obviously will depend on a large number of different factors), including the "continuum fitting" was not necessary. However, when analyzing the results obtained in the course of the present study one should keep in mind that the retrieval errors in the numerical experiments (but not the error estimations based on the error matrix calculations) contain the component stipulated by the interference from the uncertainties of the parameters which are not explicitly determined during the specific numerical experiment.

The logic of the numerical experiments was as follows:

Pressure-temperature retrieval.

Limb radiance measurements are simulated on the basis of pressure, temperature, water vapor and ozone profiles belonging to the model under test. In the process of solving the inverse problem, ozone and water vapor profiles remain unknown and are set equal to the mean profiles.

While solving the p-T retrieval problem the hydrostatic approximation was used as the additional *a priori* link between the parameters. The hydrostatic approximation for 2 neighboring altitude levels z_1 and z_2 with pressure and temperature values correspondingly p_1, T_1 and, p_2,T_2 can be written as follows:

$$p_2 = p_1 \exp\left[-\int_{z_1}^{z_2} \frac{\mu(z) g(z)}{RT(z)} dz\right] \tag{5.7}$$

where μ is air molecular mass, g is the acceleration due to gravity, R is the universal gas constant.

Assuming that at the consecutive iterative steps the deviations of pressure and temperature from the mean values p^m and T^m are δp^i, δT^i and δp^{i+1}, δT^{i+1}, we can write the linearized form of the equation (5.7). If the trapezium formula is used for integration than the final expression will be:

$$\begin{aligned} &\frac{\delta p_1^{i+1}}{p_1^m} C_1^i - \frac{\delta p_2^{i+1}}{p_2^m} C_2^i + \frac{\delta T_1^{i+1}}{T_1^m} C_3^i + \frac{\delta T_2^{i+1}}{T_2^m} C_4^i = \\ &= 1 - B_i + \frac{\delta p_1^i}{p_1^m} C_1^i - \frac{\delta p_2^i}{p_2^m} C_2^i + \frac{\delta T_1^i}{T_1^m} C_3^i + \frac{\delta T_2^i}{T_2^m} C_4^i \end{aligned} \tag{5.8}$$

where

$$B_i = \frac{p_1^i}{p_2^i} \exp\left[-\frac{\Delta Z}{2}\left(\frac{\mu_1 g_1}{RT_1^i} + \frac{\mu_2 g_2}{RT_2^i}\right)\right]$$

$$C_1^i = \frac{p_1^m}{p_1^i} B_i$$

$$C_2^i = -\frac{p_2^m}{p_2^i}$$

$$C_3^i = \frac{T_1^m}{T_1^i} B_i \frac{\Delta Z}{2} \frac{\mu_1 g_1}{R T_1^i}$$

$$C_4^i = \frac{T_2^m}{T_2^i} B_i \frac{\Delta Z}{2} \frac{\mu_1 g_2}{R T_2^i}$$

Assuming that the pressure and temperature deviation values are combined in a joint vector **x**, the formula (5.8) can be written in the vector-matrix form:

$$\mathbf{A}\mathbf{x}^{i+1}=\mathbf{Y}^i \qquad (5.9)$$

where **Y** may be considered as the "pseudo-measurement" determining the accuracy of the hydrostatic constraint with the error described by corresponding matrix E_{hyd}. The diagonal elements of the matrix E_{hyd} can be used for assignment of the accuracy of the constraint in terms, for example, of pressure values. In the present study the accuracy was set equal to 0.1% of the pressure profile. Obviously, the described approach gives the possibility to treat adequately more common case, when the hydrostatic approximation is valid with the lower accuracy due to spatial inhomogenieties of profiles in the area of observations during single MIPAS scan.

In the numerical experiments the set of linearized equations describing the radiative transfer was complemented by the set of equations (5.9) and solved in the iterative process simultaneously. The p-T crosscovariances were set equal to zero.

Ozone retrieval.

Limb radiance measurements are simulated on the basis of pressure, temperature, water vapor and ozone profiles belonging to the model under test. In the process of solving the inverse problem, the pressure and temperature profiles are set equal to profiles obtained from the results of solving the p-T task for the model under test. Water vapor profile remains unknown and is set equal to the mean profile.

Water vapor retrieval.

Limb radiance measurements are simulated on the basis of pressure, temperature, water vapor and ozone profiles belonging to the model under test. In the process of solving the inverse problem, the pressure and temperature profiles are assumed to be known exactly and are set equal to profiles obtained from the results of solving the p-T task for the model under test. Ozone profile remains unknown and is set equal to the mean profile.

In order to improve the convergence of the iterative process in the tasks of ozone and water vapor retrieval the additional constraints were applied on the solution for the first 5 iterative steps. The mentioned above modification of the Marquardt approach was used (see Eqs. 2.6.2 and 2.7.2). The matrix of additional constraint **L** was taken in the diagonal form. The diagonal values corresponded to the following variability of the solution with respect to preceding iteration:

iteration:	1	2	3	4	5
variability:	10%	10%	20%	20%	50%

At the subsequent steps there was no additional constraint applied. It should be stressed that the choice of the values of the matrix **L** diagonal does not influence the final results (when the shift of the solution is small enough).

One should keep in mind that the above mentioned tasks may be solved iteratively (for example, p-T retrieval → ozone retrieval → p-T retrieval → ozone retrieval again) in order to suppress the effect of the interference of different parameters (in case when the "wavenumber-independent continuum" is not fitted). However the investigation of this scheme is beyond the

frame of the present study. We performed the comparison of the global fit and the optimal estimation methods only for separate problems.

6. Results of the intercomparison of the global fit and optimal estimation methods

6.1 Pressure-temperature retrieval

The results of pressure-temperature retrieval are presented in the form of figures where the relative retrieval errors for pressure [%] and absolute retrieval errors for temperature [K] are plotted for the GF and OE methods at the last iteration step. Besides, in each figure the error of the initial guess is plotted also, i.e. the deviation of the mean profile from the model profile. In fact, the deviation of the initial guess from the true profile is equal to the variation of the profile taken with the opposite sign, since the variation of the profile is determined in the study as the difference between the model profile and the mean profile. The retrieval errors are displayed in the altitude range 8-65 km which corresponds to the limb scanning range. Besides figures, for each test case the characteristics of the iterative process are presented in the corresponding tables: FIS - fitting index for spectra and SSR(A) - shift of solution relative (absolute). The tables also contain the root mean square retrieval errors of the atmospheric parameters calculated for the altitude range 8 - 65 km at every iteration step.

First, we consider different test cases separately.

Model M33. P_d(pressure)=0.74·10^{-2}, P_d(temperature)=0.16·10^{-2}.

Figures 6.1 and 6.2 show the errors of the pressure and temperature profile retrievals for the model M33 which is characterized by the maximal values of normalized probability functions for pressure and temperature. The results of the pressure profile retrieval are very good: the errors for pressure are less than 0.5% in the total altitude range. Only at the height of 65 km the GF method gave the error for pressure value about 1%. The temperature profile was retrieved with the errors less than 1 K up to 60 km. The errors increase only for the levels 62 and 65 km, where they are about 1 K for the OE method and reach 5 K for the GF method. The Table 6.1 presents the characteristics of the convergence of the iterative process for the case of processing model M33. The GF method converged at the 10th iteration step and the OE method converged at the 8th step. It should be stressed that the convergence with respect to the shifts of the pressure and temperature profiles occurred at the 8th step for the GF method and at the 7th step for the OE method. However, extra iterations were necessary in order that the stabilization of the CO_2 number density profile was reached. The fitting index for spectra (FIS) at the last step was 0.97 for both methods. It should be noted that very often the FIS criterion is used for the termination of iterative process. One can see from the table 6.1 that this criterion is satisfied already after the first iteration step. However the retrieval errors for this solution are noticeably higher than the errors at the steps where the SSR and SSA are satisfied. Similar situation takes place in the other test retrievals. In the case of the GF method the minimal rms retrieval error for pressure is observed at the 3rd step (0.33%), and for temperature - at the 7th step (1.18 K). In the case of the OE method the minimal rms error for pressure constitutes 0.24% (3rd step) and for temperature - 0.45 K (4th step). However the values of rms error practically do not change at the subsequent steps for both methods. The reason for the fact that the absolute minimum of rms error is observed not at the last iteration step will be discussed below.

Model M9. P_d(pressure)=0.58·10^{-3}, P_d(temperature)=0.28·10^{-3}.

Figures 6.3 and 6.4 display the results of the numerical experiments for the model M9. The retrievals of pressure for this test case are nearly as good as for the model M33. The retrieval errors for the pressure profile do not exceed 1% for both methods in the whole altitude range. The maximal errors for pressure are observed near 8 km and 65 km where they however do not exceed 1%. The results of the pressure profile retrieval are identical for both methods up to the height of 50 km. Higher than 50 km the OE method produced slightly better accuracy. The retrievals of the temperature profile are as good as they were for the model M33 except the

level 11 km. At the height of 11 km both methods produced errors about 2 K. In the range 14-65 km the errors of the temperature profile retrieval are less than 1 K (except the error value of 2 K for the GF method at the height of 65 km). The characteristics of the convergence of the iterative process for the model M9 are given in the Table 6.2. The GF method converged at the 10th step and the OE method converged at the 7th step. However the FIS values for both methods are noticeably larger than unity (1.15). In the case of the GF method the minimal rms retrieval error for pressure is observed at the 5th step (0.43%), and for temperature - at the 4th step (0.6 K). In the case of the OE method the minimal rms error for pressure is observed at the 4th step (0.35%) and for temperature at the 4th step also (0.39 K). The rms errors at the last step differ slightly from the minimal values.

Model M39. P_d(pressure)=$0.76 \cdot 10^{-4}$, P_d(temperature)=$0.82 \cdot 10^{-4}$.

Figures 6.5 and 6.6 present the results obtained for the model M39. The retrievals of the pressure profile by both methods are practically identical. The errors for pressure are less than 1% in the whole altitude range except the altitude of 8 km, where they are about 1.1%. The results of the retrieval of the temperature profile are different in the altitude regions 8-23 km, 23-55 km, and 55-65 km. The best results are observed in the region 23-55 km, where the errors are less than 0.3 K. In the region 55-65 km the errors increase up to 1.1-1.6 K. The worst retrievals are in the lower layers where the errors reach 2 K and are oscillating. Both methods produced nearly identical results for the p-T retrieval for the considered model. The convergence of the iterative process was quite fast for both methods (see Table 6.3). The GF method converged at the 8th step and the OE method converged at the 6th step. The FIS values are identical for both methods and equal to 1.04. In the case of the GF method the minimal rms retrieval error for pressure is observed at the 2nd step (0.28%), and for temperature - at the 4th step (0.88 K). In the case of the OE method the minimal rms error for pressure is observed at the 2nd step (0.29%) and for temperature at the 4th step (0.76 K). The rms errors for pressure at the last step differ from the minimal values by about 0.12-0.15%. For temperature, the differences are negligibly small: 0.03-0.05 K.

Model M26. P_d(pressure)=$0.72 \cdot 10^{-5}$, P_d(temperature)=$0.24 \cdot 10^{-5}$.

Figures 6.7 and 6.8 present the errors of the pressure and temperature profile retrievals performed by the GF and the OE methods for the model M26. Fig. 6.7 shows that the retrieval errors for pressure are less than 1% in the whole altitude range considered for both methods. The profiles retrieved by both methods practically coincide at all heights except the vicinities of 20 km and 60 km. However the differences in these areas are quite small and do not exceed 0.2-0.3%. The largest error is observed at the height of 8 km (0.6%). The temperature profile retrievals are characterized by the errors less than 0.5 K in the altitude range 25-62 km. In this area both methods give practically the same results (the OE method gives better accuracy in the area 53-62 km). At 65 km altitude the errors increase slightly reaching the value of ~ 1 K. The largest retrieval errors show up in the altitude range 8-25 km where they reach 3 K (20 km) and 3.5 K (17 km) for the GF method and 1.5 K (20 km) and 2.5 K (17 km) for the OE method. These errors are oscillating. The characteristics of the convergence of the iterative procedure are given in the Table 6.4. The convergence of the OE method was faster than the convergence of the GF method - for the GF method 2 extra iterations were necessary in order to satisfy the convergence criteria. The OE method converged at the 7th step and the GF method converged at the 9th step. The values of the spectral fitting index are practically the same for both methods: 1.03 (GF) and 1.02 (OE). In the case of the GF method the minimal rms retrieval error for pressure is observed at the 3rd step (0.30%), and for temperature - at the 5th step (1.10 K). In the case of the OE method the minimal rms error for pressure is observed at the 2nd step (0.30%) and for temperature at the 5th step (0.80 K). The differences between the values of rms errors at the last step and at the step when the minimums are observed are quite small and constitute for pressure 0.02% and for temperature 0.05-0.09 K.

Model M44. P_d(pressure)=$0.60 \cdot 10^{-6}$, P_d(temperature)=$0.30 \cdot 10^{-6}$.

The results obtained for the model M44 are presented in Figures 6.9 and 6.10. First, it should be mentioned that the results of the pressure profile retrieval in this case are not so good as they were in the previously considered cases. The errors are worse than 1% up to the altitude

of 40 km. The maximal error is observed at the height of 14 km where it reaches 2.2%. In the altitude range 40-65 km the pressure retrieval errors are less than 1% (the error is a little bit larger in the case of the GF retrieval at the height of 65 km). The best results for the temperature profile retrieval are in the altitude range 23-65 km for the OE method and in the altitude range 23-60 km for the GF method - the errors are less than 0.3 K. Higher than 60 km the GF method errors increase up to 2.7 K. The largest errors of the temperature profile retrieval are observed in the lower layers - 8-23 km where they are as large as 2-3 K and oscillating. In the considered case the GF and the OE methods produced practically identical results up to the height of 55 km for pressure retrieval and for temperature retrieval as well. The attention should be paid to the fact of the very slow convergence of the iterative process in this case (see Table 6.5). The convergence criterion was not satisfied for both methods even at the 10th step. At this step the shift of solution for the pressure profile still was -0.66% for the GF method and -0.28% for the OE method. The correspondent values for temperature were 0.61% and 0.30%. It should be also stressed that fitting of spectra was not good also. The FIS value for the GF method was 1.28 and for the OE method it was 1.27. In the case of the GF method the minimal rms retrieval error for pressure is observed at the 4th step (1.02%), and for temperature - at the 6th step (1.19 K). In the case of the OE method the minimal rms error for pressure is observed at the 4th step (1.04%) and for temperature at the 6th step (0.86 K). The differences between the values of rms errors at the last step and at the step when the minimums are observed reach 0.4% for pressure and 0.1 K for temperature.

Model M36. P_d(pressure)=0.48·10^{-8}, P_d(temperature)=0.47·10^{-9}.

Figures 6.11 and 6.12 present the results of pressure-temperature retrievals for the model M36. As it can be seen from the Fig. 6.11 the retrieval of the pressure profile is very good. The errors are less than 0.3% for both methods. The error reaches 0.6% only at the height of 65 km for the GF method. The retrieval of the temperature profile is very good also. The errors do not exceed 0.5 K at all altitude levels except 17 km, 20 km, and 65 km. However at the levels 17 km and 20 km the errors are less than 0.8 K. The retrieval error reaches 3 K only at the height of 65 km for the GF method. The characteristics of the convergence of the iterative process are given in the Table 6.6. The iterative process converged very fast for this model: at the 5th step for the GF method and at the 4th step for the OE method. The fitting index for spectra is the same for both methods and is equal to 0.96 which is the indication of good fitting. In the case of the GF method the minimal rms retrieval error for pressure is observed at the 3rd step (0.21%), and for temperature - at the 4th step (0.68 K). In the case of the OE method the minimal rms error for pressure is observed at the 3rd step (0.16%) and for temperature at the 4th (last) step (0.24 K). After minima of the rms error were reached, the values of rms errors remained stable.

Model M31. P_d(pressure)=0.19·10^{-6}, P_d(temperature)=0.67·10^{-7}.

Figures 6.13 and 6.14 show the results obtained for the model M31. The retrieval errors are quite different in the altitude ranges 8-25 km and 25-65 km. In the region 25-65 km the retrievals for pressure and temperature are good. The errors for pressure are less than 0.5%, and the errors for temperature are less than 1 K. In the lower layers the errors considerably increase. However for the OE method the pressure profile was retrieved with errors less than 1%. But the GF method produced the pressure value at the height of 14 km with the error 1.6%. The temperature retrievals in the region 8-25 km are rather disappointing. The maximal error value for the GF method was -13 K and for the OE method it was -9 K (altitude level 17 km). At the neighboring levels 14 and 20 km the errors were about 3 K. The Table 6.7 gives the characteristics of the iterative process in this case. One can see that 10 steps were not enough for satisfying the convergence criterion. Shifts of solutions for pressure and temperature still were -0.45% and -0.89% for the GF method and -0.58% and -0.47% for the OE method. The large values of FIS (1.27 for the GF method and 1.25 for the OE method) show unsatisfactory spectral fitting. In the case of the GF method the minimal rms retrieval error for pressure is observed at the 8th step (0.33%), and for temperature - at the 4th step (2.47 K). In the case of the OE method the minimal rms error for pressure is observed at the 8th step (0.23%) and for temperature at the 4th (last) step (1.94 K). It should be noted that for the GF method the results

at the 10th step displayed rms errors for pressure by 0.19% larger than minimal value and for temperature by 0.54 K larger than minimal value. For the OE method the differences are not so significant (0.05% and 0.23 K correspondingly).

Model M46. P_d(pressure)=0.15·10^{-6}, P_d(temperature)=0.74·10^{-8}.

The last model considered was the model M46. The results for this model are displayed in Figures 6.15 and 6.16. The pressure retrieval was very good - the errors are less than 0.5% in the whole altitude range. It should be stressed that such results are to a certain extent encouraging since the deviation of the "real" pressure profile from the mean profile was very large reaching about 50% at the height of 50 km. The temperature profile retrieval was good in the altitude range 8-65 km for the OE method and in the range 20-62 km for the GF method where the errors are less than 1 K. At the height of 65 km the GF method produced the temperature retrieval error about 3 K and at the height of 17 km about 1.5 K. The iterative process converged for the GF method at the 9th step and for the OE method at the 8th step. The fitting index was 1.02 for both methods. In the case of the GF method the minimal rms retrieval error for pressure is observed at the 5th step (0.38%), and for temperature - at the 7th step (0.79 K). In the case of the OE method the minimal rms error for pressure is observed at the 2nd step (0.27%) and for temperature at the 4th step (0.38 K). There is no significant differences between the minimal values and the values at the last iteration step.

General discussion.

The overview of the test retrievals for the 8 selected atmospheric models lead to the following preliminary conclusions:

1) The results of the retrievals do not depend upon the probability of the specific profile in the statistical ensemble. This is the consequence of the fact that the inverse problem is well-determined. The set of preselected microwindows is very informative with respect to pressure and temperature and therefore there is a possibility to retrieve the "exotic" profiles with the low probability. Test cases for the models M36 and M46 prove this conclusion.
2) The retrieval errors for pressure and temperature profiles are small in the altitude range 25-60 km and are characterized by the values less than 1% and 1 K correspondingly (in some cases the errors were even smaller). This is the indication of the high information content of measurements on one side, and the indication, on the other side, of the negligibly small influence of the interfering parameters (water vapor and ozone) on the p-T retrievals in the mentioned altitude region.
3) The retrieval errors at the altitudes higher than 60 km increase. However for the OE method this increase is not significant. For the GF method the retrieval errors can be quite large: up to 3-5 K for temperature values. These results are explained by the decrease of the signal-to-noise ratio for the measurements at the upper tangent altitudes for both methods. Besides, for the GF method this is an indication of the error propagation from the upper levels (higher than 65 km) where the temperature profile was fixed to the mean profile.
4) The altitude range 8-25 km is the most problematic. There were test cases with the high accuracy retrievals (M33, M36, M46) and low accuracy retrievals as well (other cases). The low accuracy retrievals concern mainly to the temperature retrieval problem, while results of the pressure profile retrieval were satisfactory in the majority of cases (except M31 and M44). The reason for the low accuracy of the temperature and pressure retrievals is the interference from the water vapor and ozone lines outside of the target microwindows. Since the wavenumber-independent within every microwindow background continuum was neither fitted in the numerical experiments, nor accounted in a different way, the interference caused large errors for pressure and temperature in some cases.
5) The GF and the OE methods produced nearly identical results in the altitude range 25-60 km. In the ranges 8-25 km and 60-65 km the OE method showed better accuracy in some cases. The OE method demonstrated faster convergence of the iterative process. For the GF method 1-3 extra steps were necessary to satisfy the convergence criterion.
6) The analysis of the rms retrieval errors has shown that in most cases the minimal values of errors are observed not at the last iteration step (the exception is the case with the model M36). However for the most cases the differences between the rms errors at the last step and

their minimal values are insignificant. There was only one case - model M31, in which these differences were quite noticeable.

The problem of the low accuracy p-T retrievals in the lower layers should be considered in more detail. Since the retrieval errors in the altitude range higher than 25 km were quite small, the reason for large errors in the range 8-25 km is the considerable (in some cases) interference originating from the uncertainties of the water vapor and ozone profiles because of the line broadening in the lower layers. The uncertainties of the water vapor and ozone profile can influence the p-T retrieval through two mechanisms:

- the kernels of the integral equation (variational derivatives of limb radiance with respect to pressure and temperature) are calculated on the mean water vapor and ozone profiles but not real ones therefore they contain certain errors.
- the variations of the interfering profiles stipulate variations of limb radiance producing additional noise which is not accounted for in the process of solving the inverse problem;

In order to investigate the problem the model M31 was selected. For this model the largest errors for temperature were observed at 17 km altitude reaching -13 K (GF method) and -9 K (OE method). The following test retrievals were performed for both methods: the mean profiles of water vapor and ozone were substituted by the exact profiles thus simulating the solution of the joint retrieval problem with the best result for the water vapor and temperature profiles. The errors of the p-T retrieval in this test case are shown in Figures 6.17 and 6.18. The initial guesses were not plotted in order to show the peculiarities of the error behavior on a large scale. Besides the retrieval errors themselves, the error “corridors” are shown in the figures - the retrieval error estimations on the basis of error matrix calculation for the OE method. First, it should be stressed that the retrieval without the water vapor and ozone interference can be considered excellent with respect to the retrieval in the common case (see Figures 6.13 and 6.14 for comparison). The large errors in the lower layers disappeared. The retrieval errors are located almost entirely in the “corridor” estimated on the basis of error matrix calculation for the OE method. The pressure profile was retrieved by the OE method with the errors less than 0.3% in the whole altitude region. The GF method produced pressure retrieval errors less than 0.3% up to 55 km and less than 0.5% at the higher levels. The temperature profile was retrieved by the OE method with the error less than 0.5 K up to 60 km, the errors increased up to 1.3 K in the higher layers. The GF method retrieved temperature with the errors less than 0.5 K at all levels except 17 km (error -0.8 K) and 60 km (error -0.9 K). The FIS values for both the GF and OE methods appeared to be equal to 0.96. These results prove that the reason for the large errors in the lower layers was really the interference caused by the uncertainties of the water vapor and ozone profiles and indicate the necessity for either solving the problem of the multi-parameter retrieval even in case of p-T retrieval task, or performing background continuum fitting. However, the convergence of the iterative procedure even in the case of removed water vapor and ozone interference was slow. For the GF method even at the 10th step the shift of solution for pressure was -0.27% and for temperature -0.47%. For the OE method correspondent shifts were -0.24% and 0.32%. The slow convergence is the evidence of the strong dependence of the convergence speed upon the specific profiles describing the atmospheric situation and not on the water vapor and ozone interference.

The investigation of the contribution of the aforementioned mechanisms (errors in the kernels and effective noise) to the interfering effect is not a simple problem since the whole set of simulated measurements comprises very large amount of wavenumber grid points and tangent altitudes. The term “effective noise” denotes the variations of radiance caused by the uncertainties of the profiles of atmospheric parameters which are not accounted for in the retrieval process [*Pokrovsky and Timofeyev*, 1972].

In order to make the estimations of the effective noise in limb radiance measurements produced by the uncertainties of the interfering parameters, the calculations were performed of the limb radiance variations stipulated by the simultaneous variations of the water vapor and ozone profiles for the tangent altitude 17 km (where the maximal errors were observed in the common case). These calculations were done for the model M31 (bad retrieval in general case)

and for the model M36 (good retrieval in general case). The results are displayed in Figure 6.19. First, one can see from the figure that the effective noise for the model M31 was noticeably higher, especially in the vicinity of 760 cm^{-1} and 2050 cm^{-1}. However, for all wavenumbers the value of the effective noise did not exceed the NESR in the correspondent passband. On the other hand, for the model M31 in the vicinity of 760 cm^{-1} the effective noise was nearly as high as the NESR value: 0.26 (absolute) compared to 0.32 $mW/(m^2\ sr\ cm^{-1})$.

Comparison of the weighting functions for pressure and temperature calculated for the tangent height 17 km and for several wavenumber points (near 760 cm^{-1} where the maximal effective noise values are observed) showed that the maximal difference between weighting functions is about 6% if one is calculated for the mean water vapor and ozone profiles and another is calculated for the profiles of M31 model. So the errors in the kernels are unlikely to be the reason for the large retrieval errors.

The described results of the investigation of water vapor and ozone interference show on the following most probable mechanism of this interference. The main role is played by the effective noise. The values of the effective noise at each wavenumber gridpoint do not exceed the NESR value. However due to the large number of gridpoints (for example about 1000 wavenumber gridpoints for the tangent altitude 17 km) the uncorrelated random noise is suppressed as the square root of the gridpoint number. And the effective noise from the interfering species is accumulated. Therefore the effective noise plays the considerable role during the process of solving the inverse problem despite the fact that for every separate wavenumber gridpoint the effective noise value does not exceed the correspondent NESR value. It should be stressed that the fitting of the continuum which is wavenumber-independent within a microwindow would well compensate the “effective noise”.

Let us consider the problem of the rms error behavior in the iterative process. As it was mentioned above, in most cases the minimal values of errors are observed not at the last iteration step, but for the most cases the differences between the rms errors at the last step and their minimal values were insignificant. There was only one case - model M31, in which these differences were quite noticeable. We stress that model M31 was the case in which the interference effects were the most pronounced. Therefore we analyzed the behavior of the rms retrieval errors in the case when the interference effects were removed. The results are presented in the following table:

Table Model M31. σ - rms retrieval error (8-65 km). Interference effects were removed.

Step	0	1	2	3	4	5	6	7	8	9	10
	Global Fit										
σ [%] (pressure)		0.89	0.41	0.17	0.31	0.20	0.27	0.25	0.17	0.21	0.18
σ [K] (temp.)		1.03	0.96	0.55	0.82	0.53	0.44	0.49	0.40	0.50	0.33
	Optimal Estimation										
σ [%] (pressure)		0.90	0.37	0.13	0.23	0.14	0.25	0.17	0.13	0.13	0.15
σ [K] (temp.)		1.02	0.88	0.59	0.63	0.42	0.51	0.49	0.45	0.42	0.39

One can see from the Table, that both methods delivered minimal rms error for temperature at the last iteration step. The minimal errors for pressure were observed at the 3rd step for both methods, but they differ insignificantly from the values obtained at the last step. Moreover, if we take into account that we performed 2-parameter retrieval (p-T), then it is obvious that the best solution for the joint vector is delivered at the last step. Therefore one can come to the conclusion that the effects of interference can considerably influence the convergence of the solution to the best one and can make the selection of the termination criterion rather problematic.

In the conclusion we present the pressure and temperature retrieval errors for the GF and OE methods averaged over the considered 8 atmospheric models. One should keep in mind that the models were selected in such a manner that they represent situations which differ by their probability in the statistical ensemble. Therefore during averaging the errors for pressure were weighted corresponding to the probability of the pressure profiles and the errors for temperature were weighted corresponding to the probability of the temperature profiles. The estimations of the retrieval errors were done also on the basis of calculation of error matrices for pressure and temperature for 2 cases: the GF method and the OE method. It should be stressed however that the error estimations on the basis of error matrix calculations correspond to the "ideal" case when the interfering parameters are assumed to be known exactly. Therefore these error estimations give the impression on the best achievable accuracy of p-T retrieval. The results are plotted together in Figure 6.20 for pressure and in Figure 6.21 for temperature.

First, let us consider the errors obtained on the basis of error matrix calculations. One can see that there is practically no difference in the errors corresponding to the GF and OE methods in case of pressure retrieval (the difference is about 0.01%). In the considered altitude range the retrieval errors for pressure are less than 0.25%. The minimal errors are estimated to take place in the vicinity of 40 km altitude. According to the error matrix calculations the OE method is more accurate, however the profit can be considered negligibly small. The errors for temperature do not exceed 0.5 K for both methods up to 62 km altitude. The minimal errors which are about 0.1-0.2 K are estimated at the heights of 8 km and 40 km. There is the local maximum of errors at the height of 17 km for both methods. Sharp increase of errors takes place at the height of 65 km for both methods but at this altitude the errors still are less than 1 K. According to the error matrix calculations the OE method gives smaller errors, but the profit does not exceed 0.1 K and it is larger for the higher altitudes.

The analysis of the average retrieval errors obtained on the basis of the test retrievals (8 selected atmospheric models) lead to the following conclusions. First, the results for the GF and the OE methods are very similar up to the altitude of 60 km. The differences in the pressure retrieval errors are about 0.05% and in the temperature retrieval errors they are about 0.1-0.3 K. For pressure the OE method gives better accuracy in the altitude ranges 8-25 km and 55-65 km. For temperature the OE method gives better accuracy in the ranges 30-40 km and 50-56 km. The sharp increase of errors is characteristic for the GF method at the height of 65 km. In general the average retrieval errors for pressure are less than 0.5% for both methods. For temperature at the most of the altitudes the errors are less than 0.5 K (there are local maximums at 11 km, 20 km, and 65 km where the errors reach the values 0.6-1.0 K). It should be mentioned that the errors for temperature averaged over 8 selected models are in a good agreement with their estimations obtained on the basis of error matrix calculations. For pressure the agreement is not as good as it is for temperature, but still both estimations do not differ by more than 0.2-0.25%.

Summing up the results of the test pressure-temperature retrievals and the error estimations on the basis of error matrix calculations one can come to the following main conclusion: due to the high information content of limb radiance measurements in the preselected microwindows the global fit and the optimal estimation methods produce the results which do not differ significantly. This means that the contribution of the a priori information used in the optimal estimation method to the solution of the problem is negligibly small if compared to the information delivered by the limb measurements themselves. However, the a priori information plays stabilizing role in the iterative retrieval process leading therefore to more fast convergence of the iterative process and in the specific cases to smaller errors at the levels where these errors are oscillating because of the interference of the water vapor and ozone profiles.

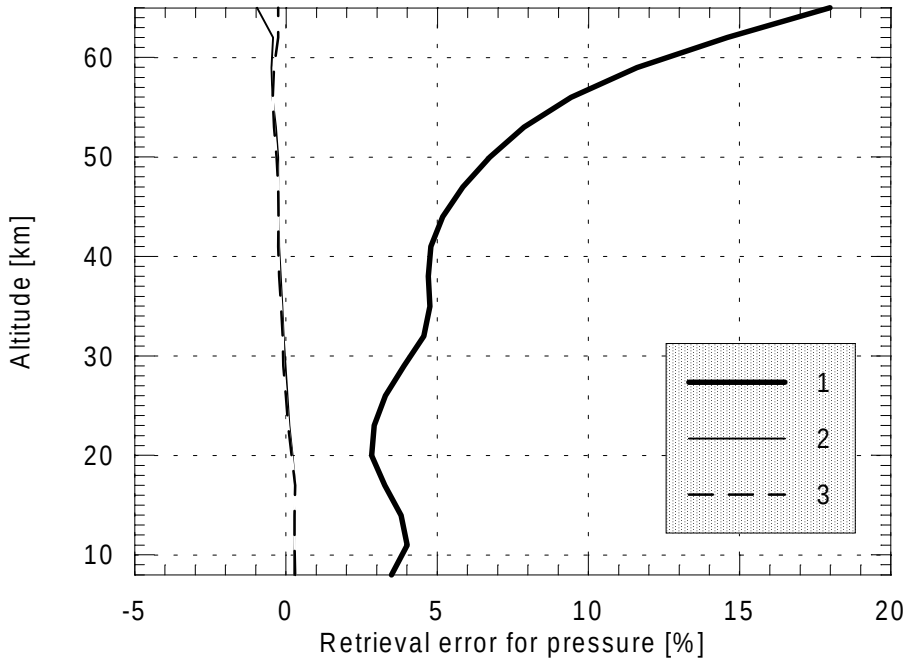

Fig. 6.1 Results of pressure retrieval. Model M33.
1 - initial guess error: deviation of the mean profile from the model profile;
2 - retrieval error in case of the GF method;
3 - retrieval error in case of the OE method.

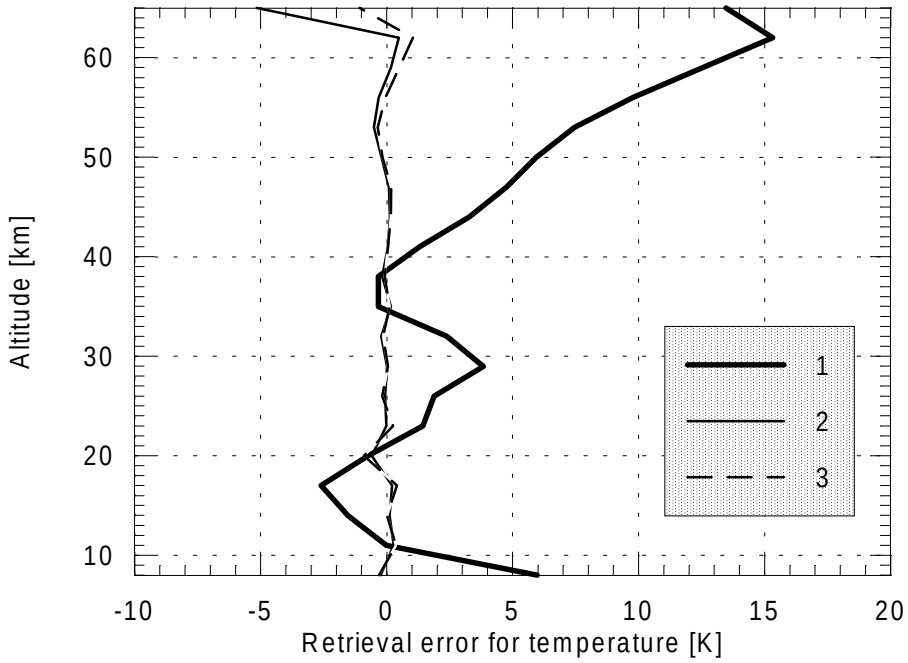

Fig. 6.2 Results of temperature retrieval. Model M33.
1 - initial guess error: deviation of the mean profile from the model profile;
2 - retrieval error in case of the GF method;
3 - retrieval error in case of the OE method.

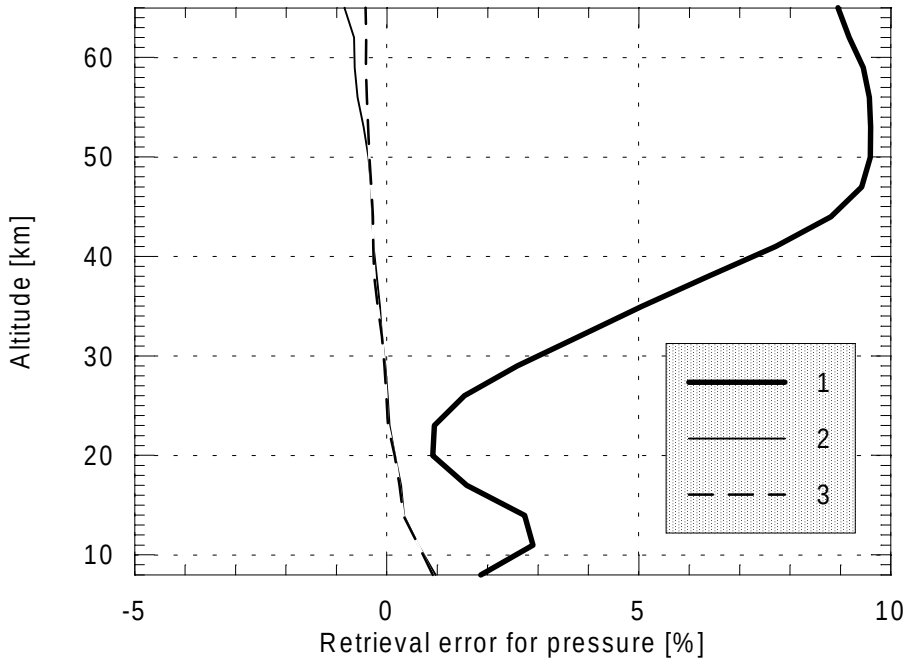

Fig. 6.3 Results of pressure retrieval. Model M09.
1 - initial guess error: deviation of the mean profile from the model profile;
2 - retrieval error in case of the GF method;
3 - retrieval error in case of the OE method.

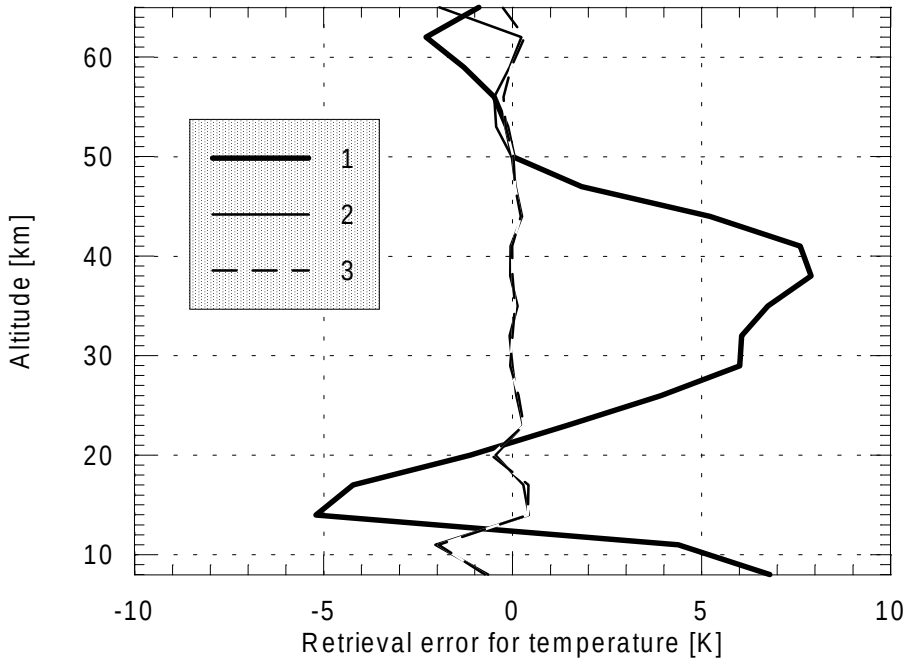

Fig. 6.4 Results of temperature retrieval. Model M09.
1 - initial guess error: deviation of the mean profile from the model profile;
2 - retrieval error in case of the GF method;
3 - retrieval error in case of the OE method.

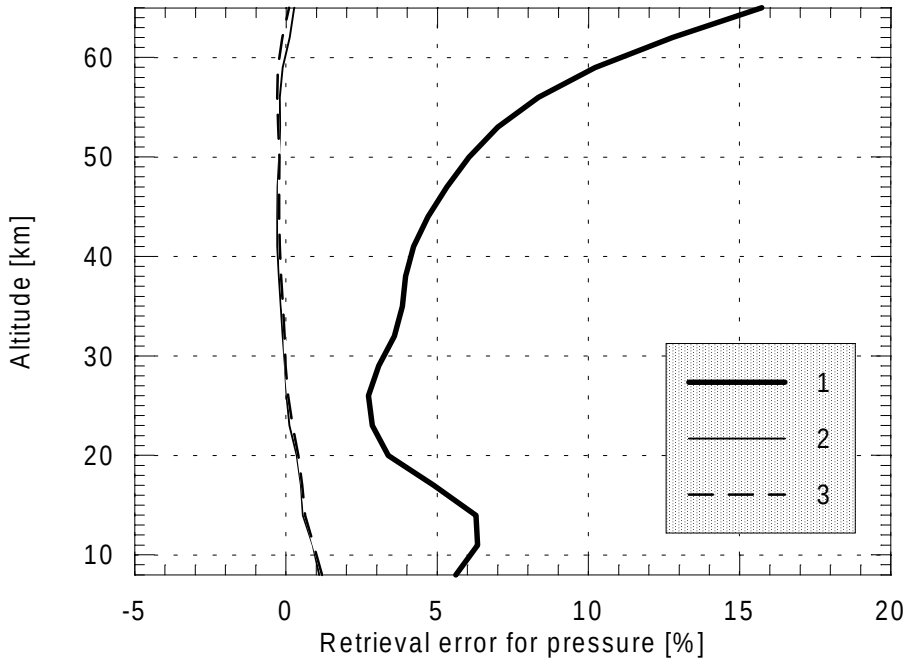

Fig. 6.5 Results of pressure retrieval. Model M39.
1 - initial guess error: deviation of the mean profile from the model profile;
2 - retrieval error in case of the GF method;
3 - retrieval error in case of the OE method.

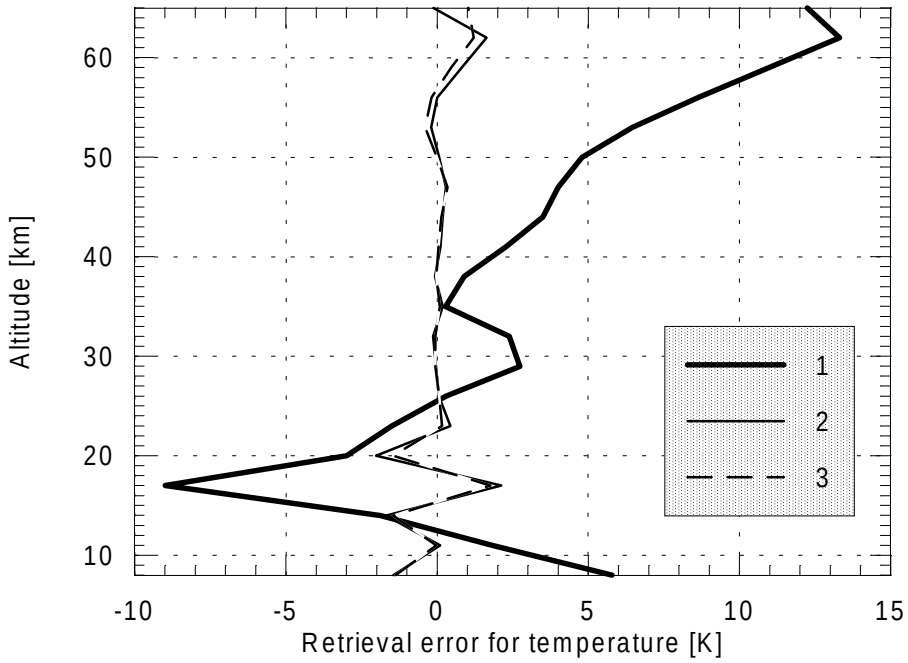

Fig. 6.6 Results of temperature retrieval. Model M39.
1 - initial guess error: deviation of the mean profile from the model profile;
2 - retrieval error in case of the GF method;
3 - retrieval error in case of the OE method.

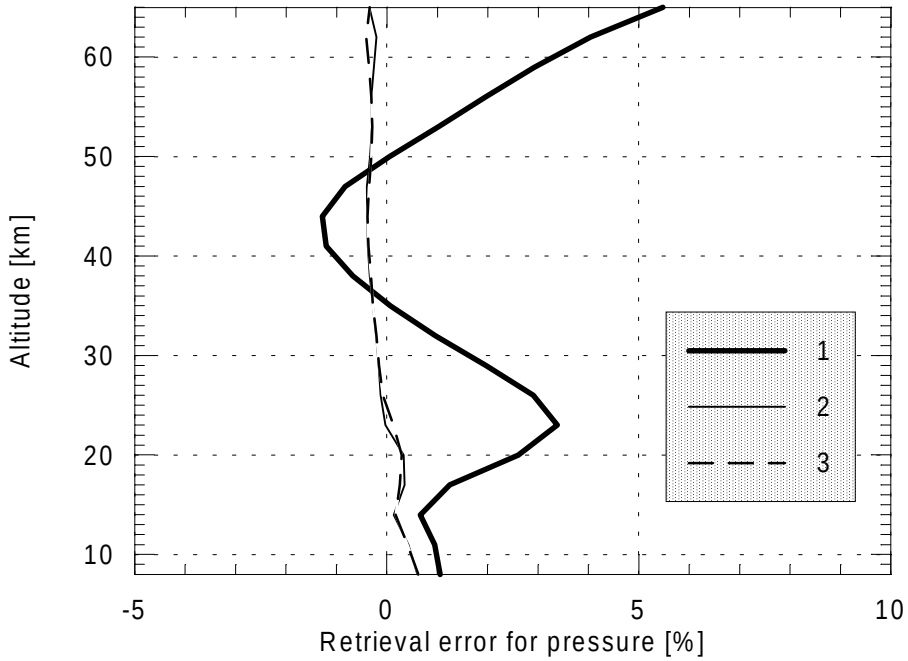

Fig. 6.7 Results of pressure retrieval. Model M26.
1 - initial guess error: deviation of the mean profile from the model profile;
2 - retrieval error in case of the GF method;
3 - retrieval error in case of the OE method.

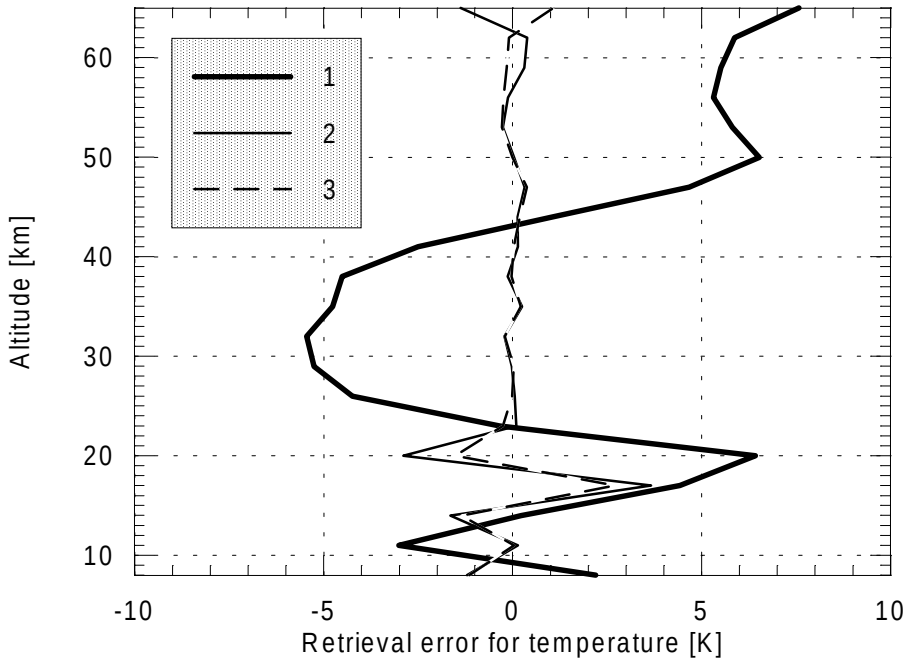

Fig. 6.8 Results of temperature retrieval. Model M26.
1 - initial guess error: deviation of the mean profile from the model profile;
2 - retrieval error in case of the GF method;
3 - retrieval error in case of the OE method.

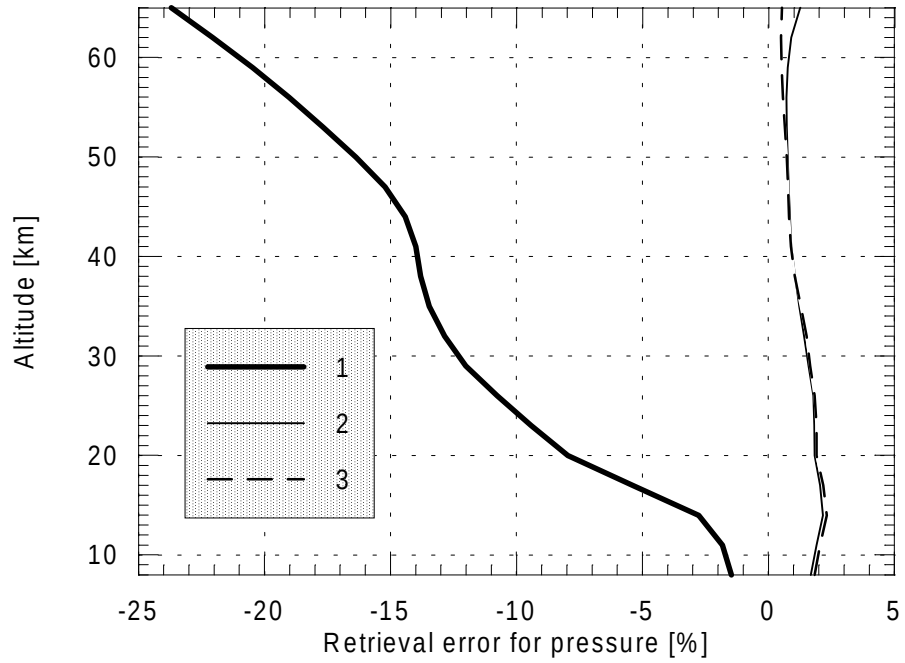

Fig. 6.9 Results of pressure retrieval. Model M44.
1 - initial guess error: deviation of the mean profile from the model profile;
2 - retrieval error in case of the GF method;
3 - retrieval error in case of the OE method.

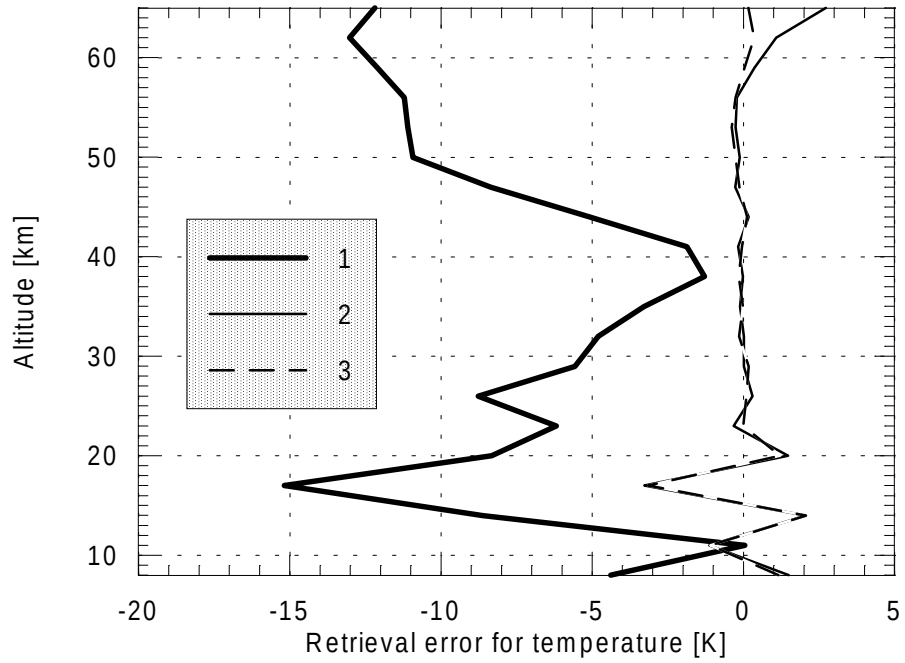

Fig. 6.10 Results of temperature retrieval. Model M44.
1 - initial guess error: deviation of the mean profile from the model profile;
2 - retrieval error in case of the GF method;
3 - retrieval error in case of the OE method.

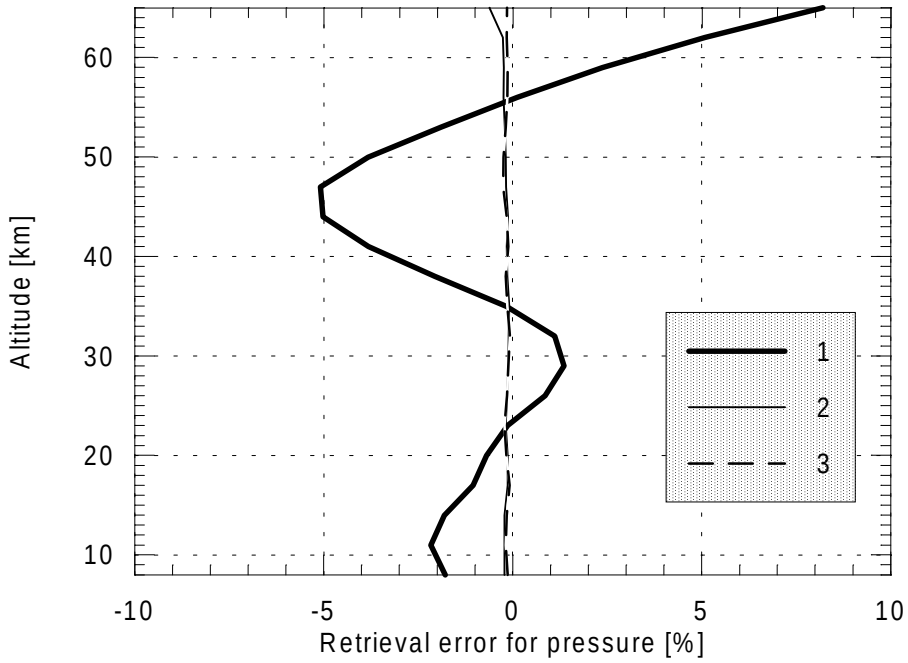

Fig. 6.11 Results of pressure retrieval. Model M36.
1 - initial guess error: deviation of the mean profile from the model profile;
2 - retrieval error in case of the GF method;
3 - retrieval error in case of the OE method.

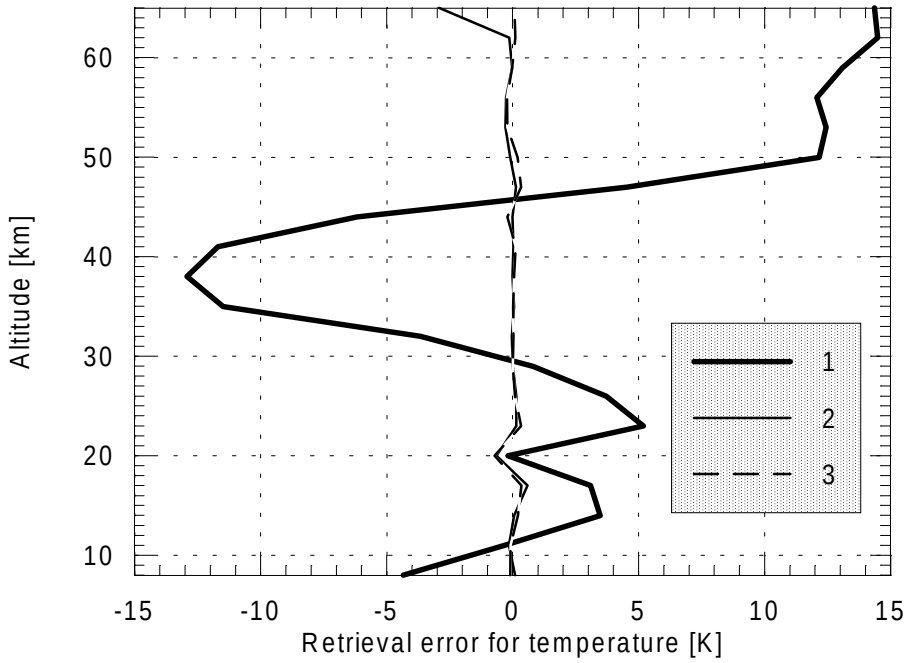

Fig. 6.12 Results of temperature retrieval. Model M36.
1 - initial guess error: deviation of the mean profile from the model profile;
2 - retrieval error in case of the GF method;
3 - retrieval error in case of the OE method.

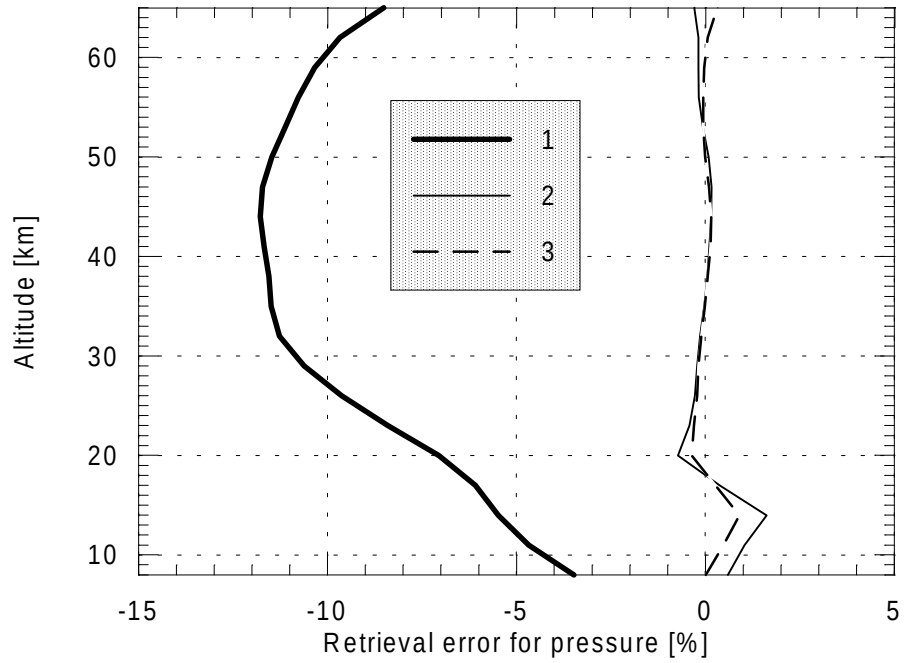

Fig. 6.13 Results of pressure retrieval. Model M31.
1 - initial guess error: deviation of the mean profile from the model profile;
2 - retrieval error in case of the GF method;
3 - retrieval error in case of the OE method.

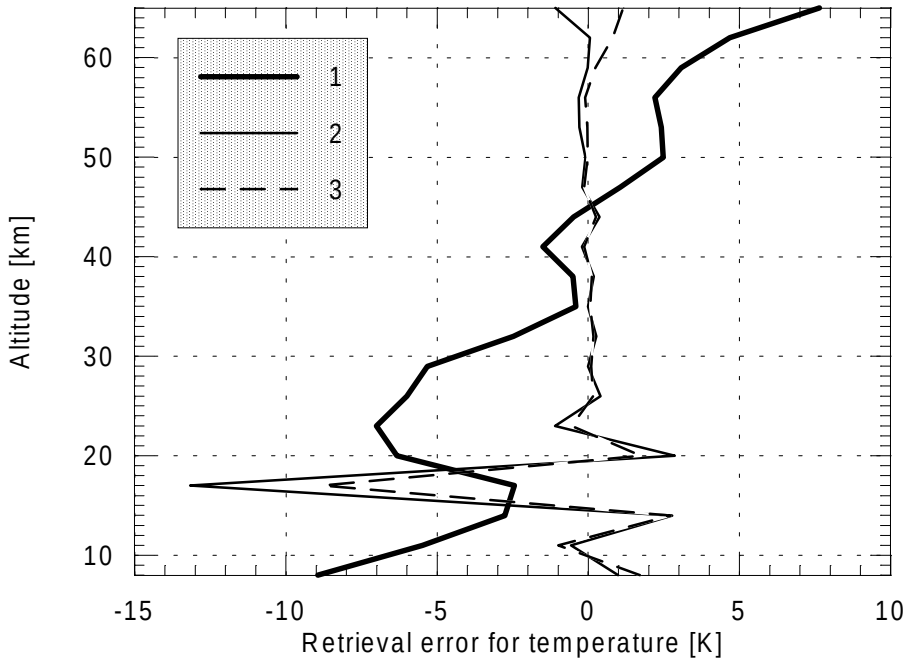

Fig. 6.14 Results of temperature retrieval. Model M31.
1 - initial guess error: deviation of the mean profile from the model profile;
2 - retrieval error in case of the GF method;
3 - retrieval error in case of the OE method.

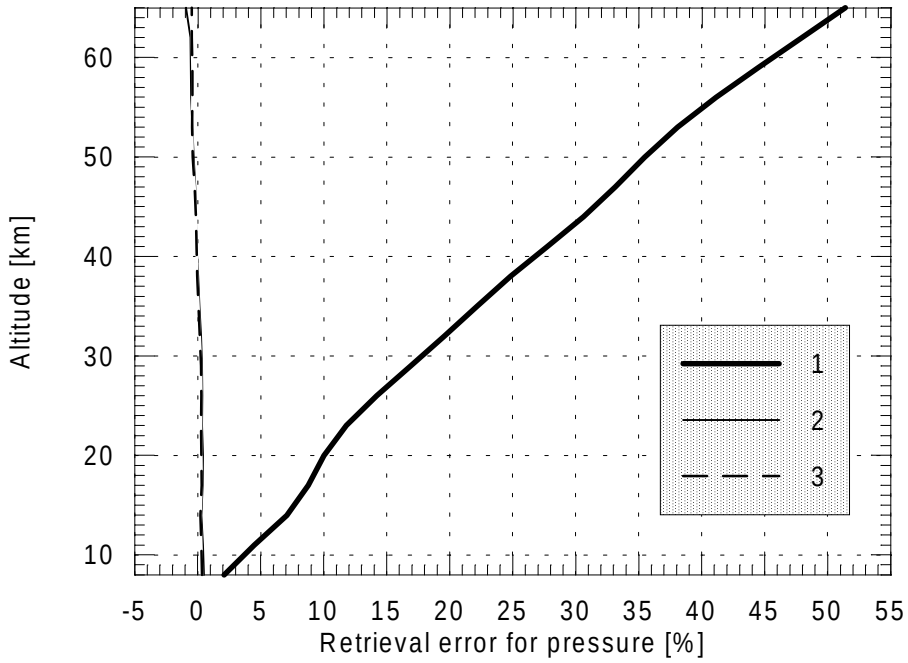

Fig. 6.15 Results of pressure retrieval. Model M46.
1 - initial guess error: deviation of the mean profile from the model profile;
2 - retrieval error in case of the GF method;
3 - retrieval error in case of the OE method.

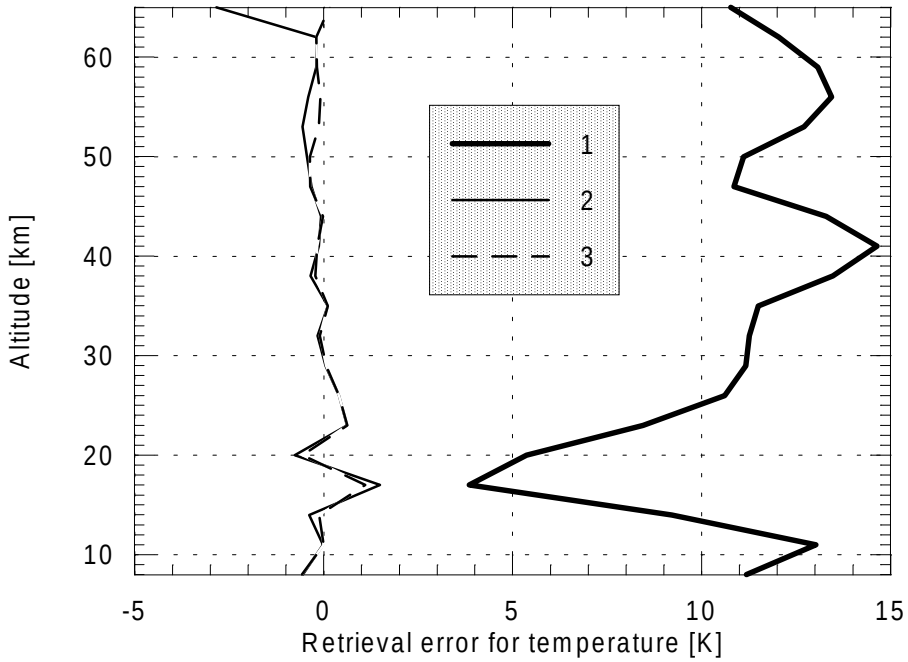

Fig. 6.16 Results of temperature retrieval. Model M46.
1 - initial guess error: deviation of the mean profile from the model profile;
2 - retrieval error in case of the GF method;
3 - retrieval error in case of the OE method.

Table 6.1 Characteristics of the convergence of the iterative process: FIS - fitting index for spectra; SSA, SSR - shift of solution absolute and relative. Model M33. σ - rms retrieval error (8-65 km).

Step	0	1	2	3	4	5	6	7	8	9	10
	Global Fit										
FIS	2.26	1.00	0.96	0.98	0.97	0.97	0.97	0.97	0.97	0.97	0.97
SSR [%] (pressure)		-17.2	-1.52	-0.46	0.60	-0.17	-0.17	0.16	-0.02	-0.06	0.04
σ [%] (pressure)		0.80	0.34	0.33	0.38	0.35	0.33	0.35	0.34	0.34	0.34
SSA[K] (temperature)		-16.9	-3.00	2.20	-1.38	0.74	0.64	-0.32	0.22	0.20	0.08
σ [K] (temp.)		1.41	1.32	1.22	1.19	1.20	1.19	1.18	1.19	1.18	1.18
	Optimal Estimation										
FIS	2.26	1.00	0.97	0.97	0.97	0.97	0.97	0.97	0.97		
SS [%] (pressure)		-21.0	-1.60	-0.22	0.40	-0.17	-0.05	0.08	-0.03		
σ [%] (pressure)		0.82	0.25	0.24	0.30	0.27	0.26	0.27	0.26		
SSA [K] (temperature)		-12.2	4.10	1.44	-1.06	0.37	0.29	-0.22	0.09		
σ [K] (temp.)		1.23	0.56	0.48	0.45	0.46	0.45	0.45	0.45		

Table 6.2 Characteristics of the convergence of the iterative process: FIS - fitting index for spectra; SSA, SSR - shift of solution absolute and relative. Model M9. σ - rms retrieval error (8-65 km).

Step	0	1	2	3	4	5	6	7	8	9	10
	Global Fit										
FIS	3.44	1.19	1.15	1.15	1.15	1.15	1.15	1.15	1.15	1.15	1.15
SSR [%] (pressure)		-9.35	-0.92	0.71	-0.50	-0.21	0.14	0.09	-0.05	-0.03	0.02
σ [%] (pressure)		0.68	0.44	0.58	0.46	0.43	0.45	0.46	0.46	0.45	0.45
SSA [K] (temperature)		9.17	5.32	-2.96	-1.75	1.19	0.64	-0.45	-0.22	0.17	0.07
σ [K] (temp.)		1.68	1.23	0.93	0.60	0.67	0.74	0.71	0.67	0.68	0.69
	Optimal Estimation										
FIS	3.44	1.19	1.15	1.15	1.15	1.15	1.15	1.15			
SSR [%] (pressure)		-16.5	3.17	-0.60	-0.39	0.11	0.09	-0.03			
σ [%] (pressure)		0.62	0.38	0.45	0.35	0.35	0.37	0.37			
SSA [K] (temperature)		-16.7	9.03	-1.95	-1.21	0.57	0.36	-0.17			
σ [K] (temp.)		1.42	1.03	0.64	0.39	0.53	0.56	0.52			

Table 6.3 Characteristics of the convergence of the iterative process: FIS - fitting index for spectra; SSA, SSR - shift of solution absolute and relative. Model M39. σ - rms retrieval error (8-65 km).

Step	0	1	2	3	4	5	6	7	8	9	10
	Global Fit										
FIS	2.32	1.06	1.05	1.04	1.04	1.04	1.04	1.04	1.04		
SSR [%] (pressure)		-14.3	-2.41	0.72	-0.18	-0.13	0.06	0.04	-0.02		
σ [%] (pressure)		1.19	0.28	0.47	0.42	0.38	0.39	0.41	0.40		
SSA [K] (temperature)		-12.1	2.75	-1.45	0.72	-0.47	-0.25	0.16	0.08		
σ [K] (temp.)		1.56	1.23	0.95	0.88	0.95	0.96	0.94	0.93		
	Optimal Estimation										
FIS	2.32	1.06	1.05	1.04	1.04	1.04	1.04				
SSR [%] (pressure)		-15.2	-2.22	0.63	-0.23	-0.05	0.05				
σ [%] (pressure)		1.18	0.29	0.50	0.43	0.41	0.43				
SSA [K] (temperature)		10.3	3.89	-1.21	0.56	-0.26	-0.13				
σ [K] (temp.)		1.51	0.95	0.79	0.76	0.78	0.79				

Table 6.4 Characteristics of the convergence of the iterative process: FIS - fitting index for spectra; SSA, SSR - shift of solution absolute and relative. Model M26. σ - rms retrieval error (8-65 km).

Step	0	1	2	3	4	5	6	7	8	9	10
	Global Fit										
FIS	1.81	1.09	1.05	1.03	1.03	1.03	1.03	1.03	1.03	1.03	
SSR [%] (pressure)		-6.53	-1.91	0.64	0.31	-0.07	-0.17	0.04	0.07	0.02	
σ [%] (pressure)		0.71	0.32	0.30	0.35	0.34	0.30	0.31	0.32	0.32	
SSA [K] (temperature)		-9.23	3.64	-1.83	1.47	-0.76	-0.69	0.38	0.32	-0.19	
σ [K] (temp.)		1.19	1.30	1.57	1.27	1.10	1.21	1.29	1.24	1.19	
	Optimal Estimation										
FIS	1.81	1.08	1.04	1.03	1.02	1.02	1.02	1.02	1.02		
SSR [%] (pressure)		-8.00	-1.75	0.63	0.19	-0.08	-0.09	0.04	0.03		
σ [%] (pressure)		0.70	0.30	0.31	0.34	0.33	0.31	0.32	0.32		
SSA [K] (temperature)		-7.27	3.68	-1.51	0.92	0.49	-0.34	-0.19	0.13		
σ [K] (temp.)		1.13	0.89	1.03	0.86	0.80	0.85	0.87	0.85		

Table 6.5 Characteristics of the convergence of the iterative process: FIS - fitting index for spectra; SSA, SSR - shift of solution absolute and relative. Model M44. σ - rms retrieval error (8-65 km).

Step	0	1	2	3	4	5	6	7	8	9	10
	Global Fit										
FIS	5.36	1.65	1.35	1.32	1.39	1.29	1.29	1.30	1.28	1.28	1.28
SSR [%] (pressure)		36.7	2.78	-1.00	-2.18	2.40	-0.33	-1.24	1.21	-0.12	-0.66
σ [%] (pressure)		2.43	2.24	1.83	1.02	1.85	1.73	1.26	1.70	1.66	1.40
SSA [K] (temperature)		20.6	-7.05	5.38	5.78	-4.14	2.76	2.98	-1.97	1.42	1.53
σ [K] (temp.)		2.91	2.17	1.27	1.39	1.72	1.19	1.24	1.48	1.21	1.22
	Optimal Estimation										
FIS	5.36	1.63	1.35	1.30	1.35	1.29	1.28	1.29	1.28	1.27	
SSR [%] (pressure)		41.0	2.68	-1.27	-1.58	1.99	-0.52	-0.69	0.83	0.23	-0.28
σ [%] (pressure)		2.40	2.21	1.67	1.04	1.79	1.58	1.30	1.62	1.54	1.42
SSA [K] (temperature)		16.5	-7.17	4.60	4.62	-3.66	1.90	1.89	-1.49	0.77	0.76
σ [K] (temp.)		2.23	1.80	0.91	1.14	1.30	0.86	0.99	1.10	0.92	0.97

Table 6.6 Characteristics of the convergence of the iterative process: FIS - fitting index for spectra; SSA, SSR - shift of solution absolute and relative. Model M36. σ - rms retrieval error (8-65 km).

Step	0	1	2	3	4	5	6	7	8	9	10
	Global Fit										
FIS	3.49	1.11	0.96	0.96	0.96	0.96	0.96				
SSR [%] (pressure)		-8.52	-1.99	0.10	0.03	-0.07	-0.01				
σ [%] (pressure)		0.75	0.22	0.21	0.21	0.22	0.22				
SSA [K] (temperature)		-16.6	-2.11	0.41	0.21	-0.18	-0.11				
σ [K] (temp.)		1.25	0.76	0.70	0.68	0.69	0.69				
	Optimal Estimation										
FIS	3.49	1.11	0.96	0.96	0.96						
SSR [%] (pressure)		-16.0	5.99	-0.5	0.02						
σ [%] (pressure)		0.94	0.17	0.16	0.16						
SSA [K] (temperature)		-14.9	16.1	0.38	0.22						
σ [K] (temp.)		1.28	0.27	0.27	0.24						

Table 6.7 Characteristics of the convergence of the iterative process: FIS - fitting index for spectra; SSA, SSR - shift of solution absolute and relative. Model M31. σ - rms retrieval error (8-65 km).

Step	0	1	2	3	4	5	6	7	8	9	10
	Global Fit										
FIS	3.58	1.78	1.37	1.34	1.36	1.27	1.31	1.25	1.27	1.27	1.27
SSR [%] (pressure)		14.3	2.44	-1.24	-2.59	1.62	1.45	-1.83	0.25	1.32	-0.45
σ [%] (pressure)		0.85	1.08	0.79	0.63	0.36	0.88	0.44	0.33	0.62	0.52
SSA [K] (temperature)		16.6	-10.1	-5.97	6.03	4.62	-3.45	2.86	-2.57	-2.61	-1.95
σ [K] (temp.)		2.66	4.11	3.64	2.47	3.14	3.60	2.84	2.77	3.31	3.11
	Optimal Estimation										
FIS	3.58	1.70	1.32	1.30	1.32	1.26	1.27	1.25	1.25	1.25	1.25
SSR [%] (pressure)		14.3	-1.93	-0.97	-1.91	1.55	0.64	-1.33	0.38	0.67	-0.58
σ [%] (pressure)		0.91	0.90	0.54	0.48	0.34	0.57	0.28	0.23	0.45	0.28
SSA [K] (temperature)		-16.4	-7.32	-4.55	4.36	3.06	2.44	2.34	1.52	-1.46	-1.02
σ [K] (temp.)		2.25	3.04	2.53	1.94	2.42	2.47	2.05	2.21	2.37	2.17

Table 6.8 Characteristics of the convergence of the iterative process: FIS - fitting index for spectra; SSA, SSR - shift of solution absolute and relative. Model M46. σ - rms retrieval error (8-65 km).

Step	0	1	2	3	4	5	6	7	8	9	10
	Global Fit										
FIS	7.63	1.39	1.08	1.03	1.03	1.03	1.02	1.02	1.02	1.02	
SSR [%] (pressure)		-33.0	-6.67	1.18	-0.77	-0.32	0.27	0.09	0.10	-0.02	
σ [%] (pressure)		6.01	0.44	0.66	0.43	0.38	0.42	0.44	0.42	0.41	
SSA [K] (temperature)		-13.7	-5.54	-3.73	2.19	1.23	-0.71	-0.41	-0.24	0.13	
σ [K] (temp.)		2.06	1.43	0.92	0.80	0.86	0.83	0.79	0.79	0.80	
	Optimal Estimation										
FIS	7.63	1.38	1.06	1.03	1.02	1.02	1.02	1.02	1.02		
SSR [%] (pressure)		-47.0	20.5	-1.58	-0.73	-0.11	0.18	-0.03	-0.04		
σ [%] (pressure)		6.13	0.27	0.51	0.31	0.30	0.33	0.32	0.31		
SSA [K] (temperature)		-34.1	31.5	-3.40	1.50	0.73	0.38	0.22	0.13		
σ [K] (temp.)		1.96	0.93	0.58	0.38	0.41	0.40	0.38	0.38		

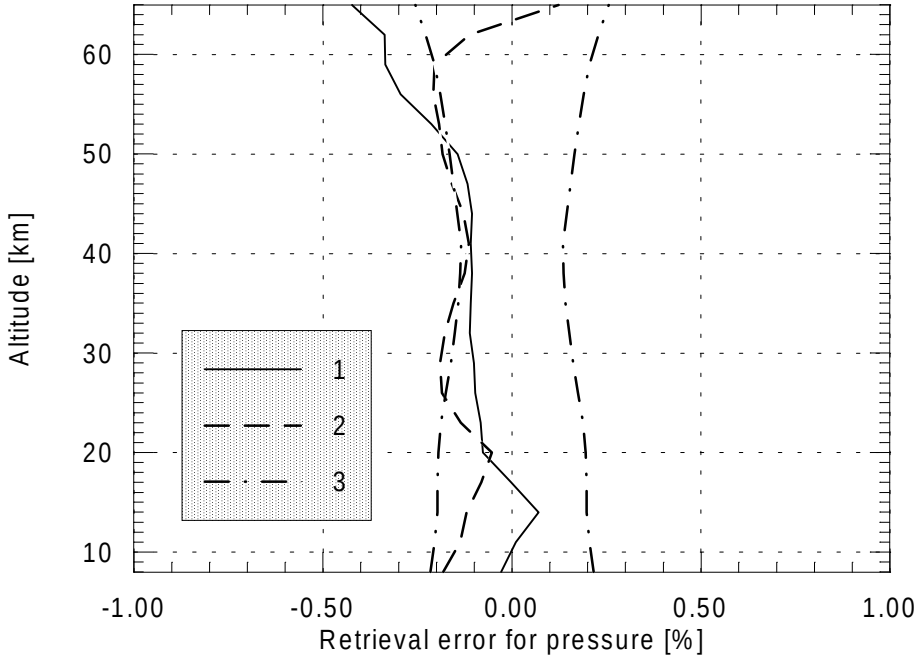

Fig. 6.17 Results of pressure retrieval. Model M31. The mean profiles of water vapor and ozone were substituted by the exact ones in order to eliminate the interference from these species.
1 - retrieval error in case of the GF method; 2 - retrieval error in case of the OE method.
3 - lines showing the "corridor" of errors estimated on the basis of the error matrix calculation.

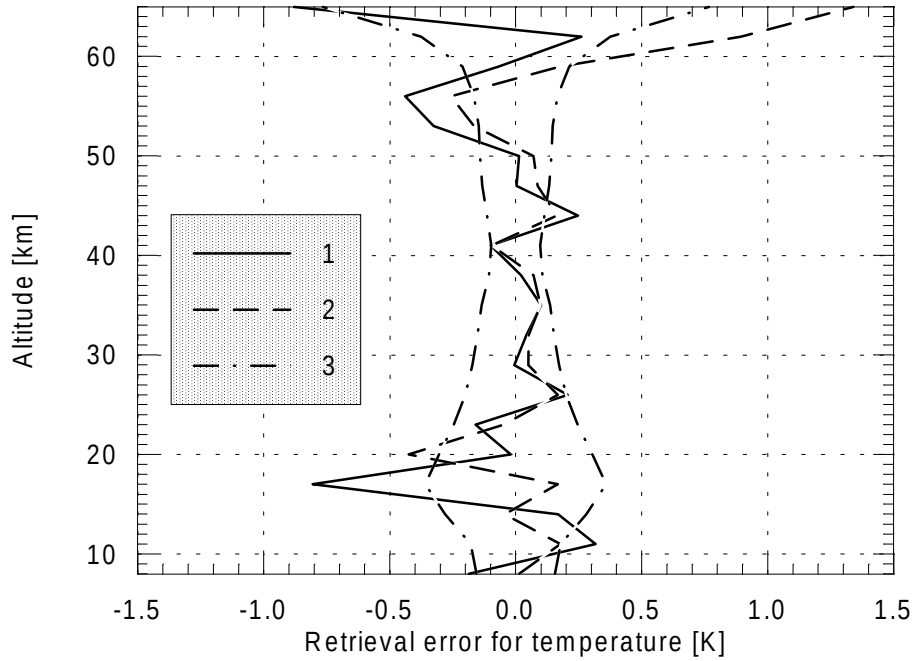

Fig. 6.18 Results of temperature retrieval. Model M31. The mean profiles of water vapor and ozone were substituted by the exact ones in order to eliminate the interference from these species. 1 - retrieval error in case of the GF method; 2 - retrieval error in case of the OE method.
3 - lines showing the "corridor" of errors estimated on the basis of the error matrix calculation.

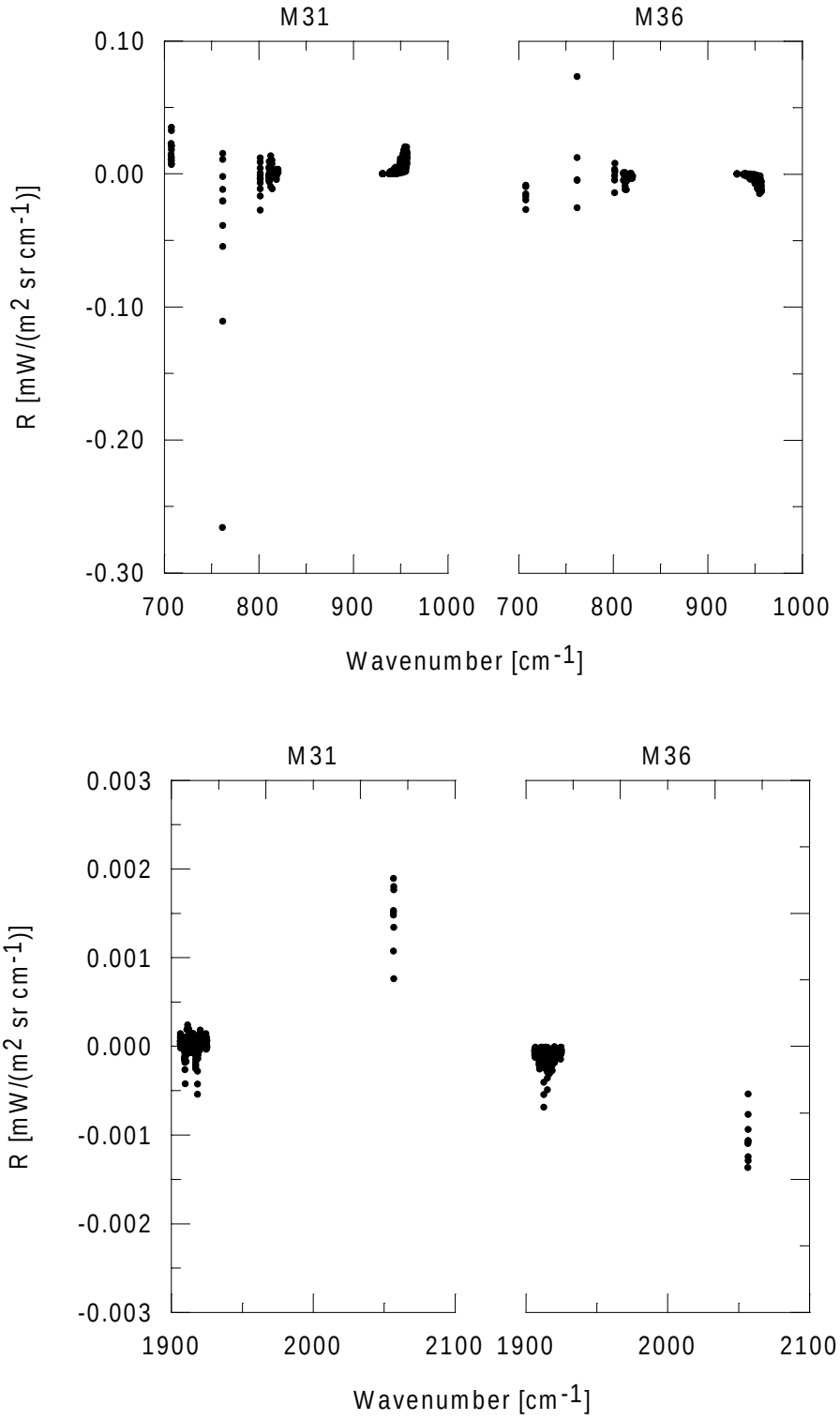

Fig. 6.19 The effective noise: variations of limb radiance stipulated by the variations of water vapor and ozone profiles. Calculations were made for the tangent altitude of 17 km for models M31 and M36 in the microwindows selected for the p-T retrieval.

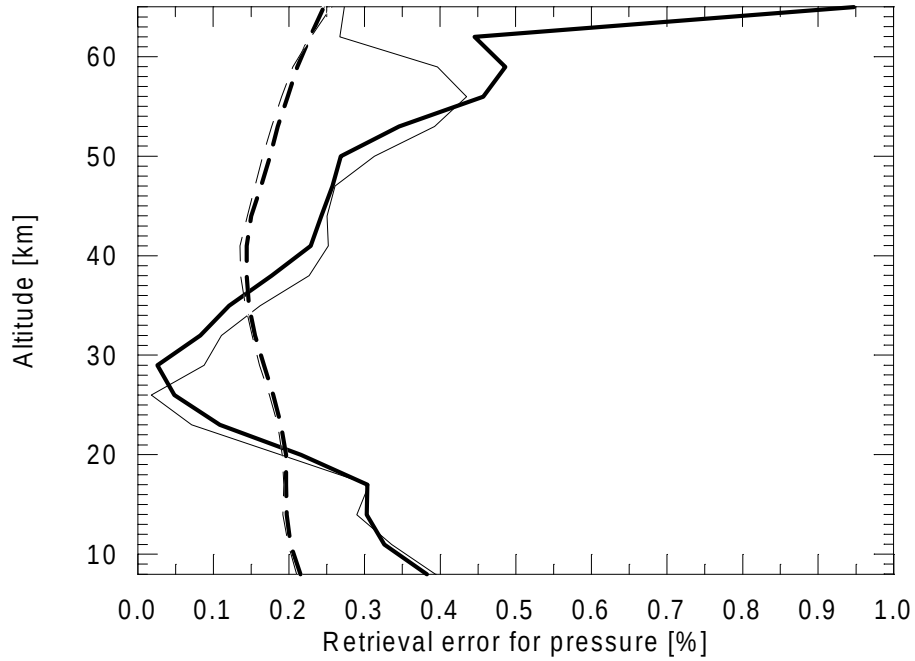

Fig. 6.20 Comparison of the retrieval errors for pressure in the case of GF method (thick lines) and OE method (thin lines). Solid lines - errors averaged with weights over 8 selected models. Long-dashed lines - errors calculated on the basis of error matrix.

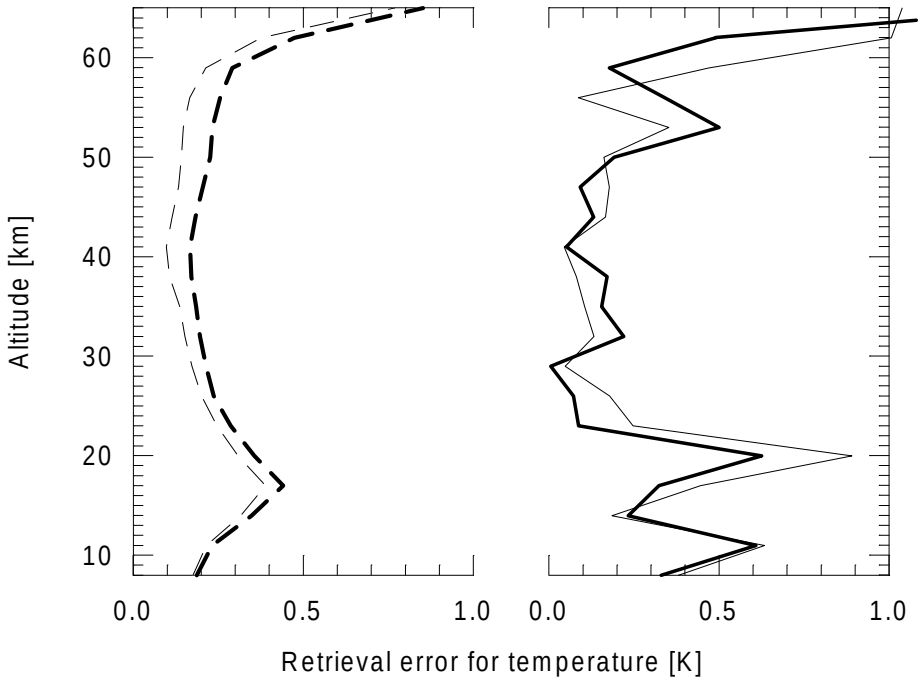

Fig. 6.21 Comparison of the retrieval errors for temperature in the case of GF method (thick lines) and OE method (thin lines). Solid lines - errors averaged with weights over 8 selected models. Long-dashed lines - errors calculated on the basis of error matrix.

6.2 The influence of random noise and initial guess on the p-T retrievals

Random noise.

The numerical experiments on the p-T retrievals which were analyzed above were performed using single random sequence modeling the MIPAS random noise. Therefore the statistical validity of the results has to be proved. In order to verify the statistical validity of the results the special additional investigations were done - the analysis of the influence of different realizations of random error sequences on the retrievals.

The influence of the random noise on the results of pressure-temperature retrievals was investigated on the basis of tests performed for the model M39. This model was selected as the typical one and is characterized by: a) high accuracy determination of pressure and temperature in the altitude range 25-55 km; b) the increase of errors in the upper and lower layers; c) convergence of the iterative process within 10 iterative steps.

Pressure-temperature retrievals were performed for the model M39 with N=6 different sequences of random noise values. The profiles of the mean retrieval error for pressure and temperature for these 6 test cases were calculated as follows:

$$\delta x(z) = \frac{1}{N}\sum_{i=1}^{N} \delta x_i(z) \tag{6.1}$$

where $\delta x_i(z)$ is the pressure (temperature) retrieval error at the altitude z corresponding to the sequence number i. The vertical profile of error scattering due to random noise was calculated using formula:

$$\delta x_{ran}(z) = \sqrt{\frac{1}{N}\sum_{i=1}^{N} (\delta x_i(z) - \delta x(z))^2} \tag{6.2}$$

The physical meaning of the error scattering is the root mean square deviation of the retrieval error from its mean value for a number of retrievals with different random noise sequences. Obviously, the comparison of the error scattering due to random noise with the full retrieval error will show the influence of the random noise on the retrieval accuracy.

Figure 6.22 presents scattering of the retrieval errors due to random noise in the pressure-temperature retrievals. Scattering was estimated for the model M39 on the basis of 6 retrievals with different random noise sequences.

First, let us consider the task of pressure retrieval. One can see from Fig. 6.22 (upper panel) that the error scattering profiles for both methods are practically identical (the difference at most of altitudes is about 0.01% and less). Only in the vicinity of 60 km the GF method is characterized by a larger error scattering reaching 0.01-0.02%, however this difference can be considered insignificant also. The error scattering profiles have the minimum in the vicinity of 25-40 km. In the lower and upper layers the error scattering values increase. If one compares figures 6.5 and 6.22 one can see that in the lower layers the error scattering due to random noise is about 10 times smaller than the pressure retrieval errors themselves (0.13% and 1.2% correspondingly at the 8 km altitude) due to the fact that the major source of errors was the interference from ozone and water vapor profiles. In the altitude range 25-65 km the pressure retrieval for the model M39 was very good and comparable with the error scattering values: 0.1% and less.

Let us consider the temperature retrieval case. The error scattering profiles for both methods are practically identical up to 60 km (the difference is about 0.02 K reaching 0.06 K only in the vicinity of 20 km altitude). In the altitude range 60-65 km the error scattering for the GF method is noticeably larger than for the OE method (the difference reaches 0.35 K at 65 km altitude). However this difference can be considered also insignificant. Up to the altitude of 60 km the error scattering is quite small and constitutes less than 0.3 K. Higher than 60 km the error scattering increase for both methods reaching 0.45 K for the OE method and 0.9 K for the GF method. The considerable increase of error scattering in the upper layers is explained by the decrease of limb radiance value for large tangent altitudes. As a consequence, the signal-to-noise ratio decreases resulting in a larger influence of random noise on the retrieval results. If

one compares figures 6.6 and 6.22 one can see that in the lower layers the error scattering due to random noise is about 6.30 times smaller than the temperature retrieval errors themselves. This is the consequence of the fact that the major error source in the lower layers is the interference from the uncertainties of the ozone and water vapor profiles. In the altitude range 25-65 km the temperature retrieval for the model M39 was very good and comparable with the error scattering values.

So the main conclusions can be formulated as follows:

a) In the lower layers the retrieval error scattering due to random noise is negligibly small relative to the errors caused by the interference from the uncertainties of the ozone and water vapor profiles. This is because the continuum which was meant to compensate for interfering species was not fitted;

b) In the layers of the high accuracy retrievals the error scattering is small and constitutes for pressure 0.05-0.1% and for temperature 0.1-0.2 K.

c) In the vicinity of 60-65 km the error scattering due to random noise increases because of the decrease of the signal-to-noise ratio and this effect is more pronounced for the GF method.

The influence of the random noise on the retrieval results was investigated only for one model M39 which was selected as the typical one. Nevertheless, the obtained conclusions can be expanded on the p-T retrieval problem as a whole because the described above test retrievals for 8 selected models revealed very high information content of measurements indicating relatively weak dependence of the results on the specific realizations of random noise sequences.

Initial guess.

It is evident from theoretical analysis of the retrieval problem that the solution must not depend on the initial guess in case when the iterative process is not diverging. For the OE method, the additional a priori information provides the uniqueness and stability of the solution. And for the GF method, the same holds true if the “implicit regularization” is correct and sufficient.

As an illustration of the fact that the solution is independent of the initial guess we present the test case with the model M31. The model M31 was selected because of the extreme errors in temperature retrieval at 17 km altitude (see Fig. 6.14). It was shown in the previous section that these extreme errors were stipulated by the strong interference from the uncertainties of the ozone and water vapor profiles. In order to prove once more this statement and analyze the influence of the initial guess on the results, the p-T retrieval was performed in which the initial guesses for pressure and temperature were exactly equal to the true profiles. The results - the solutions for temperature for the GF and the OE methods at different steps of iterative process are shown in Fig. 6.23. First, one can see that despite the fact that the initial guesses for pressure and temperature were equal to the true profiles, the retrieved profiles contained errors which were the same as in the case of another initial guess. Moreover, the convergence was as slow as it was when the initial guesses were equal to the mean profiles of atmospheric parameters. It should be stressed that the problems occurred only in the lower layers where the interference effects were significant. In the altitude range 25-65 km the retrieval accuracy was high and remained stable at all steps.

Summing up the obtained results, one can come to the following conclusions:

1) The retrieval results are independent from the initial guess for pressure and temperature because of high informativity of the MIPAS limb measurements with respect to these parameters.

2) The initial guess influences only the speed of convergence of the iterative process, however only in the case when there is no interference from the unknown atmospheric parameters.

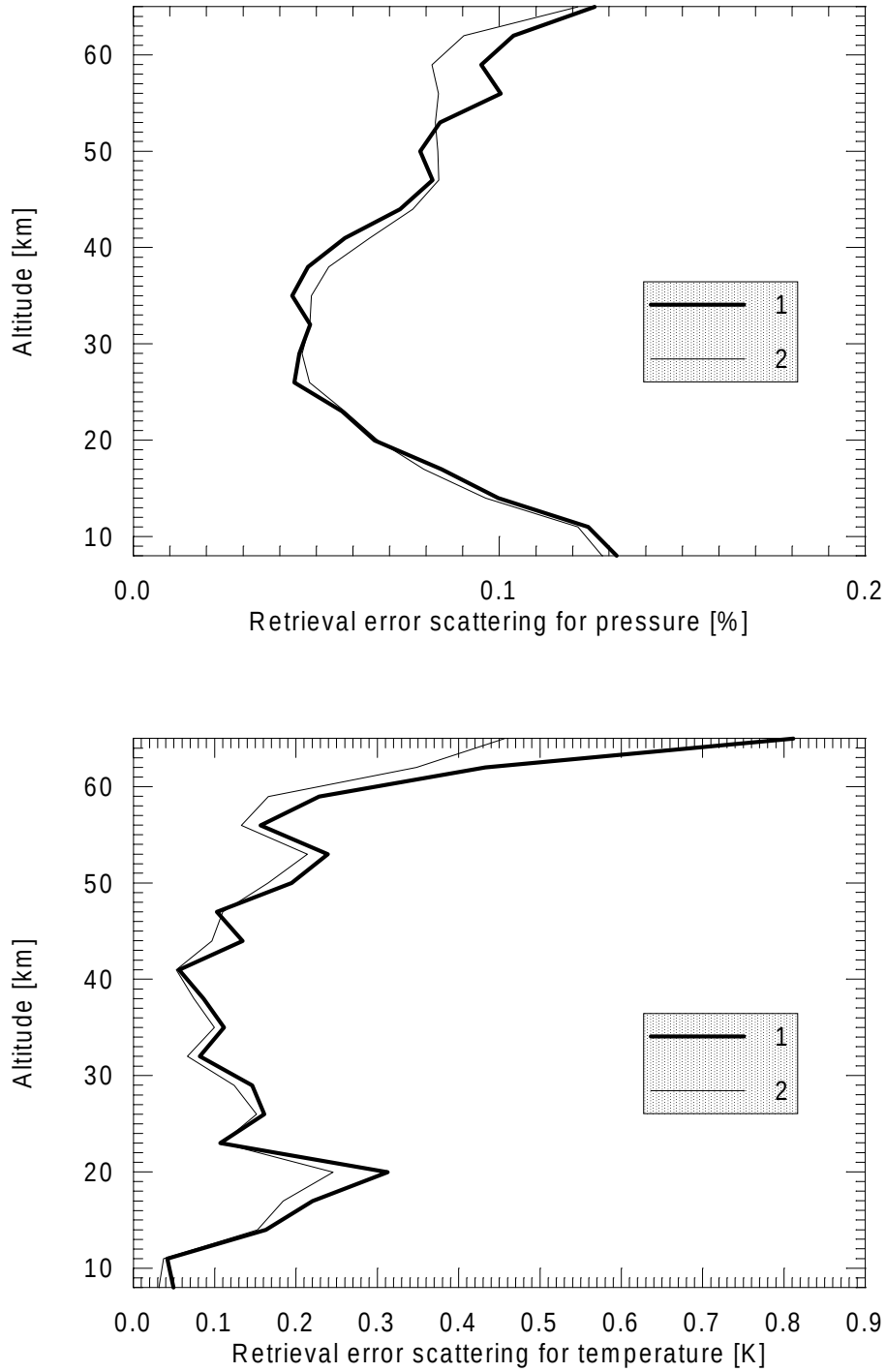

Fig. 6.22 Retrieval error scattering for the case of six different random noise realizations. Model M39. Upper panel - pressure retrieval, lower panel - temperature retrieval. 1- global fit method, 2 - optimal estimation method.

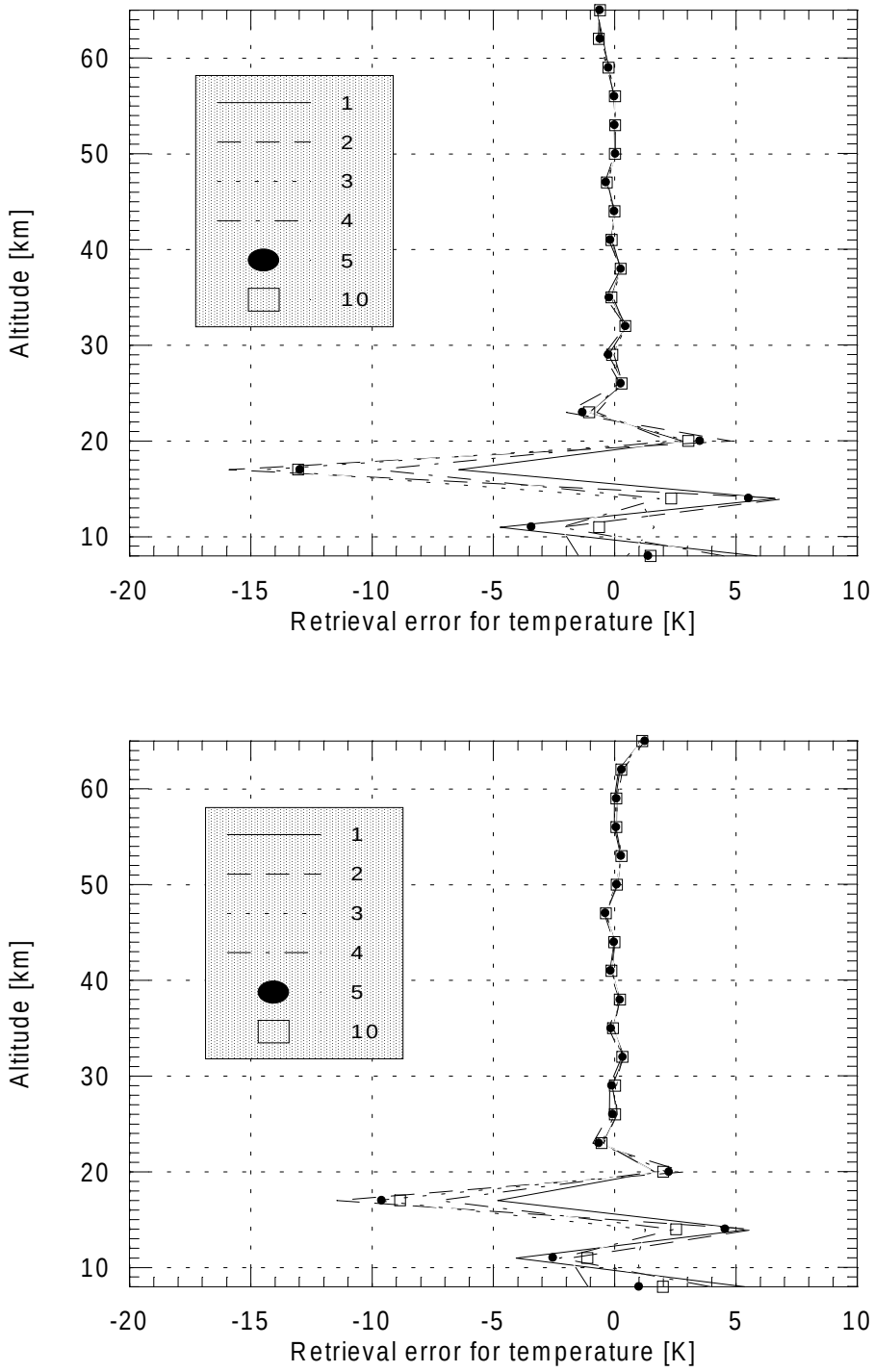

Fig. 6.23 Retrieval errors for temperature in the iterative process. Model M31. Upper panel - GF method, lower panel - OE method. Initial guess in both cases was equal to exact temperature profile. Numbers of curves correspond to the iteration numbers.

6.3 Ozone retrieval

The ozone retrieval problem appeared to be much more computer time consuming than the p-T retrieval problem due to the large number of ozone lines and broad spectral coverage of microwindows. Therefore test retrievals of ozone profiles were performed only for 6 models from the selected set of 8 models: M9, M26, M39, M33, M36, M44. However these 6 models represent the whole variety of probability density values for ozone profiles (see Table 5.2). In this sections the results of numerical experiments are presented in a way similar to one of the presentation of p-T retrieval problem results. First, we consider each model separately.

Model M9, P_d(ozone) = $0.32 \cdot 10^{-2}$.

The ozone vmr profile retrieval errors are shown in Fig. 6.24 for the GF and the OE methods. One can see that the retrieval accuracy is different in the different altitude regions. The best results can be found for the altitudes greater than 25 km. The retrieval errors for both methods are less than 5%. In the lower layers the results are not as good as for the higher layers. In the altitude range 8-25 km the retrieval errors for the GF method reach 10-17% and for the OE method they reach 10%. One can see that the OE method delivered better results in the whole altitude range: the errors are less than ones of the GF method and the profile is more smooth. The characteristics of the convergence of the iterative process are given in the Table 6.9. The iterative processes for the GF and the OE methods converged both at the 9th step. However the fitting index for spectra remained noticeably larger than unity (FIS=1.26 for both methods). The rms retrieval error calculated for the altitude range 8-65 km has the minimal value at the 1st iteration step for both methods. For the GF method it is equal to 4.43% and is about 1.4% less than the value at the last iteration step. For the OE method the minimal value is equal to 2.40% and it is about 0.8% less than the value at the last step. The reason for such behavior of the rms error will be discussed below.

Model M26, P_d(ozone) = $0.15 \cdot 10^{-3}$.

The results of the retrieval of the ozone profile for the model M26 are presented in Fig. 6.25. This model is characterized by very large variations of the ozone profile at the altitudes higher than 55 km (see Appendix 2). The deviations of the profile from the mean one are about 90%, therefore the initial guess in the upper layers is very "far" from the true profile. As a consequence, the retrieval errors are very large in the upper layers. For the GF method they exceed 50% and therefore are not shown in Fig. 6.25. The OE method delivered smaller errors which however reach 27% at 62 km altitude. Very good retrieval results are observed in the altitude range 8-55 km for the OE method: the errors are less than 5% (it should be mentioned however that there is the increase of error values in the lower layers). Very good results for the GF method are only in the range 25-55 km and in the lower layers the errors are increasing and oscillating. At the altitudes of 17 km and 20 km the errors of the GF method reach -30% and 23% correspondingly. Table 6.10 contains the FIS and SSR values for the steps of the iterative process. First, one can see that the GF method did not converge even after 10 steps. The shift of solution value still was 4.44% at the 10th step (we remind that the criterion of termination was 0.1%). Contrary, the OE method converged at the 10th step: the SSR value was 0.05%. One should notice that at the 6th step the SSR value was 15000(!). In order to avoid the confusing one should keep in mind that the SSR values are given by the relative units with respect to the solution values at the previous iteration. Therefore the large values of SSR must not be considered unrealistic because this is the case when the solution values at the previous step were relatively small with respect to the shift. The FIS values at the 10th step were about unity for both methods despite the fact that the GF method did not converge. The minimal value of the rms retrieval error is observed at the 3rd step and is equal to 147%. Such large value is a consequence of the large errors in the upper layers, where the deviation of the true profile from the mean profile is very large. For the OE method, the minimal rms error is observed at the 9th step and is equal to 6.67%. It should be stressed that at the last step the error has the same value 6.67%.

Model M39, P_d(ozone) = $0.45 \cdot 10^{-5}$.

The ozone retrieval errors for this model are presented in Fig. 6.26. One can see that the OE method delivered better results in the whole altitude range except the subrange 30-50 km where the errors of both methods were practically similar. At the lower levels (up to 25 km) the increase of errors is observed for both methods. But for the GF method the errors reach 12-23% while for the OE method the errors still are less than 10%. There is the increase of errors higher than 50 km, but for the OE method the errors still do not exceed 5% and the errors of the GF method reach 45% at the altitude of 65 km. The characteristics of the convergence of the iterative process are given in the Table 6.11. The GF method converged at the 9th step and the OE method converged at the 8th step. For both methods the FIS values are equal to 1.02. The minimal value of the rms retrieval error for the GF method is observed at the 1st iteration step and is equal to 4.56%. At the last step the rms error is considerably larger and constitutes 12.7%. For the OE method the minimal rms error is observed also at the 1st step but contrary to the GF method the difference between the minimal rms error and the rms error at the last step is insignificant - about 0.4%.

Model M33, P_d(ozone) = $0.18 \cdot 10^{-5}$.

The retrieval results for this model are displayed in Fig. 6.27 and the FIS and SSR values are given in the Table 6.12. The behavior of the retrieval errors for this model is quite similar to the behavior of errors for the model M26 discussed above. Three altitude ranges can be distinguished: 8-25 km (large errors), 25-50 km (small errors) and 50-65 km (large errors). In the range with small errors (which are about 1%) the GF and the OE methods produce practically identical results. In the ranges with large errors the OE method appeared to be more preferable. For example at 17 km and 20 km altitudes the errors of the GF method reach 10-14% and the errors of the OE method do not exceed 5%. As it was in the case of the model M26, the GF method applied to the model M33 demanded more than 10 iteration steps for convergence. At the 10th step the shift of solution was still 0.77%. The OE method satisfied the convergence criterion at the 9th step with the SSR value equal to 0.01%. The FIS values for both methods were equal to 0.97. Similar to the case with the M39 model, the minimal rms retrieval errors are observed at the 1st iteration steps for both methods. But in the considered case the difference between the minimal rms errors and the errors at the last step are noticeable for both methods. This difference for the GF method constitutes about 9% and for the OE method constitutes about 4%.

Model M36, P_d(ozone) = $0.30 \cdot 10^{-7}$.

The retrieval errors are presented in Fig. 6.28 and the characteristics of the convergence of the iterative process are presented in the Table 6.13. For this model the OE method produced very good accuracy. At all levels (except 65 km) the errors of the OE method were less than 5%. The application of the GF method resulted in large oscillating errors in the vicinity of 20 km altitude and higher than 52 km. At the altitudes of 62 km and 65 km the errors of the GF method were greater than 50% and are not shown within the scale of Fig. 6.28. At these altitudes the OE method gave the errors not exceeding 10%. In the altitude range 25-50 km both methods delivered practically the same results. The situation with the convergence of the iterative process was the same as for the models M26 and M33. At the 10th step the GF method still did not satisfy the termination criterion while the OE method converged at the 9th step. FIS values were equal to 0.96 for both methods. For the GF method the rms retrieval error has the minimum at the 1st step which is equal to 5.97%. At the last step the rms error is considerably larger and is equal to 18.7%. For the OE method the rms error has the minimum at the 8th step (2.72%) and at the last step (9th) the value is the same.

Model M44, P_d(ozone) = $0.15 \cdot 10^{-8}$.

The results of the numerical experiments for this model are presented in Fig. 6.29 and Table 6.11. This model is characteristic by the large deviation of the initial guess from the true profile. The deviation is 20-40% in the altitude range 8-50 km and increases in the upper layers. One can notice that the retrieval error profiles are slightly shifted towards the initial guess error profile for both methods. The largest retrieval errors of the GF method are below 20 km and higher than 50 km. The increase of errors of the OE method is considerable below 15 km and is

negligible at high altitudes. At 8 km altitude the error of the GF method was about 25% and the error of the OE method was 13%. The increasing and oscillating errors are observed for the GF method higher than 50 km. They reach the values of -30% (62 km) and 40% (65 km). Both methods required less than 10 iteration steps for convergence. The GF method converged at the 9th step and the OE method converged at the 8th step. FIS values were 1.02. The minimal rms retrieval error is observed for the GF method at the 2nd iteration step and is equal to 9.42%. At the last step the rms error is about 4% larger. For the OE method the minimal rms error is observed at the 5th step and is equal to 4.70%. For the OE method the difference between the minimal rms error and the rms error at the last step is very small and constitutes 0.05%.

General discussion.

The comparison of the initial guess error profiles for the considered atmospheric models show that in the most cases the true profiles have similar behavior (except model M44) since the initial guess was the same for all models. At the same time the probability density function values for the ozone profiles are quite different. There is no contradiction, since the probability density values were calculated for the profiles running from 8 km to 80 km but the figures show only the altitude range of interest 8 km - 65 km. It should be stressed once more that the major attention in the investigations was paid to the p-T retrieval problem, therefore for the ozone retrieval problem we were bounded to the models for which the p-T problem had been already solved.

In the most retrieval cases the following peculiarities of the error profiles showed up:

- the retrievals are very good for both GF and OE methods in the altitude range 25-50 km (the errors are less than 2%);
- both methods deliver larger errors below 25 km and above 50 km;
- the errors of the GF methods are considerably larger than the errors of the OE method (excluding the region of high accuracy retrievals 25-50 km);
- the convergence of the iterative process is slower for the GF method;
- the FIS values do not change noticeably after the second iteration step in each test case;
- there is no strong correlation between the final FIS value and the retrieval errors: FIS values about unity do not mean the absence of large errors.

The high accuracy retrievals in the altitude range 25-50 km are explained by the high signal-to-noise ratios (SNR) for the measurements at the corresponding tangent altitudes and by the absence of interference from other parameters. It was shown above that the p-T retrievals were good in this altitude region and the small quantity of water vapor can not produce noticeable interference.

The increase of errors in the higher layers is explained by the following mechanisms. The first mechanism is the decrease of the SNR because of the diminishing of limb radiance values. The second mechanism is the larger pressure and temperature errors in the correspondent layers. These 2 mechanisms are common for both methods. However, there is one more mechanism which is characteristic only for the GF method. Since the profiles higher than 65 km are set equal to the corresponding mean ones, the discrepancies between the true and mean profiles in the higher layers cause propagation of error to the lower layers. The errors propagate via the calculations of limb radiance values for the lower tangent altitudes (naturally, calculations include accounting of all points along the line-of-sight).

The increase of errors in the lower layers may be explained by the interference from the uncertainties in the pressure, temperature and water vapor profiles. In order to confirm this conclusion a special test retrieval was performed. Model M44 was selected for the test because both methods produced large errors in the lower layers for this model. In this test the pressure, temperature and water vapor profiles were set equal to the true profiles of the model. So the interference from these parameters was totally removed. The results of this test retrieval are displayed in Fig. 6.30. As it can be seen from the figure, the quality of the retrieval in the case when there is no interference from other parameters is very good. The comparison of figures 6.29 and 6.30 shows that the large errors in the lower layers were really caused by the interference from the uncertainties in the pressure, temperature and water vapor profiles. One

can see that the retrieval errors are in a good agreement with their estimations made on the basis of error matrix calculations for the GF and the OE methods. More detailed investigation of the contribution of each of the mentioned parameters is not discussed here because it is beyond the frame of the present study.

Special attention should be paid to the problem of convergence speed of the iterative process. As it was mentioned in the beginning of this section the problem of ozone retrieval is very computer time consuming due to the large number of ozone lines and broad spectral coverage of microwindows. In this respect the OE method has the advantage since it is converged faster. In general, test retrievals demonstrated slow convergence of the iterative process in the ozone retrieval problem and showed the necessity to work out special algorithms for the fast selection of initial guess.

Finally, we present the comparison of the ozone retrieval errors for two methods on the basis of the averaged data. As it was done in the p-T retrieval problem, we calculated root mean square error at every altitude level by averaging the results obtained for 6 selected models. While averaging we applied weighting of data in accordance with the values of the probability density function corresponding to each ozone profile. The averaged results are shown in Fig. 6.31. In this figure the error estimations made on the basis of the error matrix calculations are presented also. It is seen from the figure that the OE method is more accurate in the ozone retrieval problem. The error estimations made on the basis of error matrix calculations show that in the lower layers the accuracy of the OE method is up to 2-4% better than the accuracy of the GF method. In the upper layers the profit is about 2%. But these error estimations do not account for the error propagation effects from the higher layers in the GF method. If we consider the estimations made on the basis of averaging the results of the numerical experiments, we can see that the profit of the OE method in the higher layers is much more greater. This result is the consequence of the fact that in the ozone retrieval problem the set of measurements is not very informative in the lower and higher layers. Hence the a priori information plays noticeable role in the retrieval process by playing stabilizing role. In the altitude range 20-50 km the profit of the OE method is negligibly small due to large information content of measurements relative to these altitudes.

The error estimations which were made in different ways (error matrix and averaging) are in a very good agreement in the altitude range 25-65 km for the OE method and 25-55 km for the GF method. The differences in the lower layers are explained by the effect of interference because in the error matrix calculations it was not taken into account. And as it was just mentioned, the large averaged errors of the GF method in the upper layers (which are not even shown within the scale of the figure) are caused by the error propagation effects (which was not accounted for by the error matrix also).

The test retrievals showed that special attention should be paid to the investigation of the problem of termination of the iteration process. The test retrievals showed that the minimum of the rms retrieval error is observed not at the last iteration step. However for the OE method in most cases the rms error at the last step differed insignificantly from the minimal value. For the GF method the differences were quite large. We analyzed the behavior of the rms retrieval errors in the case when the interference effects from the uncertainties in the pressure, temperature, and water vapor profiles were removed. The results are presented in the following table:

Table Model M44. σ - rms retrieval error (8-65 km). Interference effects were removed.

Step	0	1	2	3	4	5	6	7	8	9	10
	Global Fit										
σ [%]		15.5	4.78	6.18	7.72	9.13	9.29	9.30	9.31	9.30	9.31
	Optimal Estimation										
σ [%]		16.1	4.80	0.85	0.89	0.73	0.64	0.63	0.63	0.63	

One can see that despite the fact that the interference effects were removed, the minimal rms error for the GF method is equal to 4.78% and is observed at the 2nd but not at the last iteration step. For the OE method the rms error is minimal at the last 3 steps and is equal to 0.63%. One can see also that the errors of the GF method are by more than one order of magnitude larger than the errors delivered by the OE method. This is due to the mechanism of the error propagation effect in the GF method which causes the considerable increase of the GF errors in the upper layers.

So one can arrive to the following main conclusion: in the ozone retrieval problem the optimal estimation method is more preferable than the global fit method in the lower and higher layers and there is practically no difference between the methods in the altitude range 20-50 km.

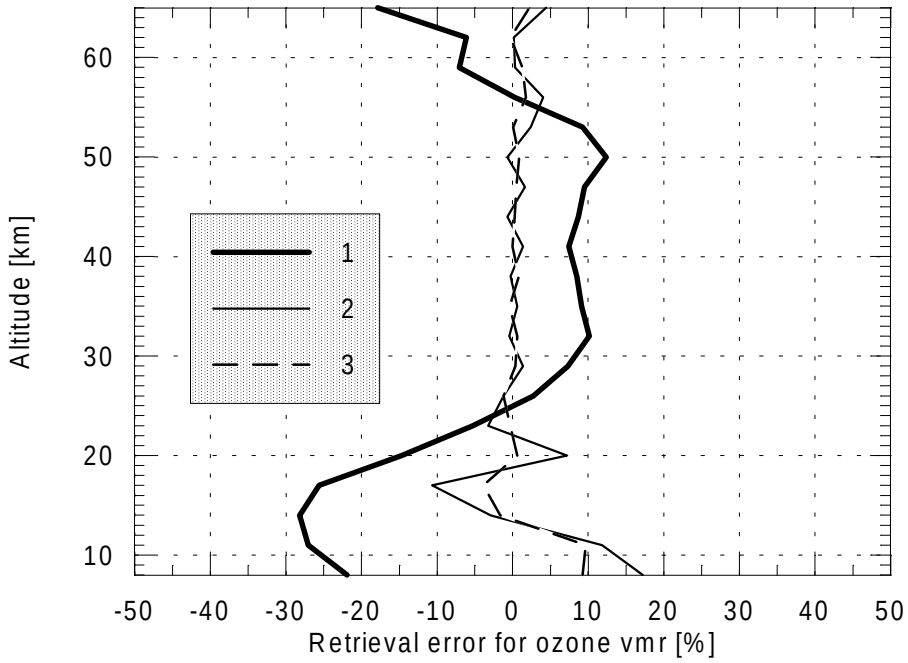

Fig. 6.24 Results of ozone retrieval. Model M09.
1 - initial guess error: deviation of the mean profile from the model profile;
2 - retrieval error in case of the GF method;
3 - retrieval error in case of the OE method.

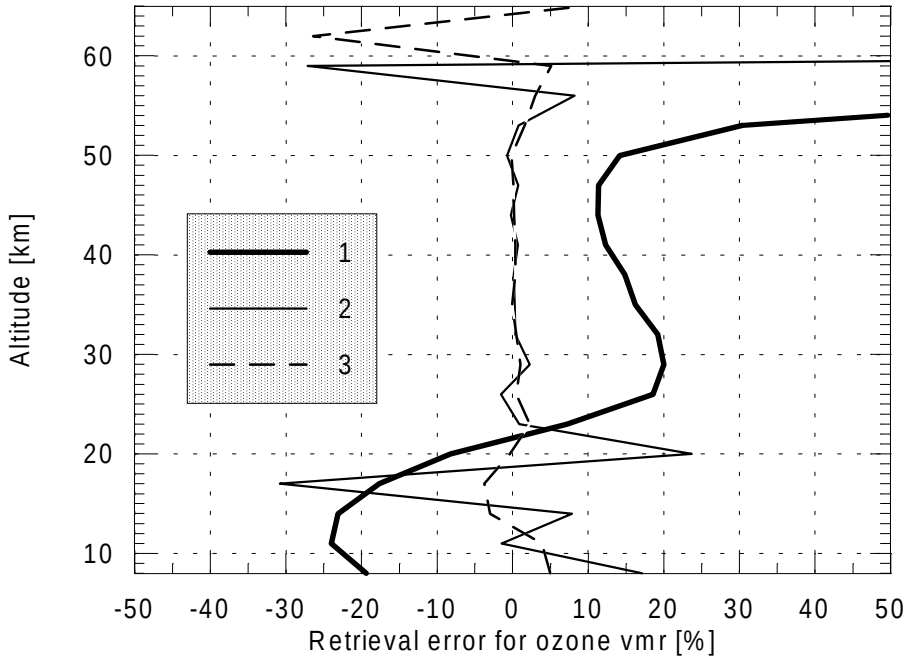

Fig. 6.25 Results of ozone retrieval. Model M26.
1 - initial guess error: deviation of the mean profile from the model profile;
2 - retrieval error in case of the GF method;
3 - retrieval error in case of the OE method.

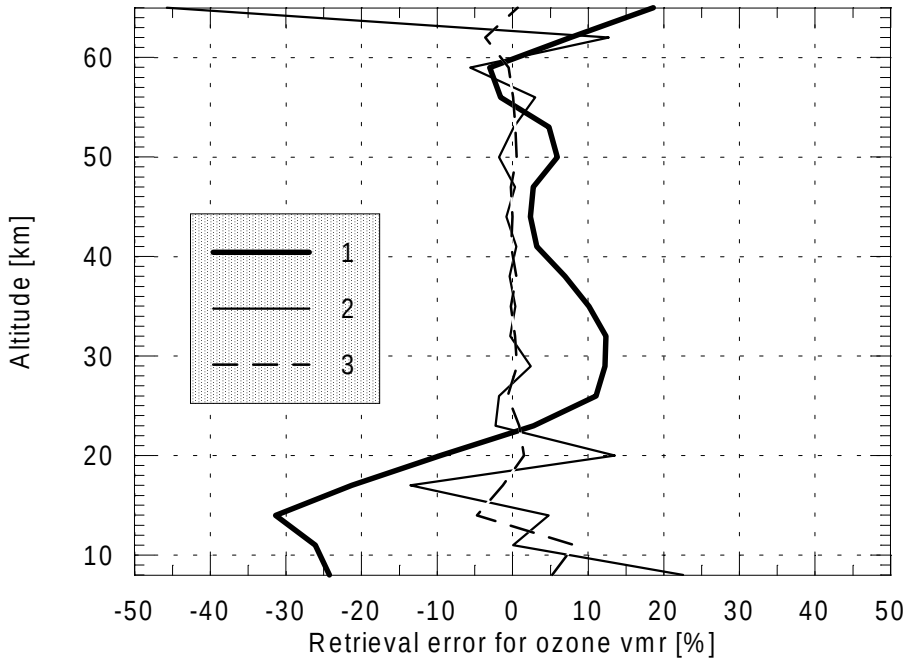

Fig. 6.26 Results of ozone retrieval. Model M39.
1 - initial guess error: deviation of the mean profile from the model profile;
2 - retrieval error in case of the GF method;
3 - retrieval error in case of the OE method.

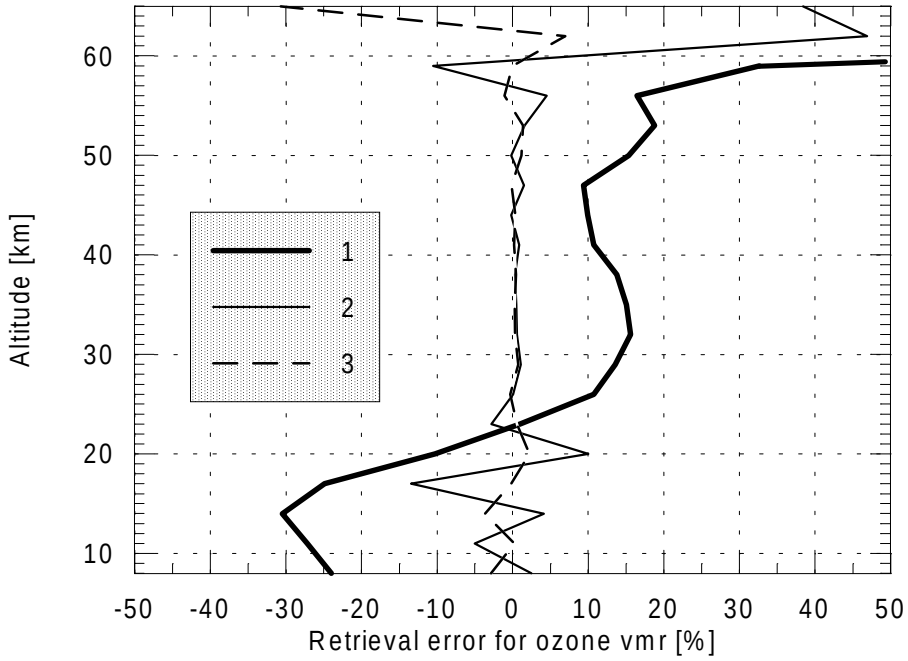

Fig. 6.27 Results of ozone retrieval. Model M33.
1 - initial guess error: deviation of the mean profile from the model profile;
2 - retrieval error in case of the GF method;
3 - retrieval error in case of the OE method.

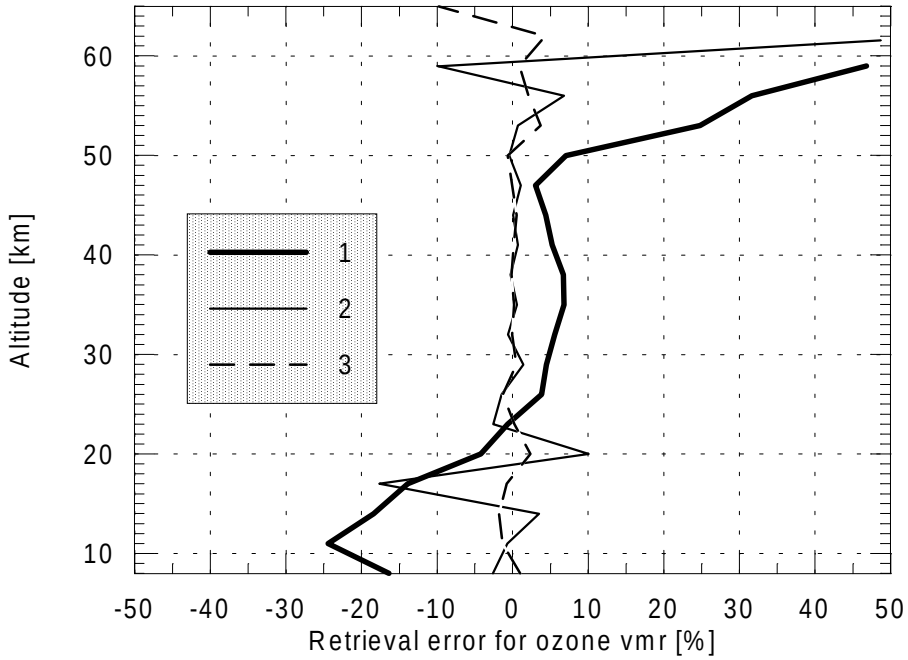

Fig. 6.28 Results of ozone retrieval. Model M36.
1 - initial guess error: deviation of the mean profile from the model profile;
2 - retrieval error in case of the GF method;
3 - retrieval error in case of the OE method.

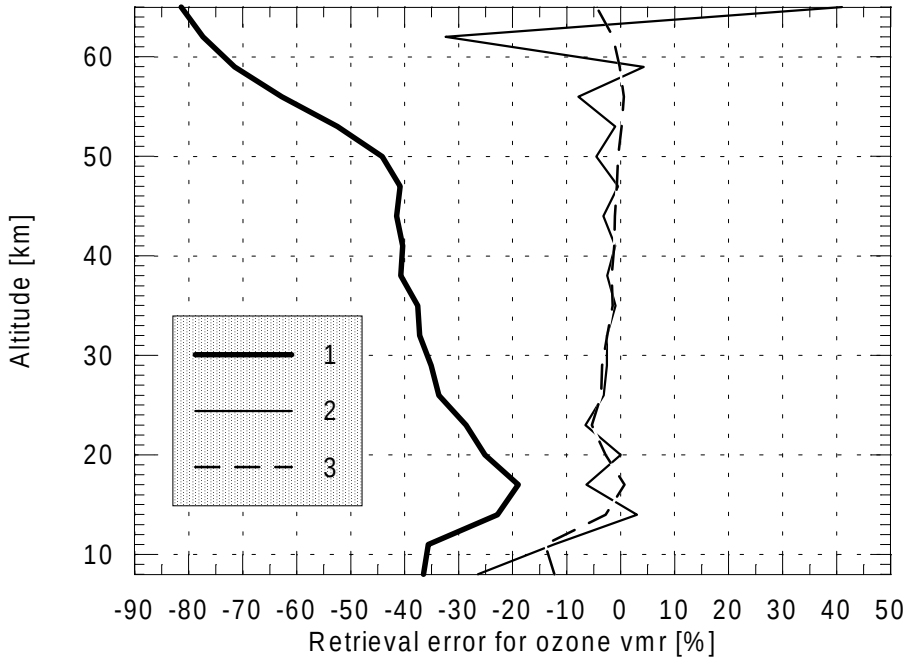

Fig. 6.29 Results of ozone retrieval. Model M44.
1 - initial guess error: deviation of the mean profile from the model profile;
2 - retrieval error in case of the GF method;
3 - retrieval error in case of the OE method.

Table 6.9 Characteristics of the convergence of the iterative process. Ozone retrieval. Model M9. FIS - spectral fitting index, SSR - shift of solution. σ - rms retrieval error (8 - 65 km).

Step	0	1	2	3	4	5	6	7	8	9	10
	Global Fit										
FIS	1.37	1.26	1.26	1.26	1.26	1.26	1.26	1.26	1.26	1.26	
SSR [%]		51.3	7.44	3.52	-0.79	0.44	0.35	-0.19	0.11	-0.08	
σ [%]		4.43	5.61	5.86	5.78	5.79	5.82	5.80	5.81	5.80	
	Optimal Estimation										
FIS	1.37	1.26	1.26	1.26	1.26	1.26	1.26	1.26	1.26	1.26	
SSR [%]		45.3	4.99	14.7	10.1	23.6	8.32	6.71	-0.12	-0.01	
σ [%]		2.40	3.07	3.22	3.24	3.26	3.26	3.25	3.25	3.25	

Table 6.10 Characteristics of the convergence of the iterative process. Ozone retrieval. Model M26. FIS - spectral fitting index, SSR - shift of solution. σ - rms retrieval error (8 - 65 km).

Step	0	1	2	3	4	5	6	7	8	9	10
	Global Fit										
FIS	1.39	1.02	1.01	1.01	1.01	1.01	1.01	1.01	1.01	1.01	
SSR [%]		-52.5	-61.7	-76.9	104.	47.2	15.7	22.1	12.7	-7.0	4.44
σ [%]		174.	173.	146.	150.	157.	153.	158.	155.	157.	156.
	Optimal Estimation										
FIS	1.39	1.02	1.01	1.01	1.01	1.01	1.00	1.00	1.00	1.00	
SSR [%]		-58.8	-44.6	-97.8	544.	-99.9	15000	-74.0	-11.0	-0.27	0.05
σ [%]		175.	174.	149.	148.	22.9	8.12	6.79	6.68	6.67	6.67

Table 6.11 Characteristics of the convergence of the iterative process. Ozone retrieval. Model M39. FIS - spectral fitting index, SSR - shift of solution. σ - rms retrieval error (8 - 65 km).

Step	0	1	2	3	4	5	6	7	8	9	10
	Global Fit										
FIS	1.14	1.02	1.02	1.02	1.02	1.02	1.02	1.02	1.02	1.02	
SSR [%]		47.3	-14.6	-19.7	-8.94	-4.64	0.68	-0.35	0.12	-0.04	
σ [%]		4.56	7.63	11.2	12.1	12.6	12.7	12.7	12.7	12.7	
	Optimal Estimation										
FIS	1.13	1.02	1.02	1.02	1.02	1.02	1.02	1.02	1.02		
SSR [%]		42.1	-7.07	14.0	9.20	19.0	6.35	5.19	0.06		
σ [%]		2.26	2.69	2.64	2.59	2.60	2.61	2.62	2.62		

Table 6.12 Characteristics of the convergence of the iterative process. Ozone retrieval. Model M33. FIS - spectral fitting index, SSR - shift of solution. σ - rms retrieval error (8 - 65 km).

Step	0	1	2	3	4	5	6	7	8	9	10
	Global Fit										
FIS	1.19	0.97	0.97	0.97	0.97	0.97	0.97	0.97	0.97	0.97	0.97
SSR [%]		-66.4	-87.0	1042.	-12.1	26.7	-6.79	9.03	-3.57	1.65	0.77
σ [%]		5.24	20.0	12.4	10.4	14.8	13.0	15.2	14.2	14.6	14.4
	Optimal Estimation										
FIS	1.20	0.97	0.97	0.97	0.97	0.97	0.97	0.97	0.97	0.97	
SSR [%]		-60.3	-42.0	-21.9	-12.0	-19.8	-7.56	-10.8	-0.26	-0.01	
σ [%]		3.57	8.07	10.4	9.88	8.42	7.87	7.15	7.15	7.15	

Table 6.13 Characteristics of the convergence of the iterative process. Ozone retrieval. Model M36. FIS - spectral fitting index, SSR - shift of solution. σ - rms retrieval error (8 - 65 km).

Step	0	1	2	3	4	5	6	7	8	9	10
	Global Fit										
FIS	1.04	0.96	0.96	0.96	0.96	0.96	0.96	0.96	0.96	0.96	0.96
SSR [%]		-70.4	69.0	24.8	1.53	26.6	-6.61	8.98	-3.45	-1.56	0.74
σ [%]		5.97	13.7	14.9	14.8	19.0	17.3	19.4	18.5	18.9	18.7
	Optimal Estimation										
FIS	1.05	0.96	0.96	0.96	0.96	0.96	0.96	0.96	0.96	0.96	
SSR [%]		-61.3	-40.1	-32.6	-19.2	-25.2	-14.9	-23.4	0.67	-0.01	
σ [%]		5.76	6.24	8.21	7.28	4.96	3.96	2.74	2.72	2.72	

Table 6.14 Characteristics of the convergence of the iterative process. Ozone retrieval. Model M44. FIS - spectral fitting index, SSR - shift of solution. σ - rms retrieval error (8 - 65 km).

Step	0	1	2	3	4	5	6	7	8	9	10
	Global Fit										
FIS	4.02	1.29	1.12	1.12	1.12	1.12	1.12	1.12	1.12		
SSR [%]		294.	46.9	23.9	7.15	-8.21	-1.46	-0.3	-0.07		
σ [%]		18.0	9.42	10.1	11.6	13.4	13.8	13.8	13.8		
	Optimal Estimation										
FIS	4.03	1.29	1.12	1.12	1.12	1.12	1.12	1.12	1.12	1.12	
SSR [%]		215.	46.9	40.2	18.6	62.9	23.3	25.2	-0.47	0.03	
σ [%]		17.4	7.15	4.88	4.73	4.70	4.71	4.75	4.75	4.75	

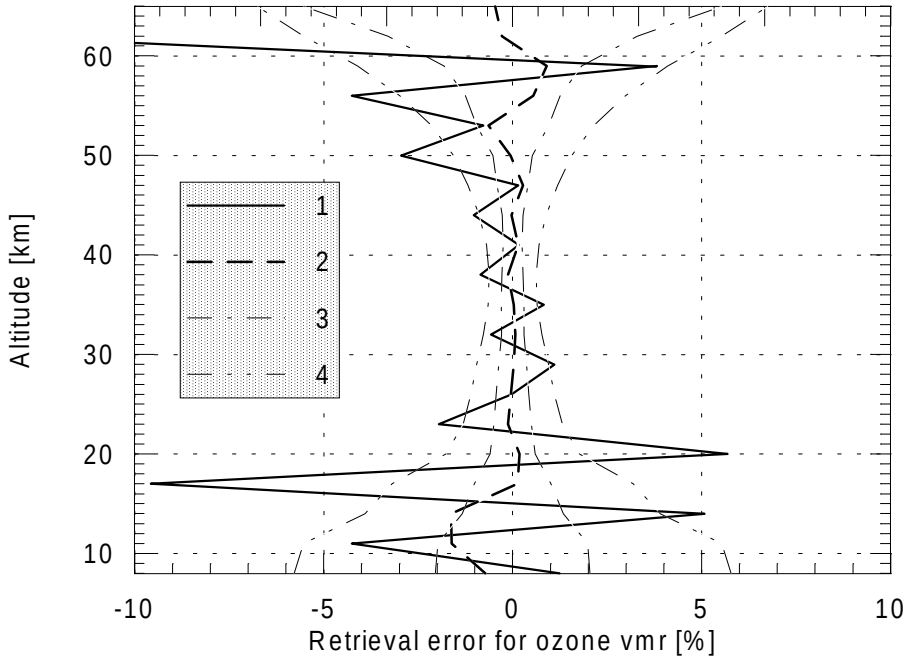

Fig. 6.30 Results of ozone retrieval. Model M44. The profiles of pressure, temperature and water vapor were set equal to the exact ones in order to eliminate the interference from these species. 1 - retrieval error in case of the GF method; 2 - retrieval error in case of the OE method. 3,4 - "corridors" of errors estimated on the basis of error matrix calculations for OE and GF methods correspondingly.

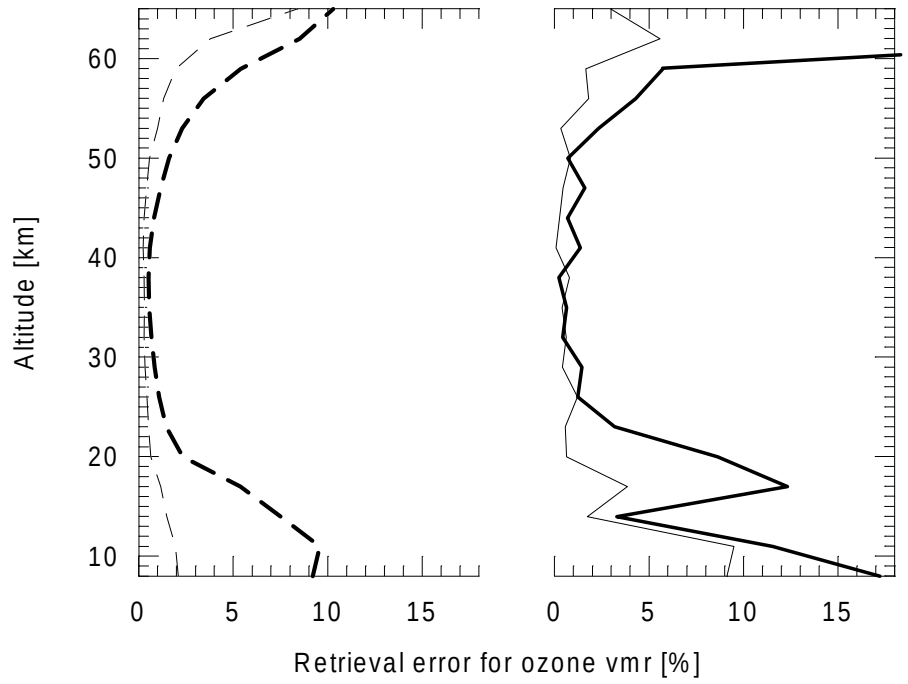

Fig. 6.31 Comparison of the retrieval errors for ozone vmr in the case of GF method (thick lines) and OE method (thin lines). Solid lines - errors averaged with the weights over 6 selected models. Long-dashed lines - errors calculated on the basis of error matrix.

6.4 Water vapor retrieval

The water vapor test retrievals were performed similar to the retrievals of ozone profiles. Pressure and temperature profiles were set equal to the profiles obtained as the solution of the p-T retrieval problem. The ozone profile in each model was set equal to the mean profile. The limb radiance measurements were simulated on the basis of true profiles of all parameters. Hence, the additional sources of errors were: the errors of pressure-temperature determination in the p-T task and the uncertainty of the ozone profile. Test retrievals were terminated after 4 models of the selected set of atmospheric models were investigated because the results revealed divergence of the iterative process in 3 of 4 cases at the 8 km altitude level for the selected values of SSR. The reason for the divergence of the iterative process will be discussed below. First, we consider 4 test retrievals which were performed.

Model M33. P_d(water vapor)=0.53·10^{-3}.

The errors of the retrieval of water vapor profile for the model M33 are shown in Fig. 6.32. As it can be seen from the figure, the retrieval errors are characterized by oscillations in the whole altitude range for both GF and OE methods. However in the range 11-55 km the errors are within the corridor of 10%. The errors of both methods at the altitude of 8 km are extremely large and reach 60%. The increase of errors is observed also at the higher levels where the errors of the GF method reach 35% and the errors of the OE method reach 20%. The characteristics of the convergence of the iterative process are given in the Table 6.15. The analysis showed that both methods did not converge even after 10 steps. Moreover, the analysis of the retrieval errors at every step revealed that the retrieval errors at 8 km altitude were permanently increasing from step to step - so the process really diverged. This effect took place despite the relatively small values of fitting index for spectra which remained about 0.96-0.97 in the iterative process. The test retrieval results for the GF and the OE methods displayed practically no difference up to the altitude of 25 km. In the range 25-55 km the OE method delivered more smooth solution. The rms error has the minimum at the 2nd step for both the GF and the OE methods and constitutes correspondingly 5.68% and 6.12%. At the 10th step the rms error for the GF method was 3 times greater than the minimal value and for the OE method - 2 times greater.

Model M33. P_d(water vapor)=0.11·10^{-4}.

The results obtained for the model M36 are shown in Fig. 6.33. For this model the same effect as for the model M33 was observed. The iterative process diverged for the altitude of 8 km. After the 10th step the retrieval error at 8 km altitude for the GF method was 35% and for the OE method it was -60%. In the altitude range 11-55 km the retrievals were satisfactory. For the most altitudes (except 20 km) the errors did not exceed 5% for both methods. In the range 11-25 km both methods delivered practically the same results. But in the range 25-55 km the solution was more smooth for the OE method. In the upper layers the errors of the GF method increased noticeably up to -50% but the errors of the OE method remained within the 10% corridor. The characteristics of the iterative process are summarized in the Table 6.16. One can see the absence of convergence for both methods. As it was mentioned above, the divergence occurred only for the altitude of 8 km. The FIS value was quite low - about 0.96. The minimal rms error for the GF method is observed at the 1st iteration step and constitutes 5.31%. For the OE method the minimal rms error is observed at the 3rd step and constitutes 4.25%. At the 10th step both methods delivered rms errors considerably larger than the minimal values.

Model M26. P_d(water vapor)=0.49·10^{-5}.

The results of the retrievals are demonstrated in Fig. 6.34. The characteristic feature is the very large errors in the lower layers up to approximately 25 km. For the altitudes except 8 km the retrieval errors were even larger than the errors of the initial guess and were oscillating. At 17 and 20 km altitude the errors of the GF method reached 45% and the errors of the OE method reached 20-30%. Above 25 km altitude both methods produced satisfactory results with the errors about 5% and less. For the considered case the results delivered by both methods were practically similar and smoothing of solution by the OE method was not

observed. The characteristics of the iterative process are given in the Table 6.17. Though the criterion of convergence (shift of solution less than 0.1%) was not satisfied even after the 10th step, the process was converging (very slowly). The shift of solution for the GF method was -0.81% and for the OE method it was -0.79%. The retrieved values at "critical" 8 km altitudes remained stable. It should be stressed that despite the tendency to converge the errors in the lower layers were very large. The minimal rms error for the GF method is observed at the 2nd step (13.7%) and for the OE method - at the 4th step (8.9%). As a consequence of the convergence, the rms errors at the 10th iteration step differ from the minimal values only by about 2%.

Model M44. P_d(water vapor)=$0.69 \cdot 10^{-8}$.

The errors of water vapor profile retrieval for the model M44 are shown in Fig. 6.35. similar to the previous cases, the errors in the lower layers were very large. At 8 km altitude both methods produced errors up to 90% which were larger than the initial guess error. There was the local maximum of errors at 17 km altitude: 30%. The GF method delivered good results in the range 20-55 km (the errors less than 5%). Higher than 55 km the GF method errors increased noticeably (50% and more) and started oscillating. The OE method errors were less than 5% starting from 20 km and up to 65 km. Again the iterative process did not converged (see Table 6.18). At the 10th step the shift of solution for the GF method was -40.5% and the shift of solution for the OE method was 35.5%. The analysis of errors at every step revealed the same effect as in the previous cases: the process diverged at the 8 km altitude. The minimal rms errors for both methods are observed at the 1st step. As a consequence of the divergence of the iterative process, the rms errors at the 10th step are considerably larger than minimal values.

General discussion.

The divergence of the iterative process for three of the four initial test cases was the reason to terminate test retrievals and to investigate the problem. Since the analysis of the p-T and ozone retrieval tasks showed the great influence of the interfering parameters on the results of the specific retrievals, the logical step was to eliminate the interference in the water vapor retrieval task. Similar to the p-T and ozone retrieval tasks, the interference seemed to be the most probable reason for the divergence. For the test with the eliminated interference the model M36 was chosen which was characterized by bad quality retrieval despite small errors of the initial guess. The numerical experiment was performed with the pressure, temperature and ozone profiles equal to exact ones. The water vapor determination errors obtained for this case are shown in Fig. 6.36. If one compare Figs. 6.33 and 6.36, one can see that in the ideal case of known interfering profiles the retrievals are very good. The errors for both methods are mainly less than 5% up to 55 km altitude. The OE method produced error less than 1% at the "critical" altitude 8 km. The results of the GF method were not as good as for the OE method - at 8 km altitude the error was still 6.8%. The test retrieval in the case of eliminated interference confirmed that the water vapor retrieval task is very sensitive to the interference. If we take into account the low FIS values even in the cases when the process diverged, we can come to the conclusion that this interference influences the water vapor retrieval to a great extent through the mechanism of erroneous kernels of the integral equation rather than through the effective noise in limb radiance measurements. However the detailed investigation of the contribution of both mechanisms was beyond the frame of the present study.

Despite the fact that test retrievals were terminated, the comparison of the retrieval errors for the GF and the OE methods was done similar to the p-T and ozone tasks. The errors averaged over 4 test cases (with weights corresponding to the probability density function values) were considered as well as the errors obtained from the error matrix calculations. One should keep in mind, however, that due to small quantity of test cases the averaged error estimations can not be considered very representative, but still are illustrative. Fig. 6.37 shows these error estimations. First we consider the error estimations made on the basis of error matrix calculations. One can see that up to 45 km altitude the GF and the OE methods deliver practically identical errors. At the higher altitudes the errors of the OE method are about 2% less than of the GF method. The results averaged over 4 test cases show the same tendency (right part of Fig. 6.37). The GF and the OE methods produced close results up to 45 km

(except the region 25-35 km). In the higher layers the OE method appeared to be more precise (by about 5% and even much more at 62 and 65 km altitude).

The test retrievals showed that special attention should be paid to the investigation of the problem of termination of the iteration process. The test retrievals showed that similar to the case of ozone retrieval the minimum of the rms retrieval error is observed not at the last iteration step. We analyzed the behavior of the rms retrieval errors in the case when the interference effects from the uncertainties in the pressure, temperature, and ozone profiles were removed. The results are presented in the following table:

Table Model M36. σ - rms retrieval error (8-65 km). Interference effects were removed.

Step	0	1	2	3	4	5	6	7	8	9	10
	Global Fit										
σ [%]		5.79	7.71	9.43	9.89	10.0	10.0	10.0	10.0	10.0	10.1
	Optimal Estimation										
σ [%]		4.48	3.92	3.34	2.97	2.84	2.80	2.80	2.79	2.78	2.78

One can see that despite the fact that the interference effects were removed, the minimal rms error for the GF method is equal to 5.79% and is observed at the 1st but not at the last iteration step. For the OE method the rms error is minimal at the last 2 steps and is equal to 2.78%. One can see also that the errors of the GF method are several times larger than the errors delivered by the OE method. This is due to the mechanism of the error propagation effect in the GF method which causes the considerable increase of the GF errors in the upper layers.

So the main conclusions may be formulated as follows:

a) in the water vapor retrieval problem the interference of other parameters dramatically influences the results and in most cases masks the determination of water vapor profile in the vicinity of 8 km impossible;

b) the GF and the OE methods deliver practically the same results up to the altitude of 45 km, in the higher layers the OE method is much preferable.

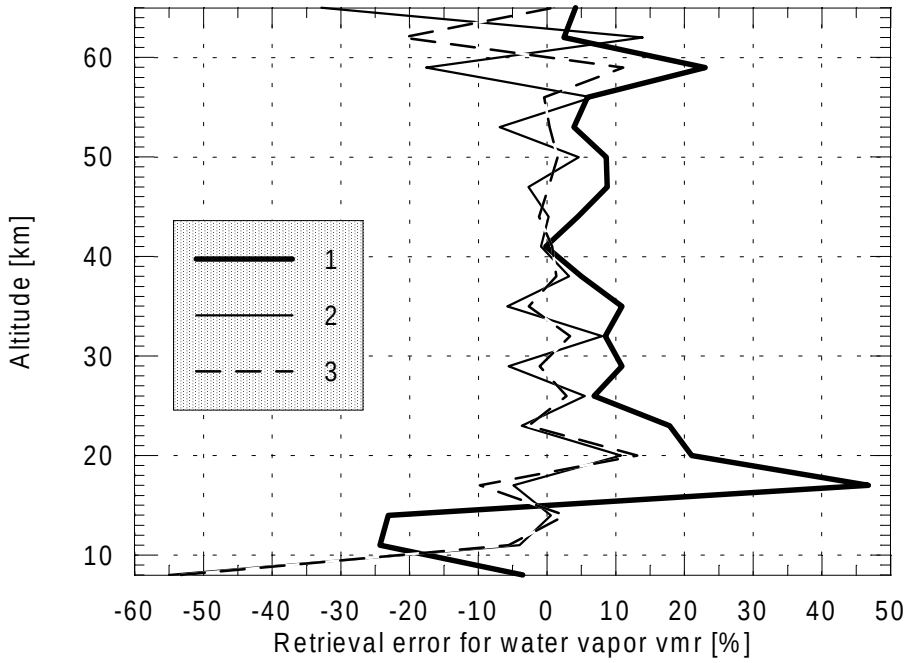

Fig. 6.32 Results of water vapor retrieval. Model M33.
1 - initial guess error: deviation of the mean profile from the model profile;
2 - retrieval error in case of the GF method;
3 - retrieval error in case of the OE method.

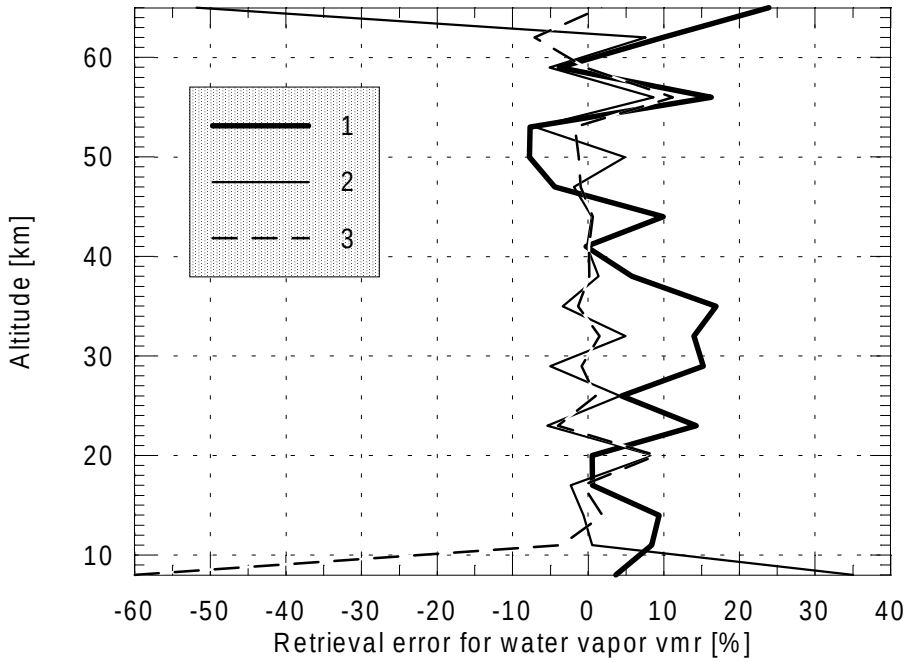

Fig. 6.33 Results of water vapor retrieval. Model M36.
1 - initial guess error: deviation of the mean profile from the model profile;
2 - retrieval error in case of the GF method;
3 - retrieval error in case of the OE method.

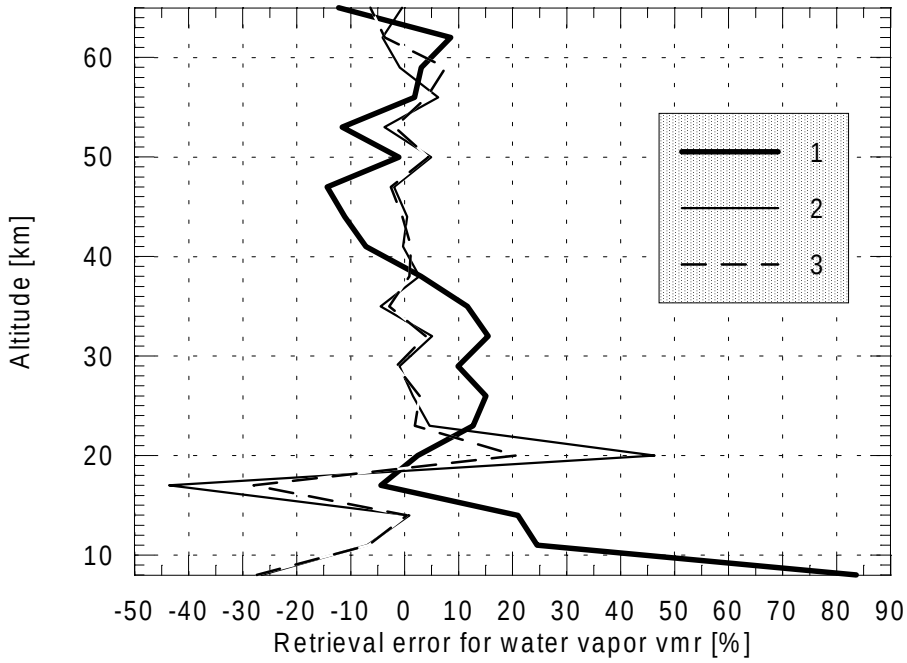

Fig. 6.34 Results of water vapor retrieval. Model M26.
1 - initial guess error: deviation of the mean profile from the model profile;
2 - retrieval error in case of the GF method;
3 - retrieval error in case of the OE method.

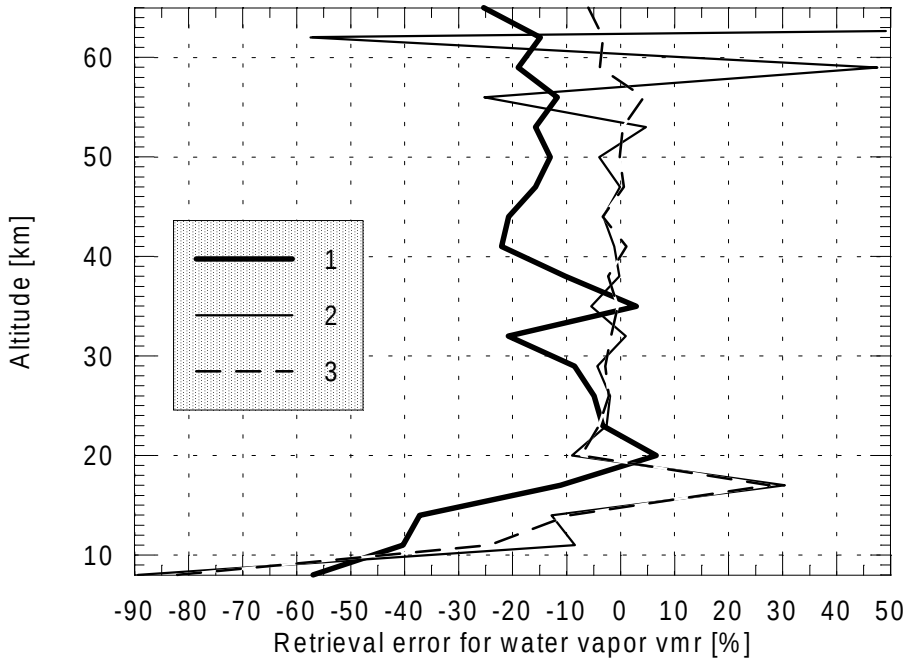

Fig. 6.35 Results of water vapor retrieval. Model M44.
1 - initial guess error: deviation of the mean profile from the model profile;
2 - retrieval error in case of the GF method;
3 - retrieval error in case of the OE method.

Table 6.15 Characteristics of the convergence of the iterative process. Water vapor retrieval. Model M33. FIS - spectral fitting index, SSR - shift of solution. σ - rms retrieval error (8 - 65 km).

Step	0	1	2	3	4	5	6	7	8	9	10
	Global Fit										
FIS	1.05	0.97	0.96	0.96	0.96	0.96	0.96	0.97	0.97	0.96	0.96
SSR [%]		-53.0	37.4	7.52	-7.70	-13.0	-15.6	-21.8	-16.5	8.67	-3.58
σ [%]		9.01	5.68	6.63	7.71	11.2	12.8	15.0	16.4	15.8	15.9
	Optimal Estimation										
FIS	1.05	0.97	0.96	0.96	0.96	0.96	0.96	0.96	0.97	0.97	0.97
SSR [%]		-54.7	38.6	-13.3	-7.59	-8.18	-10.5	-14.8	-20.1	-15.6	7.71
σ [%]		9.65	6.12	6.28	6.31	6.76	7.88	9.73	12.2	14.0	13.7

Table 6.16 Characteristics of the convergence of the iterative process. Water vapor retrieval. Model M36. FIS - spectral fitting index, SSR - shift of solution. σ - rms retrieval error (8 - 65 km).

Step	0	1	2	3	4	5	6	7	8	9	10
	Global Fit										
FIS	1.02	0.96	0.96	0.96	0.96	0.96	0.96	0.96	0.96	0.96	0.96
SSR [%]		-24.8	-12.4	-19.7	-10.8	-15.5	2.68	3.23	3.86	4.58	5.39
σ [%]		5.31	6.75	9.00	10.3	12.5	12.9	13.1	13.5	14.0	14.7
	Optimal Estimation										
FIS	1.03	0.96	0.96	0.96	0.96	0.96	0.96	0.96	0.97	0.97	0.97
SSR [%]		-19.6	-17.4	-30.0	-22.2	-28.6	-7.57	-10.2	-14.0	-18.7	-18.4
σ [%]		4.97	4.54	4.25	4.34	4.97	6.01	7.51	9.50	11.9	14.0

Table 6.17 Characteristics of the convergence of the iterative process. Water vapor retrieval. Model M26. FIS - spectral fitting index, SSR - shift of solution. σ - rms retrieval error (8 - 65 km).

Step	0	1	2	3	4	5	6	7	8	9	10
	Global Fit										
FIS	1.08	1.00	0.98	0.97	0.98	0.98	0.97	0.97	0.97	0.97	0.97
SSR [%]		-40.5	19.0	-25.1	-23.4	-12.5	9.57	-3.45	0.59	0.59	-0.81
σ [%]		16.2	13.7	15.1	14.3	16.4	15.5	15.8	15.8	15.7	15.8
	Optimal Estimation										
FIS	1.08	0.99	0.97	0.97	0.97	0.97	0.97	0.97	0.97	0.97	0.97
SSR [%]		-25.0	-14.4	-21.8	-24.2	-10.7	7.59	-2.69	-0.89	-0.66	-0.79
σ [%]		13.5	9.92	9.42	8.90	11.2	10.1	10.5	10.5	10.4	10.5

Table 6.18 Characteristics of the convergence of the iterative process. Water vapor retrieval. Model M44. FIS - spectral fitting index, SSR - shift of solution. σ - rms retrieval error (8 - 65 km).

Step	0	1	2	3	4	5	6	7	8	9	10
	Global Fit										
FIS	1.35	1.02	0.99	0.99	0.99	1.00	1.03	1.01	1.01	1.01	1.01
SSR [%]		97.9	24.2	-60.5	-83.5	927.	-47.4	-23.4	-16.0	36.3	-40.5
σ [%]		17.6	24.7	35.4	42.3	43.5	46.6	48.4	49.3	49.3	50.0
	Optimal Estimation										
FIS	1.33	1.01	0.99	0.99	1.00	1.12	1.09	1.01	1.00	1.01	1.01
SSR [%]		42.0	14.4	-17.7	-29.5	-66.5	151.	58.6	22.0	-16.1	35.5
σ [%]		13.7	14.6	16.0	18.2	21.8	20.9	20.9	20.7	21.0	20.5

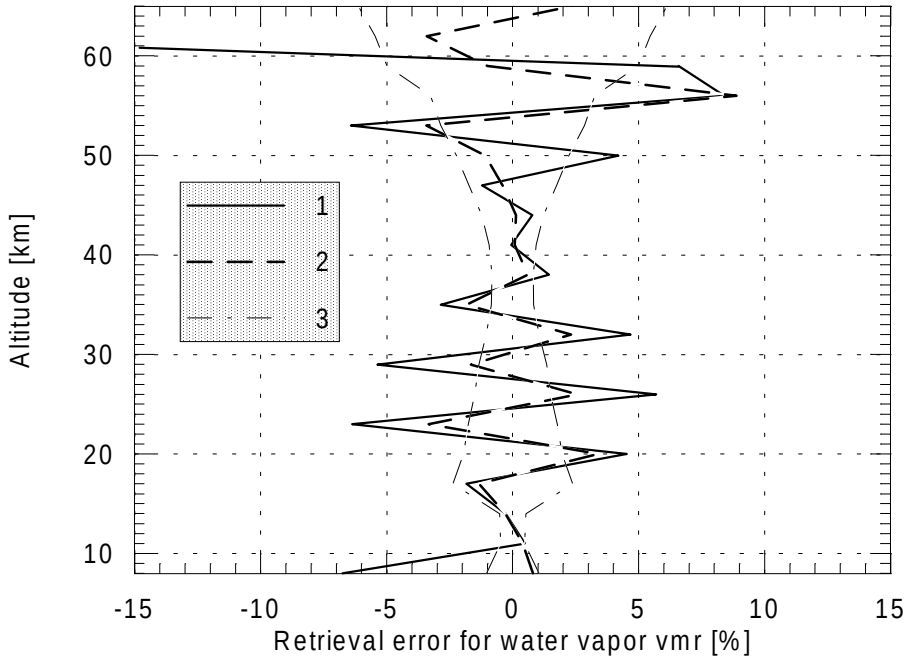

Fig. 6.36 Results of water vapor retrieval. Model M36. The profiles of pressure, temperature and ozone were set equal to exact ones in order to eliminate the interference from these species.

1 - retrieval error in case of the GF method; 2 - retrieval error in case of the OE method;

3 - lines showing the "corridor' of errors for the OE method estimated on the basis of error matrix calculation.

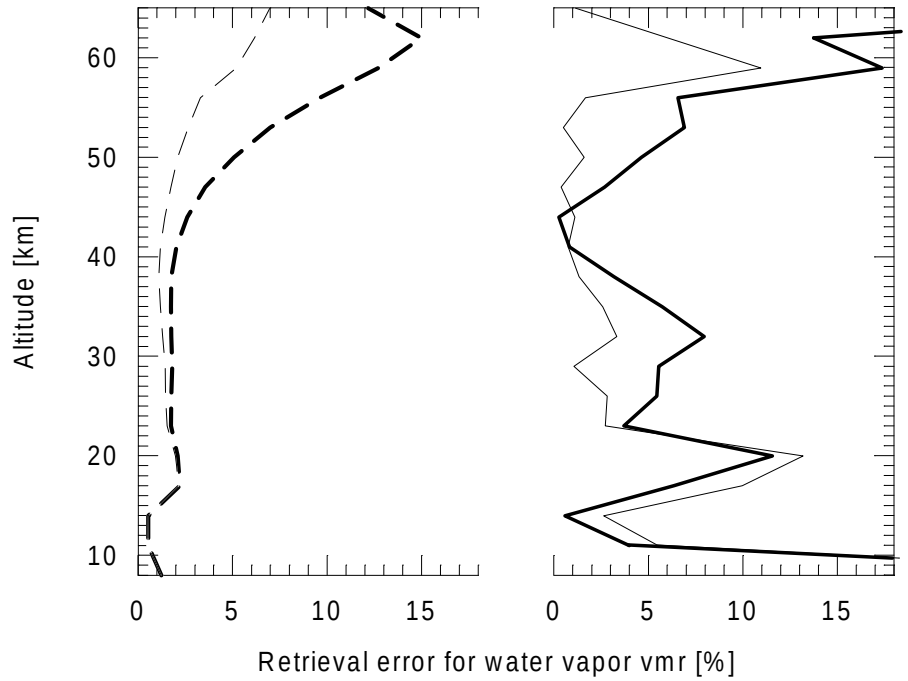

Fig. 6.37 Comparison of the retrieval errors for water vapor vmr in the case of GF method (thick lines) and OE method (thin lines). Solid lines - errors averaged with the weights over 6 selected models. Long-dashed lines - errors calculated on the basis of error matrix.

6.5 Comparison of the retrieval errors for the cases of processing measurements in the microwindows and broad spectral regions

In order to estimate the potential accuracy of the retrieval of atmospheric parameters the retrieval errors were estimated on the basis of the error matrix calculations for the case of measurements in broad spectral regions. The ozone and water vapor retrieval tasks were investigated. The pressure-temperature retrieval task was not considered since:

- this task is more specific due to the fact that it is primary and basic with respect to the retrieval of gaseous content and therefore the interference effects (which are strong for continuous spectral intervals) must be excluded in one way or another;
- the numerical experiments showed that the retrieval accuracy for pressure and temperature profiles was sufficiently high when the preselected set of microwindows was used.

For the ozone and water vapor retrieval tasks it is assumed that pressure and temperature profiles are already known. Of course, the interference effects from other parameters remain important, but they can be suppressed for example in the process of iterative consecutive solution of inverse problems with respect to interfering parameters.

For the ozone retrieval task the limb radiance measurements were simulated in the following continuous spectral regions covering all preselected microwindows:

1) 705- 785 cm^{-1}
2) 1030-1140 cm^{-1}
3) 1730-1745 cm^{-1}
4) 1820-1845 cm^{-1}
5) 2080-2135 cm^{-1}

The total wavenumber coverage was 285 cm^{-1}. (The total wavenumber coverage of the microwindows was 80 cm^{-1}.)

For the water vapor retrieval task the following set of spectral intervals was used (preselected microwindows are completely covered by these intervals):

1) 1350 - 1500 cm^{-1}
2) 1600 - 1710 cm^{-1}
3) 1820 - 2000 cm^{-1}

The total wavenumber coverage was 440 cm^{-1}. (The total wavenumber coverage of the microwindows was 110 cm^{-1}.)

Limb radiance measurements were simulated for all tangent altitudes at each wavenumber gridpoint.

The results of the comparison of the retrieval errors for ozone are shown in Fig. 6.38. Let us consider first the GF method. Comparison of the curves 1 and 3 shows that measurements in broad spectral regions have considerably higher information content than the measurements in the preselected microwindows in the altitude regions 8-20 km and 55-65 km. The improvement of the retrieval accuracy in the lower layers reaches 6% and in the upper layers it reaches 4%. In the altitude region 20-55 km the improvement of the retrieval accuracy is not as significant as in the lower and upper layers and constitutes 1% and less.

The situation for the OE method differs from the situation for the GF method. The improvement of the retrieval accuracy due to the utilization of measurements in broad spectral intervals is not as large as it was in the case of the GF method. The improvement is less than 1% up to 60 km and in the upper layers it reaches 2%.

The obtained results may be interpreted in a different manner if one considers the relative improvement of retrieval accuracy, but not the absolute values. Under such a consideration, the utilization of measurements in broad spectral intervals in the case of the GF method results in the improvement of the retrieval accuracy by a factor of 3 in the lower layers and by a factor of 1.5-2 in the upper layers. In the case of the OE method the retrieval accuracy is improved by a factor of 1.5-2 up to the altitude of 15 km.

It should be emphasized that from the point of retrieval accuracy the application of the OE method to the processing of measurements in the preselected microwindows may be considered more preferable than the application of the GF method for processing of

measurements in broad spectral intervals. The retrieval errors for the OE method and measurements in the microwindows are less than the errors of the GF method and measurements in the broad regions up to the altitude of 63 km. Only in the vicinity of 65 km the errors of the GF method (broad intervals) are about 2% less than the errors of the OE method (microwindows).

The results of the comparison of the retrieval errors for water vapor are shown in Fig. 6.39. One can see that the situation differs from the situation for ozone. For the GF method the improvement of the retrieval accuracy due to utilization of measurements in broad intervals is insignificant up to the altitude of 50 km and constitutes less than 1%. In the upper layers the improvement is larger, however it does not exceed 3.5%. For the OE method the improvement is less than 1% throughout the altitude region of interest.

The obtained results lead to the following conclusions:

1) For the ozone retrieval task the information content of measurements in the preselected microwindows is very high for both methods with respect to the altitude region 20-55 km. The utilization of measurements in broad spectral intervals may noticeably improve the retrieval accuracy in the lower and upper layers if the GF retrieval method is used. If the OE method is used for the retrievals the set of preselected microwindows may be considered highly informative throughout the altitude region 8-65 km.

2) For the water vapor retrieval problem the preselected set of microwindows is highly informative with respect to the whole altitude region of interest 8-65 km for the OE method and with respect to the altitude range 8-50 km for the GF method. There is no considerable improvement of the retrieval accuracy in the lower layers in the case of utilization measurements in broad spectral intervals since the accuracy delivered by measurements in the preselected microwindows is already sufficiently high.

One important remark should be given. The estimation of the retrieval accuracy on the basis of error matrix calculations was performed under the assumption of eliminated interference from the uncertainties of the profiles of atmospheric parameters which are not retrieved. As it was shown in the previous sections, such interference may be significant in the lower layers if microwindows are processed. In case of processing measurements in broad spectral intervals the interference effects are expected to play much more important role. Therefore one should keep in mind that the utilization of the measurements in broad spectral intervals will require in practice the solution of multi-parameter inverse problem or the iterative consecutive solution of single-parameter inverse problems.

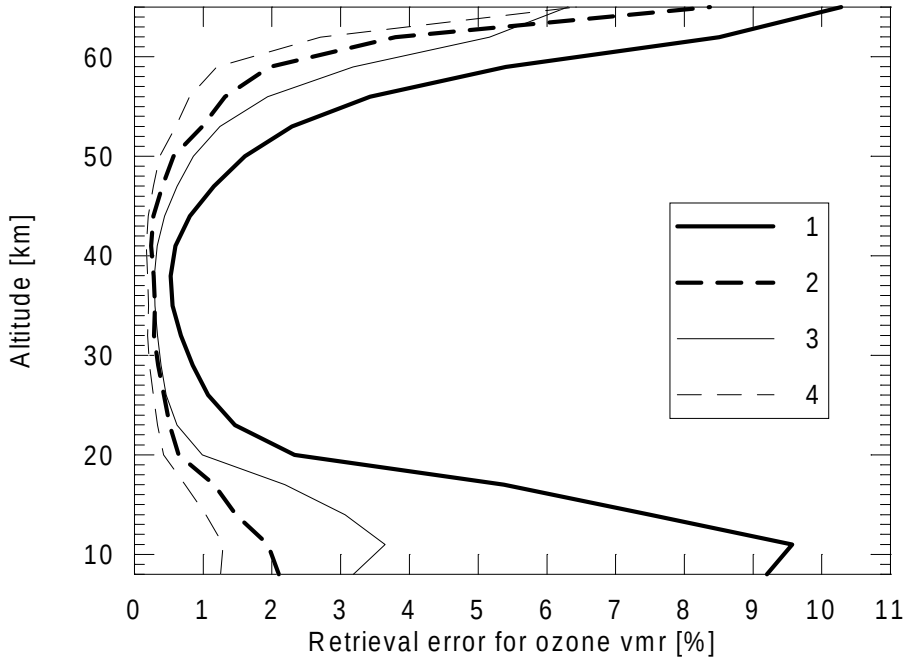

Fig. 6.38 The ozone retrieval errors estimated on the basis of error matrix calculations.
1 - GF, microwindows; 2 - OE, microwindows;
3 - GF, broad spectral intervals, 4 - OE, broad spectral intervals.

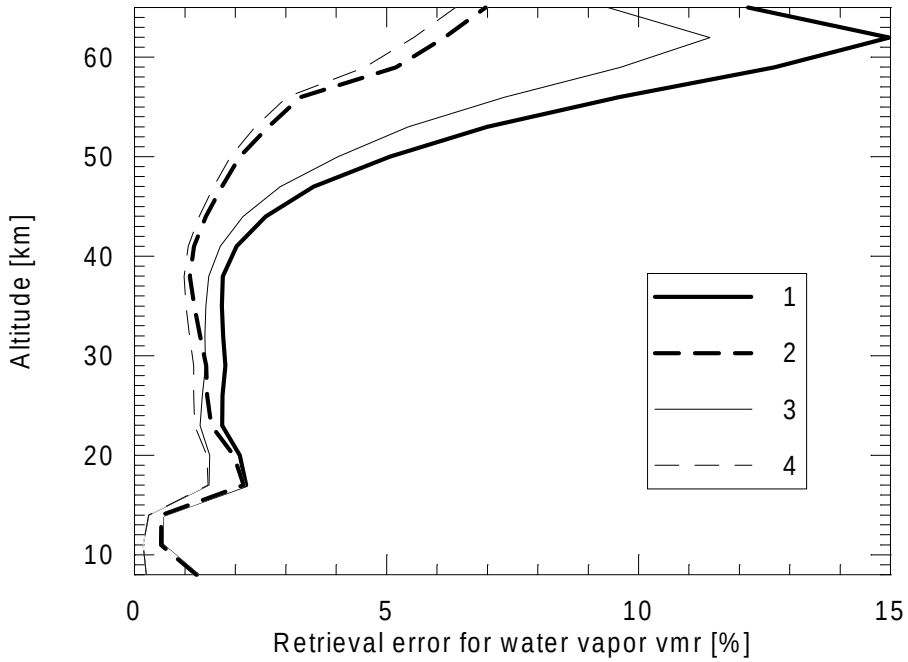

Fig. 6.39 The water vapor retrieval errors estimated on the basis of error matrix calculations.
1 - GF, microwindows; 2 - OE, microwindows;
3 - GF, broad spectral intervals, 4 - OE, broad spectral intervals.

6.6 The influence of the fine structure of profiles and atmospheric conditions on the retrieval accuracy.

The results of the numerical experiments performed for the selected set of models and described in the previous sections give the possibility to analyze the influence of the fine structure of profiles and atmospheric conditions on the retrieval accuracy. First, we must define what is meant by the term “fine structure of profiles”. The nature of the global fit method gives the possibility in the considered case to retrieve profiles of atmospheric parameters only at the altitude points which coincide with the tangent heights of measurements. The arbitrary altitude grid can not be used since in this case the inverse problem may become not well-determined for the GF method. Therefore we can define the fine structure as the peculiarities of the profiles with the characteristic scale not less than 3 km. Contrary to the GF method, the optimal estimation method is not bounded to the specific altitude grid because of the regularization of the inverse problem provided by the a priori information. However in the present study the altitude grid was chosen the same for both methods for the sake of the comparison of the results. So for the OE method we shall also consider the fine structure of profiles with the characteristic scale not less than 3 km. Obviously, the analysis of the fine structure has to be focused to the areas of considerable change of the gradient of the deviation of the mean profile from the model profile, i.e. to the areas where the deviation profiles are not smooth. The background for such a consideration is the linearization of the radiative transfer equation and the formulation of the inverse problem with respect to the deviations of the true profile from the mean profile.

It should be stressed that the specific limb scanning scenario is the primary mechanism which determines the possibility for the retrieval of the fine structure of profiles. In the present study we do not perform the rigorous investigation of the problem since we are bounded to the planned limb scanning scenario with vertical spacing of 3 km.

First, let us examine the p-T retrieval task. First, we pay attention to the fact that due to very smooth pressure profiles it makes no sense to analyze their fine structure. So we focus on the temperature retrievals. The most suitable for the consideration is the model M36 since the interference effects for this model were very small. One can see from the figure 6.12 that in the altitude region 11-26 km the gradient of the deviation of the mean temperature profile from the model profile changes its sign 3 times (the deviation profile is oscillating). Such a peculiarity may be treated as an example of fine structure. One can also see from figure 6.12 that the retrieval errors for temperature are very small in the altitude region under analysis. This is the evidence of the fact that both methods deliver accurate retrievals of the temperature values in the areas where the temperature profile has some peculiarities. The illustration is presented in Fig. 6.40 where the retrieved profiles are plotted but not the retrieval errors. As it can be seen from the figure, the temperature values at 17, 20 and 23 km are retrieved with high accuracy and the peculiar feature of the profile is adequately described. However, one can see a slight tendency to smoothing the profile at the altitude of 20 km, but still the errors do not exceed 1 K at this level.

Another example of the successful retrieval of the peculiarity of the temperature profile is the model M44, the vicinity of 26 km, where the local peak of the deviation of the mean profile from the model profile is located (see Fig. 6.10). One can see from figure 6.10 that the temperature retrieval errors at the altitude of 26 km are about 0.2 K for both methods. Similar situation is observed for the model M46 in the vicinity of 41 km (see Fig. 6.16).

In general, the following conclusion can be made: the fine structure of temperature profiles with the characteristic vertical scale not less than 3 km can be successfully retrieved by both methods in the altitude range 25-50 km where the interference effects are negligibly small. In the lower layers the elimination of these effects is the necessary prerequisite for the accurate retrievals.

As far as the ozone retrieval problem is concerned, we may point out that no general conclusions on the possibility to retrieve the fine structure of profiles can be made since the

selected model profiles do not have noticeable peculiarities. We can mention as an example only the good retrieval of the profile in the vicinity of 17 km for the model M44 (the area of the local minimum of the deviation of mean profile from the model profile), see Fig. 6.29. The investigation of the possibilities to retrieve fine structure of ozone profiles requires special modeling but the elimination of the interference effects must be done prior to this activity.

Contrary to the ozone test retrievals, the water vapor profiles of the models selected for the numerical experiments have many peculiarities. One can see from figures 6.32-6.35 that the deviations of the mean profile from the model profiles are not smooth and the sign of the gradient of the deviation profile is changing frequently. The most vivid example of the retrieval of fine structure of water vapor profile is the model M44, the altitude region 29-40 km. As it can be seen from the figure 6.35, in this altitude region the deviation of the mean profile from the model profile has the local peak. Fig. 6.35 also shows that the retrieval errors delivered by both methods are about 5% and less in this region. As an additional illustration we present Fig. 6.41 where the retrieved profiles are displayed but not the retrieval errors. Fig. 6.41 demonstrates successful retrieval of the peculiarities of the water vapor profile by both methods. However, the OE method delivers better results, for example for the level 35 km. In general one can conclude that in the altitude region 25-50 km the fine structure of profiles can be retrieved with good accuracy. The conclusion of the possibility to detect the fine structure in the lower layers can be made only after the interference effects are eliminated.

Now we pass to the discussion of the influence of atmospheric conditions on the retrieval accuracy. By the term “atmospheric conditions” we shall denote the whole set of parameters describing the atmospheric state including parameters which are to be retrieved and interfering ones. As it was shown in the previous sections for all considered tasks, the retrieval accuracy does not depend upon the specific profile in the statistical ensemble which is retrieved. The numerical experiments demonstrated high accuracy retrievals of all profiles in the altitude ranges where the interference effects were negligibly small. The vivid example can be presented: the good retrieval of the pressure profile for the model M44, see Fig. 6.9 (this was the case when the true pressure profile was considerably “far” away from the mean profile). Therefore the retrieval accuracy is influenced by the atmospheric conditions only through the mechanism of the error interference caused by the uncertainties of the parameters which are not controlled in the retrieval process. This conclusion was verified for all tasks and described in previous sections.

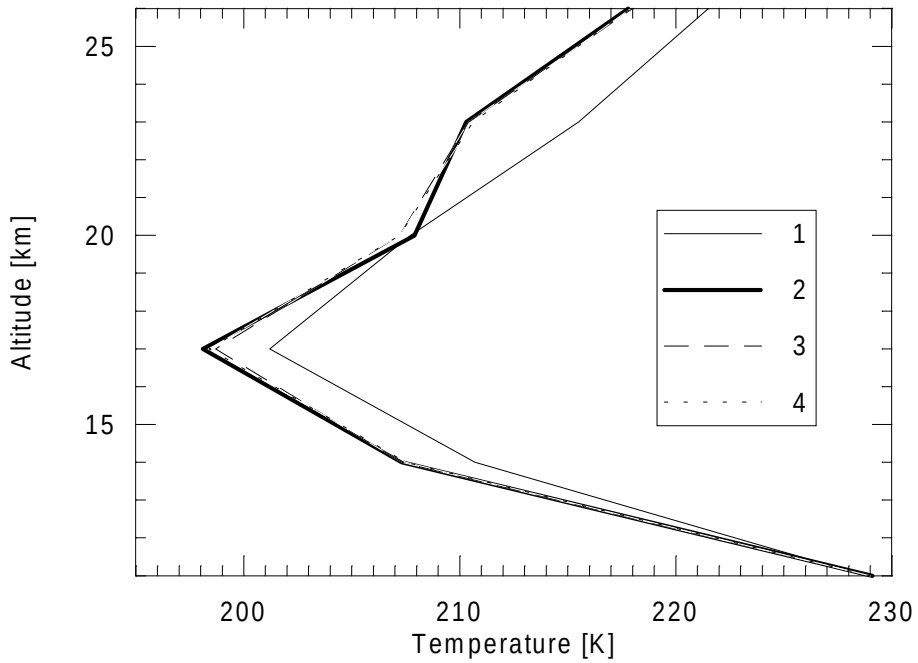

Fig. 6.40 The example of the retrieval of temperature profile. Model M36.
1 - mean profile, 2- model profile, 3 - retrieval by the GF method, 4 - retrieval by the OE method.

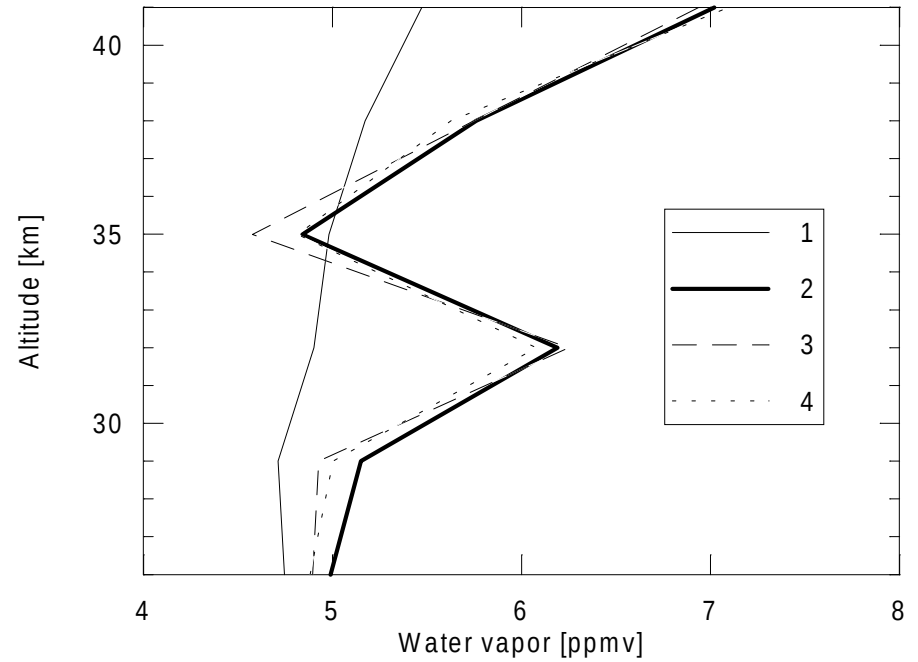

Fig. 6.41 The example of the retrieval of water vapor profile. Model M44.
1 - mean profile, 2- model profile, 3 - retrieval by the GF method, 4 - retrieval by the OE method.

6.7 The influence of the angular resolution of the instrument on the retrieval error estimations

The retrieval error estimations were made in the present study on the basis of several assumptions, in particular the assumption of the infinitesimal angular resolution of measurements. In order to estimate the influence of the finite angular resolution (FOV convolution function) on the retrieval accuracy of the parameters under investigation, several test calculations were performed. In these test calculations the above mentioned assumption was removed and the FOV function of the instrument was considered.

The FOV function which was used in the calculations is shown in figure 6.42. This function (5-point trapezium with the nodes at -2.0, -1.4, 0.0, 1.4, 2.0 km) is the one assumed for the MIPAS instrument.

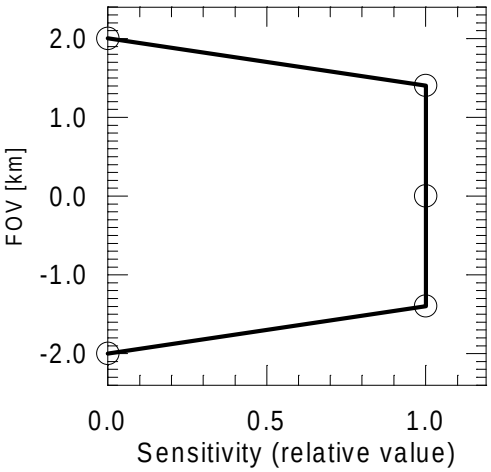

Fig. 6.42 FOV convolution function. The Y-axis shows the distance from the nominal tangent altitude.

Pressure-temperature retrieval.

First, the influence of the finite angular resolution on the retrievals was estimated on the basis of the error matrix calculations. Figure 6.43 shows the accuracy of the pressure and temperature retrieval for 2 cases: for the case of infinitesimal angular resolution and for the case of the convolution with the FOV function. One can see that the differences between the results obtained for these cases are very small. For the pressure retrieval the maximal difference is about 0.02 % and for the temperature retrieval it is about 0.08 K.

For the pressure retrieval the accuracy is lower in case of the finite spectral resolution up to the altitude of 45 km. In the vicinity of 55-60 km the accuracy of the retrieval in case of finite resolution is better than the accuracy in case of infinite resolution. However, this improvement is negligibly small.

For the temperature retrieval the accuracy is lower in the case of finite angular resolution in the altitude region 20-65 km and at the altitude point 8 km. In the layers 11-17 km the accuracy is better in the case of finite resolution than in the case of infinitesimal resolution.

This behavior of the retrieval accuracy profiles is caused by 2 mechanisms through which the FOV convolution function influences the retrievals. First, the weighting functions become more wide if compared to the case of infinitesimal resolution. Hence, the retrieval accuracy should become lower. However, due to the fact that the radiance is increasing for lower tangent altitudes approximately according to the exponential law and the FOV function is symmetrical, the radiance convoluted with the FOV function increases also, thus leading to the improvement of the signal-to-noise ratio. This is the second mechanism which causes the improvement of accuracy (contrary to the first mechanism). In different layers the first or second mechanism prevails leading correspondingly to the lowering or improvement of the retrieval accuracy.

As an example of the numerical experiment accounting for the FOV function, we present here the results of the pressure-temperature retrieval for the model M31. This model was selected since previous results displayed very good retrieval in the middle and upper layers and at the same time the oscillations in the lower layers (due to the uncertainties of the ozone and water vapor profiles). The retrieval errors for pressure and temperature for the model M31 in the case of the finite angular resolution are presented in figure 6.44. For the sake of comparison, previous results are also shown (infinitesimal angular resolution).

One can notice that there is a considerable difference in the results of the pressure profile retrieval below 35-40 km. The errors of both methods in the case of finite angular resolution are much larger than in the case of infinite resolution and reach the maximal value of 5% at 8 km altitude. The retrieval errors for both methods in the case of the finite resolution are practically identical. For the temperature profile retrieval there is no influence of the FOV function on the results above 25 km. Below 25 km, in the area of oscillations, the errors in the case of the FOV convolution function are larger than the errors in the case of infinitesimal resolution by about 5 K.

The accuracy estimations made on the basis of error matrix calculations showed that the influence of the finite angular resolution on the accuracy should be negligibly small throughout the atmosphere, and the results of the numerical experiment which was made as an example delivered noticeable differences in the lower layers. However there is no contradiction, since the error matrix does not take into account the possible uncertainties of the interfering atmospheric parameters. And in the case when the interference is large, the convolution with the FOV function amplifies the effect of the accuracy degradation through the above mentioned first mechanism.

Ozone and water vapor retrieval.

For the ozone and water vapor retrieval tasks we present the estimation of the influence of the finite angular resolution on the retrieval accuracy made on the basis of error matrix calculations.

Figure 6.45 (upper panel) shows the retrieval errors for ozone profiles. One can see that the influence of the finite angular resolution on the ozone retrieval accuracy is negligibly small for the optimal estimation method. The difference between the considered cases does not exceed 0.1%. Contrary to the optimal estimation method, the noticeable differences are delivered by the global fit method: about 3% in the lower and upper layers and about 1% in the altitude region 11-50 km. The reason for such an effect is that the measurements are not so informative with respect to the ozone profile as with respect, for example, to the pressure and temperature profiles in the p-T retrieval task. Therefore the changes of the weighting functions produce larger effect on the retrieval errors. However, in the case of the OE method, the additional a priori information plays noticeable role in the retrieval process diminishing the effect produced by the FOV function.

The lower panel of the figure 6.45 shows the retrieval errors for water vapor profiles. One can see that the influence of the finite angular resolution on the water vapor retrieval accuracy is very small for the optimal estimation method. The difference between the considered cases is about 1.5% only in the vicinity of 17 km, and for the other altitudes it is less than 1%. As it was in the case of the ozone profile retrieval, the global fit method delivers larger differences which constitute about 2% above 17 km and reach 5% in the vicinity of 65 km altitude. Below 17 km the differences are very small.

Conclusion.

The estimations of the influence of the finite angular resolution of measurements on the retrieval accuracy made on the basis of the error matrix calculations have shown the following:

1) The influence of the finite resolution on the pressure-temperature retrieval is negligibly small for both OE and GF methods given tangent height spacing of 3 km and FOV of 3 km.

2) The influence of the finite resolution on the ozone retrieval is negligibly small for the OE method, but for the GF method the corresponding effect is equal to the lowering of accuracy by about 1-3%.

3) The influence of the finite resolution on the water vapor retrieval is small for the OE method, but for the GF method the corresponding effect is equal to the lowering of accuracy by about 2-5%.

The test retrieval of pressure and temperature profiles showed that the uncertainties of the interfering parameters can amplify the influence of the FOV function on the retrieval accuracy. However, the relative behavior of the error profiles for the OE and the GF methods remains the same as in the case of the infinitesimal angular resolution.

Therefore, the results obtained in the course of the study under the assumption of the infinitesimal angular resolution measurements are a good estimate even for the general case which accounts for the FOV convolution function.

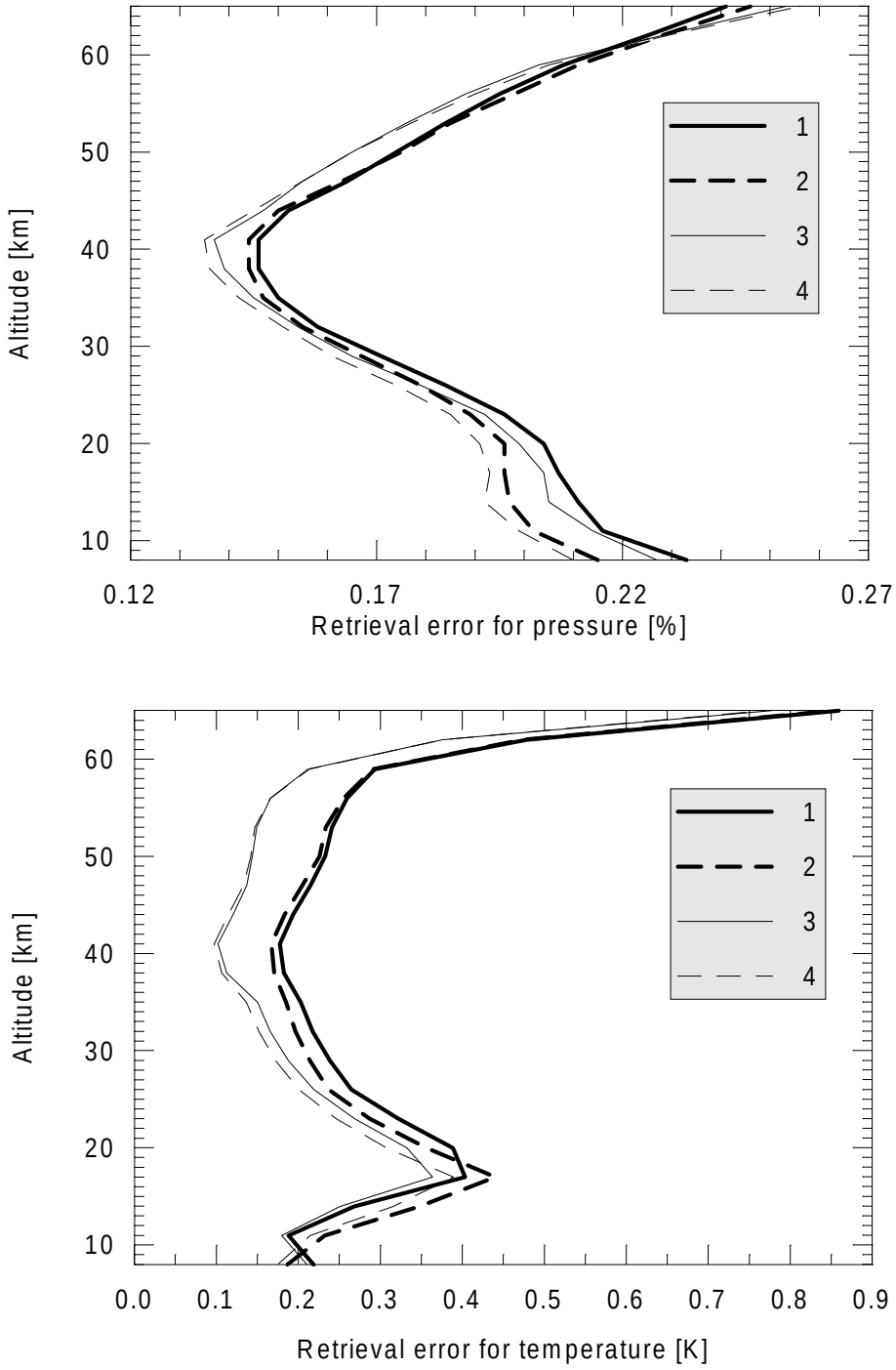

Fig. 6.43. Comparison of the pressure and temperature retrieval errors (upper and lower panels correspondingly) in the cases of infinite and finite angular resolution of the instrument.

1 - GF method, FOV is taken into account;
2 - GF method, infinite angular resolution;
3 - OE method, FOV is taken into account;
4 - OE method, infinite angular resolution.

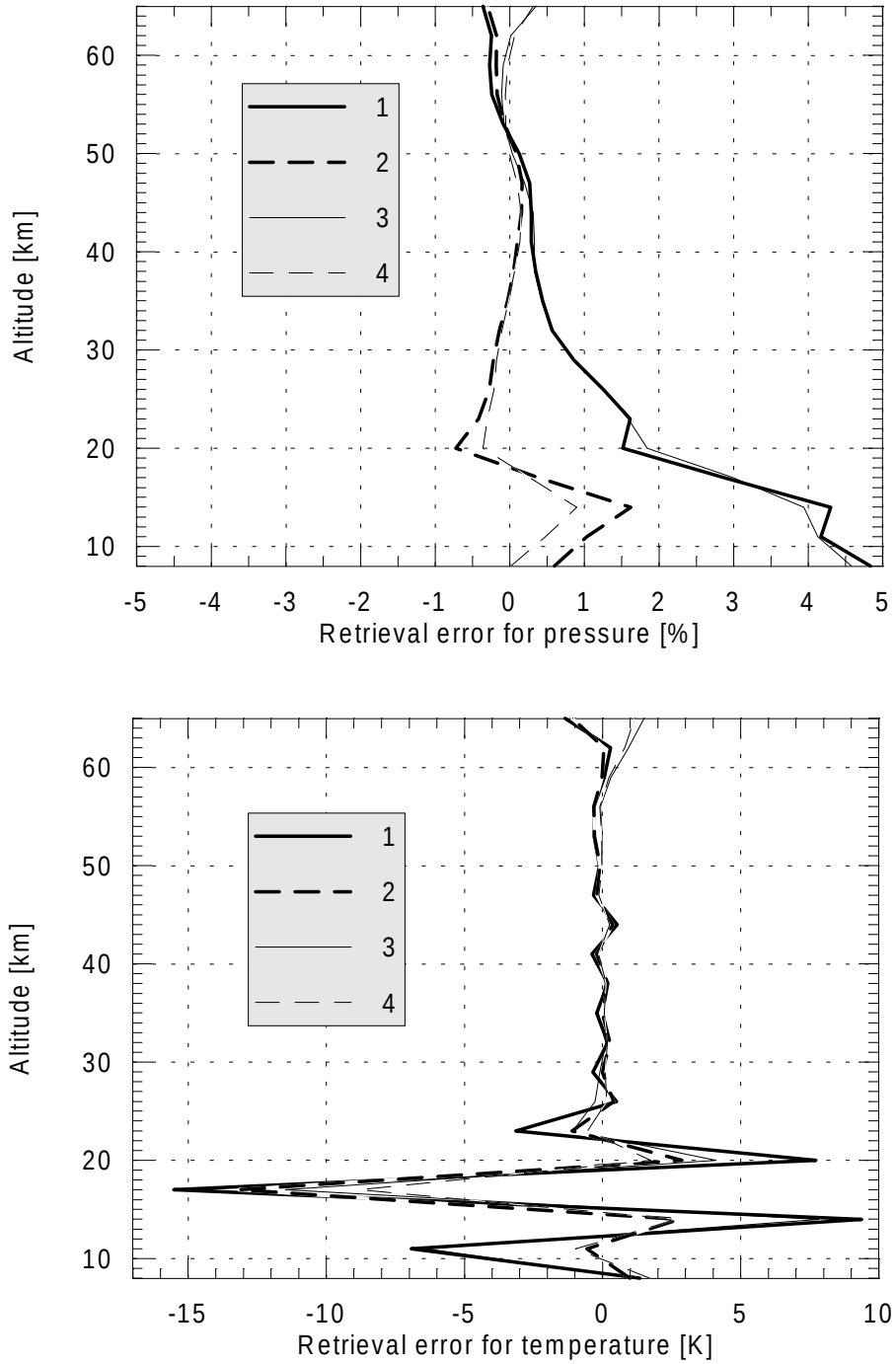

Fig. 6.44. The results of pressure and temperature retrieval in the numerical experiment (upper and lower panels correspondingly).

1 - GF method, FOV is taken into account;
2 - GF method, infinite angular resolution;
3 - OE method, FOV is taken into account;
4 - OE method, infinite angular resolution.

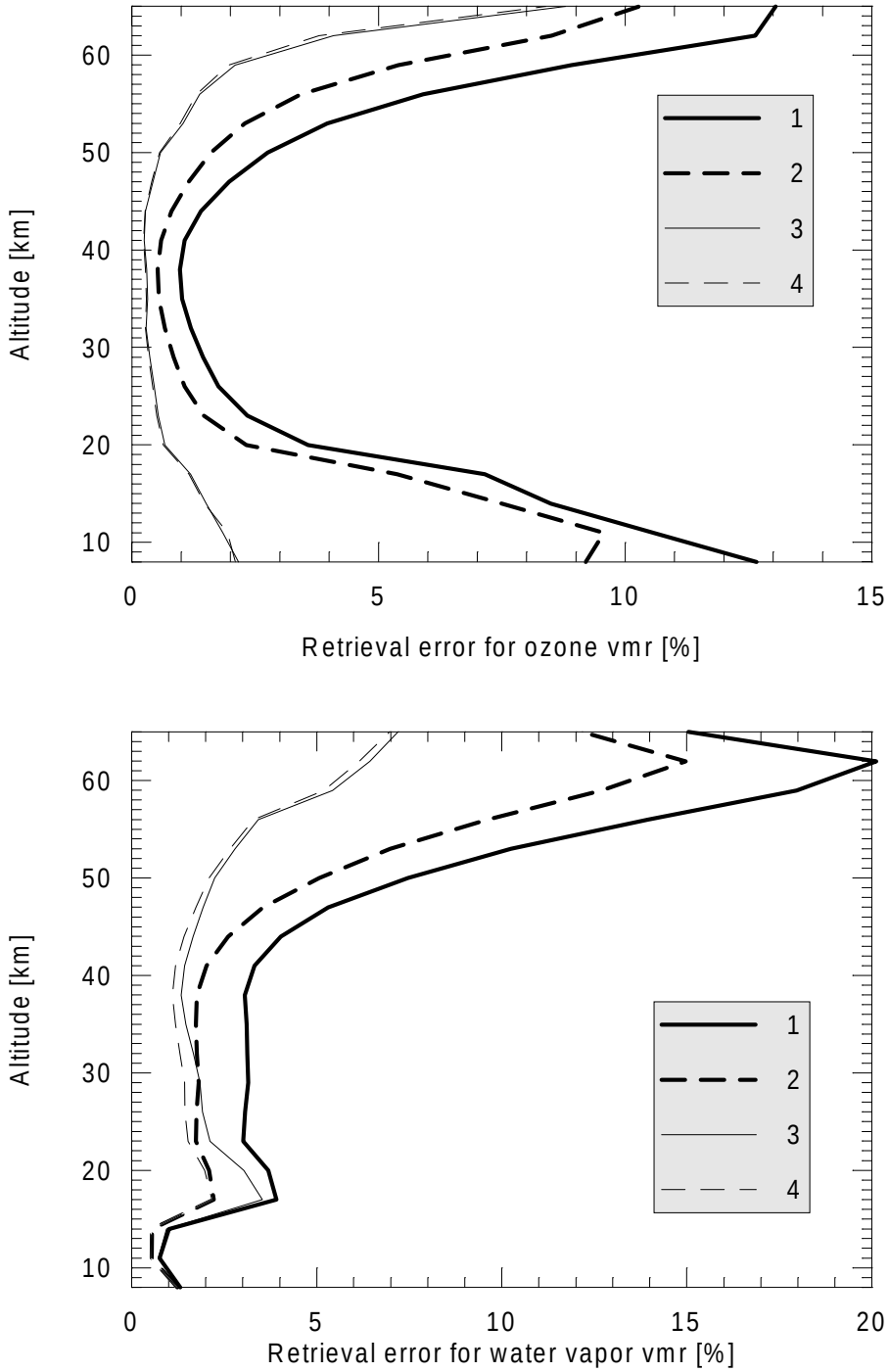

Fig. 6.45. The results of ozone and water vapor retrieval in the numerical experiment (upper and lower panels correspondingly).

1 - GF method, FOV is taken into account;
2 - GF method, infinite angular resolution;
3 - OE method, FOV is taken into account;
4 - OE method, infinite angular resolution.

6.8 The influence of the hydrostatic approximation constraint on the p-T retrievals

Finally we present the estimation of the influence of the hydrostatic approximation constraint on the accuracy of the retrieval of the pressure and temperature profiles. Figure 6.46 shows the accuracy estimations based on the error matrix calculations for the cases when the hydrostatic constraint was included in the retrieval algorithm and not included. (It should be noted that all the results presented above were obtained accounting the hydrostatic constraint.)

One can see from figure 6.46 (upper panel) that in case of the retrieval without hydrostatic constraint the accuracy for the pressure profile is quite different for the GF and the OE methods. The maximal difference is about 1% and is observed at the altitude of 17 km. Above 25 km altitude the difference is not large and is about 0.1-0.2%. We stress that when hydrostatic constraint is applied, there is practically no difference between the accuracy estimations for the GF and the OE methods. As an illustration, we presented (by the dots) the accuracy estimations for the GF/OP (global fit / onion peeling) algorithm without hydrostatic constraint reported by *Clarmann et al.* [1995]. One can see that there is a good qualitative agreement in the vertical behavior of the accuracy profiles. However, the estimations reported by Clarmann et al. [1995] appear to be about 0.5-1% larger than ones obtained in the present study. It should be kept in mind, however, that the algorithmic and computational implementations of the retrieval procedure were to a certain extent different in the present study and in the study by *Clarmann et al.* [1995]. For example, in the present study the inverse problem was set with respect to the CO_2 number density and fixing of the CO_2 volume mixing ratio was implemented with the help of additional constraint which involved the pressure and temperature profile variations together with the variations of the CO_2 number density. Furthermore: (1) in the study by *Clarmann et al*. [1995] the noise correlations were taken into account; (2) these authors took interlayer parameter correlations in an a posteriori manner, rather than during the fit.

The results corresponding to the temperature retrieval are presented in the bottom panel of Figure 6.46. As it can be seen, the application of the hydrostatic constraint does not have a significant influence on the temperature profile retrieval accuracy (the differences between the estimation for the considered cases do not exceed 0.05 K. For the global fit method, there are practically no differences up to the altitude of 17 km, but above this altitude the effect is much more pronounced. If the hydrostatic constraint is added to the GF method, the improvement of accuracy of the temperature profile retrieval can reach up to 0.5-1 K in the altitude region 40-65 km. The estimation of the accuracy of the temperature profile retrieval by the GF/OP method without hydrostatic constraint obtained in the study by *Clarmann et al.* [1995] is shown by dots. Good qualitative agreement with the results of the present study is observed throughout the atmosphere and good qualitative agreement takes place up to about 30 km altitude. Contrary to the pressure profile retrieval, the estimations of the temperature profile retrieval accuracy obtained by *Clarmann et al.* [1995] are smaller than ones obtained in the present study. Possible reasons for such descrepancy were mentioned above. The detailed investigation of the discrepancies was beyond the scope of present work.

In conclusion, we stress that different aspects of the application of hydrostatic constraint require special analysis because of considerable horizontal averaging which occurs because of limb observation geometry, satellite movement and not infinitesimal time of limb scanning.

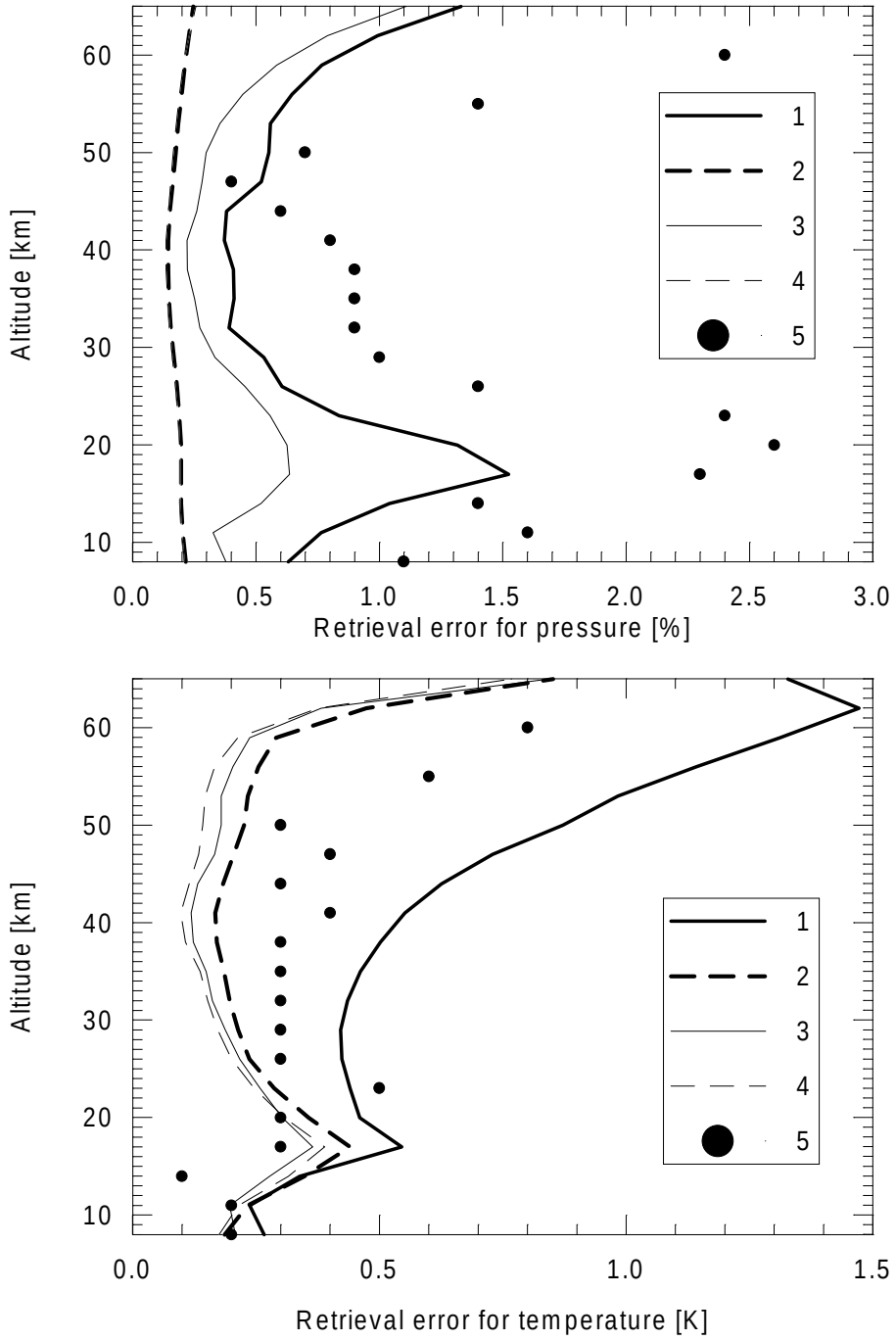

Fig. 6.46. The influence of the hydrostatic constraint on the accuracy of pressure and temperature retrievals.

1 - global fit, without constraint

2 - global fit, with constraint

3 - optimal estimation, without constraint

4 - optimal estimation, with constraint

5 - retrieval without hydrostatic constraint: error estimations by *Clarmann et al.* [1995]

7. Conclusions and recommendations

In the course of the present study 3 inverse problems were investigated on the basis of numerical experiments: pressure-temperature retrieval, ozone profile retrieval and water vapor profile retrieval from the limb radiance measurements. The aim of the investigations was to compare the applicability of the global fit and the optimal estimation methods to the processing of the data. The measurement scenario was taken close to that of the planned MIPAS space mission. The following simplifications were used: infinitesimal angular resolution of measurements, uncorrelated random noise, no offset and gain calibration errors. The limb measurements were simulated in the microwindows preselected for the appropriate retrieval tasks, but fitting of the background quasicontinuum (for the compensation of the contribution from interfering parameters) was not performed. The assumptions and simplifications mentioned above, however, do not influence the relative comparison of the global fit and the optimal estimation methods and the results which were obtained in the course of the study should be a good estimate for more general case.

Pressure-temperature retrieval task.

The retrieval errors for pressure and temperature profiles are small in the altitude range 25-60 km and are characterized by the values less than 1% and 1 K correspondingly (in some cases the errors were even smaller). This is the indication of the high information content of measurements on one side, and the indication, on the other side, of the negligibly small influence of the interfering parameters (water vapor and ozone) on the p-T retrievals in the mentioned altitude region.

The retrieval errors at the altitudes higher than 60 km increase. However for the OE method this increase is not significant. For the GF method the retrieval errors can be quite large: up to 3-5 K for temperature values. These results are explained by the decrease of the signal-to-noise ratio for the measurements at the upper tangent altitudes for both methods. Besides, for the GF method this is an indication of the error propagation from the upper levels (higher than 65 km) where the temperature profile is required by the GF method to be fixed to a priori profile.

The altitude range 8-25 km is the most problematic for p-T retrieval. There were test cases with the high accuracy retrievals and low accuracy retrievals as well. The low accuracy retrievals concern mainly to the temperature retrieval problem, while results of the pressure profile retrieval were satisfactory in the majority of cases (it should be noted that the hydrostatic constraint was implemented in the retrieval algorithm). It was shown that the low accuracy of the temperature and pressure retrievals in the lower layers is stipulated by the interference from the uncertainties of the ozone and the water vapor profiles. This is due to the fact that the microwindows were defined for simultaneous fitting of the background continuum (which would compensate for interference), but in the present study such fitting was not done.

The GF and the OE methods produced nearly identical results in the altitude range 25-60 km. In the ranges 8-25 km and 60-65 km the OE method showed better accuracy in some cases. Besides, the OE method demonstrated faster convergence of the iterative process. For the GF method 1-3 extra steps were necessary to satisfy the convergence criterion.

The results of the retrievals do not depend upon the probability of the specific profile in the statistical ensemble. This is the consequence of the fact that the inverse problem is well-determined. The set of preselected microwindows is very informative with respect to pressure and temperature and therefore there is a possibility to retrieve even the “exotic” profiles which have the low probability to appear.

So the following main conclusion can be made: due to the high information content of limb radiance measurements in the microwindows preselected for p-T retrieval the global fit and the optimal estimation methods produce the results which do not differ significantly (the error estimations made on the basis of error matrix calculations confirm this conclusion). This means that the contribution of the a priori information used in the optimal estimation method is negligibly small if compared to the information delivered by the limb measurements

themselves. However, the a priori information plays stabilizing role in the iterative retrieval process thus leading to more fast convergence of the iterative process and in the specific cases to smaller errors at the levels where these errors are oscillating because of the interference of the water vapor and ozone profiles.

Test retrievals with different random sequences of the detector noise values showed that the scattering of retrieval errors is quite small and does not influence the results and conclusions obtained for specific random sequence which was used in the majority of tests.

It was shown also that the retrieval results do not depend on the selection of the initial guess and on the atmospheric state (fine structure of profiles): in the altitude range 25-60 km the retrieval accuracy was very high for all models considered and both retrieval methods.

Ozone retrieval task.

In the most retrieval cases the following peculiarities showed up:

- the retrievals are very good for both GF and OE methods in the altitude range 25-50 km (the errors are less than 2%);
- both methods deliver larger errors below 25 km and above 50 km. In the lower layers the errors of the GF method can reach 30% and the errors of the OE method can reach 15%. In the upper layers the errors of the GF method can reach hundreds of percent while the errors of the OE method - only dozens of percent;
- the errors of the GF method are considerably larger than the errors of the OE method (excluding the region of high accuracy retrievals 25-50 km);
- the convergence of the iterative process is slower for the GF method.

High accuracy retrievals in the altitude range 25-50 km demonstrate high information content of the preselected set of microwindows with respect to the ozone profile in this area. As a consequence, there is practically no difference between the results delivered by the global fit and the optimal estimation methods at the correspondent altitudes.

It was shown that the increase of errors in the lower layers is explained by the interference from the uncertainties in the pressure, temperature and water vapor profiles.

In the upper layers the decrease of accuracy is caused by the decrease of signal-to-noise ratio for both methods and additionally by error propagation effect for the GF method.

So the following main conclusion can be made: in the ozone retrieval problem the optimal estimation method is more preferable than the global fit method in the altitude ranges 8-20 km and 50-65 km and there is practically no difference between the methods in the altitude range 20-50 km. This conclusion is confirmed by the test retrievals and by the error estimations on the basis of error matrix calculations. Another advantage of the optimal estimation method is its faster convergence.

Water vapor retrieval task.

The water vapor retrieval problem appeared to be very sensitive to the interference from the uncertainties of pressure, temperature and ozone profiles. In most of test retrievals the iterative process diverged at the 8 km altitude level for the selected values of SSR. It was shown that the divergence was the consequence of the interference from the uncertainties in the pressure, temperature and ozone profiles. As a consequence the region 8-25 km was characterized by the large retrieval errors for both methods reaching dozens of percent.

The most accurate retrievals took place in the altitude range 25-45 km for both methods where the errors were mainly less than 5%. However in this region the OE method delivered more smooth solution.

In the region 45-65 km the errors increased due to the decrease of signal-to-noise ratio for both methods. Additionally for the GF method the error propagation effect was another error source and in some cases the GF method delivered errors of more than 50% at the upper altitudes.

So the main conclusions may be formulated as follows: a) in the water vapor retrieval problem the interference of other parameters dramatically influences the results and in most cases makes the determination of water vapor profile in the vicinity of 8 km impossible ; b) the

GF and the OE methods deliver practically the same results up to the altitude of 45 km, in the higher layers the OE method is much preferable.

Recommendations.

The analysis of the numerical experiments showed, first of all, that there may be a considerable influence of the uncertainties of the interfering parameters on the retrieval accuracy of the target parameters. Therefore it is necessary to utilize completely the advantages of the microwindow concept and to perform the fitting of the wavenumber-independent background quasicontinuum which includes such type of interference implicitly.

The analysis of the numerical experiments also revealed the areas of further research activities aimed to develop efficient algorithms and computer codes for the processing of the MIPAS data.

1) It can be recommended to perform the numerical experiments on the retrieval of the vertical profiles of atmospheric parameters other than pressure, temperature, ozone and water vapor with a simultaneous fitting of the background quasicontinuum.
2) It is necessary to make special investigations of the efficiency of different criteria of termination of the iterative process and to select the optimal criterion (it was shown that the criterion based on spectral fitting did not deliver the best results, and in the presence of the interference effects the criterion based on the shift of solution sometimes also failed).
3) The problem of speeding up the convergence of the iterative process also requires attention. The possible solution is the selection of the initial guess by special high performance algorithm.
4) The influence of the offset and gain calibration error on the retrieval accuracy should be investigated.
5) Since the non-LTE effects are present for a number of absorption bands of atmospheric gases it can be recommended to investigate the retrieval accuracy accounting for these effects.

Acknowledgments

The authors express their gratitude to Prof. Dr. W.L.Smith for the TIGR data and to Dr. M.Gunson and Dr. P.DeCola for the ATMOS data.

References

Abbas, M.M., et al., Finite fields of view effects on inversion of limb thermal emission observations, *J.Geoph Res.*, **90**, No D2, 3903-3909, **1985.**

Anderson, G.P., S.A.Clough, F.X.Kneizys, J.H.Chetwynd, and E.P.Shettle. AFGL Atmospheric Constituent Profiles (0-120km). AFGL-TR-86-0110, Environmental research papers, N 954, 43p., **1986**.

Backus, G.E., and J.F. Gilbert, Uniqueness in the inversion of inaccurate gross Earth data, *Philos. Trans. R. Soc. London, Ser. A,* **266**, 123-192, **1970.**

Bailey, P.L., and J.C. Gille, Inversion of limb radiance measurements: An operational algorithm, *J.Geoph Res.*, **91**, No. D2, 2757-2774, **1986.**

Carlotti, M., Global fit approach to the analysis of limb-scanning atmospheric measurements, *Appl. Opt.*, **27**, No. 15, 3250-3254, **1988.**

Clarmann, T.v., H. Fischer, and H. Oelhaf, Instabilities in retrieval of atmospheric gas profiles caused by the use of atmospheric level models, *Appl. Opt.*, **30**, No. 21, 2924-2925, **1991**.

Clarmann, T.v., et al., Retrieval of stratospheric O_3, HNO_3 and $ClONO_2$ profiles from 1992 MIPAS-B limb emission spectra: method, results and error analysis, *J. Geoph. Res.*, **98,** No. 11, 26495-26506, **1993a**.

Clarmann, T.v., H. Oelhaf, and H. Fischer, Retrieval of atmospheric O_3, HNO_3 CFC-11, and CFC-12 profiles from MIPAS-B-89 limb emission spectra, *Appl. Opt.*, **32**, No. 33, 6808-6817, **1993b**.

Clarmann, T.v., A.Linden, and H.Oelhaf, The simultaneous retrieval of pressure and temperature from the MIPAS limb emission spectra. Final report. ESA purchase order No 131253, Institut für Meteorologie und Klimaforschung, Kernforschungszentrum Karlsruhe / Universität Karlsruhe, **1994**.

Clarmann, T.v., A.Linden, and G.Echle, The retrieval of pressure and temperature from MIPAS limb emission spectra. *Final Report. ESA Purchase Order No. 142957.* Institut für Meteorologie und Klimaforschung, Forschungszentrum Karlsruhe / Universität Karlsruhe, **1995.**

Conrath, B.J., Vertical resolution of temperature profile obtained from remote radiation measurements, J.Atmos.Sci., Vol. 29, No 7, pp. 1262-1271, **1972**.

Dudhin, A., and N.Livesey, Validation of temperature measurements from the improved stratospheric and mesospheric sounders. J.Geoph.Res., Vol. 100, No D6, pp. 9795-9809, **1996**.

Echle, G., H. Oelhaf, and A. Wegner, Measurements of atmospheric parameters with MIPAS, Final Report, Institut fur Meteorologie and Klimaforschung, Kernforschungszentrum/ Universitat Karlsruhe, 327 pp., **1992**.

Echle, G., H. Oelhaf, and A. Wegner, On the potential of IR limb emission spectroscopy for the measurement of stratospheric composition, *J. Quant. Spec. Rad. Trans.*, **52**, No. 3/4, 253-265, **1994**.

Echle, G., H.Oelhaf, T.v.Clarmann, and M.Schmidt, Definition of spectral intervals for the retrieval of trace gas concentrations from MIPAS limb emission spectra, *Final Report. ESTEC Contract No. 10993/94/NL/PR*, April **1995**.

Endemann, **M.,** P. Garé, D.J. Smith, K. Hoerning, B. Fladt, and R. Geßner, MIPAS Design Overview and Current Development Status. Proceedings Europto Series, „Optics in Atmospheric Propagation, Adaptive Systems, and Lidar Techniques for Remote Sensing", A.D. Devir, A. Hohnle, and C. Werner (Eds.), European Symposium on Satellite Remote Sensing III, 24-26 Sep. **1996**, Taormina, Italy *SPIE* Volume 2956, pp 124 - 135.

Fischer, H., and H.Oelhaf, Remote sensing of vertical profiles of atmospheric trace constituents with MIPAS limb-emission spectrometers, *Appl. Opt.*, **35**, No 16, pp. 2787-2796, **1996.**

Gille, J.C., and F.B. House, On the inversion of limb radiance measurements : Temperature and thickness, *J. Atm. Sci.*, **28,** 1427-1442, **1971.**

Gille, J.C., and J.M. Russell III, The limb infrared monitor of the stratosphere: experimental description, performance and results, *J. Geoph. Res.*, **89**, No. D4, 5125-5140, **1984.**

Gille, J.C., et al., Validation of temperature retrievals obtained by the Limb Infrared Monitor of the Stratosphere (LIMS) experiment on Nimbus 7, *J. Geoph. Res.*, **89,** No. D4, 5115-5124, **1984.**

Hollweg, H.-D., V.S.Kostsov, G.Schlüssel, P.Schlüssel, Yu.M.Timofeyev, M.V.Tonkov, A.V.Polyakov, and N.N.Filippov, Interaction at mm and Optical Frequencies. Part II: Specific Atmospheric Absorption and Emission Features: Investigation and Modeling. Final Report. ESA ESTEC Contract No. 10603/93/NL/NB. Zentrum für Meeres- und Klimaforschung der Universität Hamburg, Meteorologisches Institut, **1995**.

Houghton, J.T., F.W. Taylor, and C.D. Rodgers, Remote Sounding of Atmospheres, *Cambridge University Press*, Cambridge, **1984**.

Humlicek, J., Optimized computation of the Voigt and complex prbability functions, JQSRT, Vol. 27, No 4, pp. 437-444, **1982**.

Kondratyev, K.Ya., and Yu.M. Timofeyev, Thermal Sounding of the Atmosphere from Satellites, *Gidrometeoizdat*, Leningrad (in Russian), **1970.**

Kondratyev, K.Ya., and Yu.M. Timofeyev, Meteorological Sounding of the Atmosphere from Space, *Gidrometeoizdat*, Leningrad (in Russian), **1978.**

Kostsov, V.S., H.Fischer, Yu.M.Timofeyev, and H.Oelhaf, Numerical modeling of the influence of non-LTE effects on the MIPAS balloon and satellite limb radiance

measurements. Wissenschaftliche Berichte FZKA 5860, Forschungszentrum Karlsruhe, December **1996**.

Kumer, J.B., and J.L. Mergenthaler, Pressure, temperature and ozone profile retrieval from simulated atmospheric earth-limb infrared emission, *Appl. Opt.*, **30,** No. 9, 1124-1131, **1991.**

Marquardt, D.W., An algorithm for the least-squares estimation of nonlinear parameters, *J. Soc. Appl. Math*, **11,** 431, **1963.**

Marks, C.J., and C.D. Rodgers, A retrieval method for atmospheric composition from limb emission measurements, *J. Geoph. Res.*, **98,** 14939-14953, **1993.**

Norton, R.H., and R.Beer, New apodizing functions for Fourier spectrometry, *J. Opt. Soc. Am.*, Vol. 66, No 3, pp. 259-264, March **1976**.

Oelhaf, H., and H. Fischer, Measurements of minor constituents in the middle atmosphere from IR limb emission spectra - a feasibility study. Universitat Munchen - Meteorologisches Institut, Wissenschaftliche Mitteilung, Nr. 47, Februar 1983, 182 pp., **1983.**

Pokrovsky, O.M., and Yu.M. Timofeyev, Common statistical approach to solution of inverse problems of atmospheric optics, *Meteor. and Hydrol*., 1, 72-81, (in Russian), **1972.**

Polyakov, A.V., On the matter of using a priori statistical information for solving the non-linear inverse problems of atmospheric optics, *Earth Res. from Space*, 3, 11-17 (in Russian), **1996.**

Polyakov, A.V. and Rozanov V.V., Iterative method of solving the non-linear inverse problems with using *a priori* information, *Trudi of GosNICPR*, 33, 99-103 (in Russian), **1989.**

Reber C.A., The upper atmosphere research satellite (UARS), *Geophys. Res. Lett.*, Vol.20, 1215-1218, **1993**.

Remsberg, E.E. et al., The validation of NIMBUS 7 LIMS measurements of ozone, *J. Geoph. Res.*, **89**, No. D4, 5161-5178, **1984.**

Rodgers, C.D, Some theoretical aspects of remote sounding in the Earth's atmosphere, *Journ. Quant. Spect. Rad. Trans*, **11**, 767-777, **1971.**

Rodgers, C.D., Retrieval of atmospheric temperature and composition from remote sounding measurements of thermal radiation, *Rev. Geoph. Space Phys.*, **14,** 609-624, **1976.**

Rodgers, C.D., Characterization and error analysis of profiles retrieved from remote sensing measurements, *J. Geoph. Res.*, **95,** 5587-5595, **1990.**

Russell III, J.M., et al., Validation of water vapor results measured by the Limb Infrared Monitor of the Stratosphere experiment on Nimbus 7, *J. Geoph. Res.*, **89**, No. D4, 5115-5124, **1984.**

Strand, O.N., and E.R. Westwater, The statistical estimation of the numerical solution of a Fredholm integral equation of the first kind, *Journ. Assoc. Mach.*, **15**, 100, **1968.**

Tikhonov, A.N., and V.Ya. Arsenin, Solutions of Ill-Posed Problems, *Winston*, Washington, **1977.**

Timofeyev , Yu.M., Satellite methods of study of gaseous content of atmosphere (a review), *Izvestiya, Atm. and Ocean. Physics*, **25**, 451-472 (English transl.), **1989**.

Turchin, V.F., M.S. Malkevich, and I.A. Gorchakova, Applying of statistical regularization method to retrieve atmospheric vertical temperature profile, *Izvestiya, Atm. and Ocean. Physics*, **5**, 5 (in Russian), **1968**.

Turchin, V.F., V.P. Kozlov, and M.S. Malkevich, Applying the methods of mathematical statistics for solving ill-posed problems, *Progress in Physical Sciences*, **102**, 3, 345-386 (in Russian), **1970**.

Appendix 1: Variations of profiles in the atmospheric models

Pressure profile deviations [%] for the models M1-M12

Z,km	M 1	M 2	M 3	M 4	M 5	M 6	M 7	M 8	M 9	M10	M11	M12
80.	19.7	20.9	44.5	-12.9	-11.4	4.1	-12.7	-9.3	-15.8	-13.8	-16.5	3.9
77.	16.9	20.1	38.7	-11.1	-9.3	4.8	-13.5	-10.7	-12.7	-10.2	-14.0	3.8
74.	16.6	18.5	35.8	-10.3	-8.1	5.0	-13.7	-11.2	-10.3	-7.8	-12.3	4.2
71.	16.6	16.3	33.2	-10.3	-7.5	4.1	-12.8	-11.0	-9.1	-6.8	-11.1	5.2
68.	15.6	13.4	28.4	-10.9	-7.8	2.4	-11.8	-10.9	-8.5	-6.7	-10.1	5.8
65.	13.1	9.8	22.6	-11.4	-8.5	0.2	-11.7	-10.9	-8.2	-7.3	-9.2	5.0
62.	10.1	6.4	17.8	-11.3	-9.3	-1.8	-11.4	-10.3	-8.4	-8.4	-9.1	3.5
59.	7.7	3.6	14.0	-11.0	-10.0	-3.5	-10.5	-9.5	-8.6	-9.5	-9.2	2.1
56.	5.8	1.5	11.0	-10.7	-10.4	-4.8	-9.9	-8.9	-8.7	-10.4	-9.3	1.0
53.	4.3	-0.1	8.7	-10.6	-10.5	-5.7	-9.4	-8.5	-8.8	-11.0	-9.4	0.1
50.	3.1	-1.4	6.7	-10.3	-10.6	-6.3	-8.8	-8.0	-8.8	-11.4	-9.4	-0.6
47.	2.2	-2.4	5.0	-9.9	-10.3	-6.7	-8.2	-7.6	-8.6	-11.5	-9.3	-1.1
44.	1.8	-2.8	3.7	-9.4	-9.4	-6.7	-7.7	-6.9	-8.1	-11.2	-8.8	-1.1
41.	2.0	-2.5	3.0	-8.7	-7.8	-6.4	-7.3	-6.0	-7.2	-10.5	-7.9	-0.5
38.	2.6	-1.5	2.7	-8.1	-5.7	-5.9	-7.2	-5.1	-6.0	-9.5	-6.8	0.3
35.	3.0	-0.1	2.5	-7.6	-3.7	-5.1	-7.0	-4.5	-4.8	-8.3	-5.7	1.2
32.	2.8	1.0	2.3	-7.1	-2.2	-4.3	-6.4	-3.9	-3.7	-7.0	-4.9	1.6
29.	2.0	1.5	1.7	-6.5	-1.3	-3.6	-4.9	-3.2	-2.5	-5.7	-4.4	1.5
26.	1.1	1.4	1.1	-5.8	-0.9	-3.2	-3.2	-2.7	-1.5	-4.2	-4.0	0.9
23.	0.6	1.0	1.1	-4.8	-1.0	-2.5	-2.1	-2.5	-0.9	-2.9	-3.7	0.4
20.	0.7	0.6	1.7	-3.3	-1.7	-1.3	-1.4	-2.3	-0.9	-1.6	-3.6	0.5
17.	1.5	0.3	3.4	-1.4	-3.0	1.0	-0.3	-2.4	-1.6	-0.2	-3.1	0.9
14.	2.2	0.3	4.7	-0.2	-4.2	3.1	0.4	-3.3	-2.7	0.8	-2.2	1.1
11.	2.4	1.0	4.3	-0.2	-5.2	3.5	0.8	-4.4	-2.8	0.9	-2.1	0.6
8.	2.0	1.3	3.0	-1.0	-5.2	2.8	1.1	-3.8	-1.8	0.5	-2.6	0.5

Pressure profile deviations [%] for the models M13-M24

Z,km	M13	M14	M15	M16	M17	M18	M19	M20	M21	M22	M23	M24
80.	-8.9	-9.0	-12.5	-4.8	-4.5	14.3	-15.5	38.7	34.0	-1.3	6.5	1.3
77.	-5.3	-9.6	-11.2	-2.8	-1.1	12.8	-12.5	36.7	32.7	-4.6	5.7	0.4
74.	-3.4	-9.0	-10.1	-1.9	0.6	12.0	-9.8	35.3	31.3	-6.0	4.8	-1.0
71.	-3.1	-7.8	-8.7	-1.5	0.9	11.7	-7.7	33.2	28.6	-6.4	4.4	-2.5
68.	-3.3	-6.5	-7.8	-1.5	0.6	11.7	-6.5	30.0	25.0	-6.5	4.7	-2.5
65.	-3.7	-5.3	-7.1	-1.5	0.0	11.6	-5.5	26.4	21.4	-6.0	5.5	-0.5
62.	-4.1	-4.4	-6.5	-1.6	-0.8	11.2	-4.5	22.5	17.9	-4.3	6.4	1.8
59.	-4.3	-3.7	-6.2	-1.9	-1.3	10.7	-3.8	19.1	14.9	-2.1	6.8	3.6
56.	-4.4	-3.2	-6.1	-2.3	-1.5	10.2	-3.4	16.2	12.4	-0.4	7.2	5.2
53.	-4.4	-2.9	-5.9	-2.7	-1.5	9.6	-3.2	13.7	10.3	1.1	7.4	6.6
50.	-4.1	-2.6	-5.8	-3.2	-1.1	9.0	-3.3	11.5	8.7	2.3	7.4	7.9
47.	-3.8	-2.4	-5.5	-3.8	-0.7	8.3	-3.6	9.4	7.3	3.1	7.0	8.7
44.	-3.5	-2.5	-5.0	-4.3	-0.4	7.5	-4.0	7.7	6.4	3.5	6.3	8.6
41.	-3.6	-3.0	-4.3	-4.5	-0.5	6.7	-4.4	6.4	5.8	3.3	5.0	7.4
38.	-3.9	-3.9	-3.6	-4.6	-0.8	5.9	-4.8	5.3	5.6	2.6	3.6	5.7
35.	-4.1	-4.7	-2.9	-4.6	-0.9	5.1	-5.1	4.1	5.5	1.6	2.4	4.1
32.	-4.2	-5.0	-2.6	-4.4	-0.5	4.6	-4.9	2.5	5.1	0.4	1.5	2.8
29.	-4.0	-4.6	-2.5	-4.1	0.1	4.3	-4.1	0.6	4.4	-0.8	1.0	1.8
26.	-3.8	-4.0	-2.4	-3.8	0.7	3.9	-3.5	-1.0	3.8	-1.7	0.9	1.6
23.	-3.3	-3.3	-2.2	-3.6	1.4	3.8	-3.5	-2.2	3.4	-2.4	0.8	2.0
20.	-3.0	-2.4	-2.0	-3.7	2.5	4.0	-3.6	-2.8	3.2	-2.7	0.7	2.4
17.	-1.6	-1.5	-2.1	-4.0	3.7	4.3	-3.8	-1.7	3.3	-3.3	0.6	2.1
14.	0.5	-1.5	-2.3	-3.7	3.8	4.5	-3.3	0.6	3.9	-3.8	0.0	0.9
11.	1.6	-1.3	-2.1	-3.1	2.8	4.3	-2.0	1.9	3.8	-3.3	0.0	-0.6
8.	1.6	-0.5	-1.7	-2.7	1.7	3.5	-1.0	1.8	2.6	-2.2	0.9	-0.7

Pressure profile deviations [%] for the models M25-M36

Z,km	M25	M26	M27	M28	M29	M30	M31	M32	M33	M34	M35	M36
80.	-20.7	-4.0	-27.3	7.2	0.8	-11.5	4.4	-1.2	-18.9	-17.1	20.8	-10.9
77.	-20.2	-6.1	-26.9	8.1	2.7	-8.4	6.4	0.7	-19.7	-17.3	20.6	-11.7
74.	-19.6	-8.0	-25.7	7.8	4.1	-6.2	7.8	1.2	-20.0	-18.4	19.3	-12.0
71.	-18.4	-8.2	-23.8	7.0	4.5	-4.5	8.1	1.3	-19.3	-19.3	17.5	-11.2
68.	-15.9	-6.8	-21.4	7.1	4.7	-2.6	8.2	1.2	-17.6	-18.5	15.8	-9.7
65.	-12.8	-5.2	-18.4	8.2	5.1	-0.4	9.3	1.4	-15.2	-16.1	13.6	-7.6
62.	-9.4	-3.9	-14.6	9.1	5.4	1.5	10.7	1.6	-12.7	-13.3	11.3	-4.8
59.	-5.9	-2.9	-10.8	9.5	5.4	2.8	11.5	1.8	-10.4	-10.9	9.5	-2.3
56.	-3.0	-1.9	-7.7	9.6	5.2	3.8	12.1	1.9	-8.6	-8.9	8.2	-0.1
53.	-0.5	-1.0	-5.2	9.6	4.9	4.5	12.5	1.9	-7.3	-7.1	7.3	1.9
50.	1.9	0.0	-2.8	9.5	4.6	5.1	13.0	2.1	-6.3	-5.6	6.4	4.0
47.	3.7	0.8	-0.7	9.2	4.3	5.3	13.3	2.3	-5.5	-4.3	5.6	5.4
44.	4.2	1.3	0.3	8.7	4.1	5.0	13.4	3.0	-4.9	-3.0	5.4	5.3
41.	3.2	1.2	-0.1	8.0	3.8	4.0	13.2	4.0	-4.6	-1.8	5.8	4.0
38.	1.3	0.7	-1.5	7.3	3.6	2.6	13.1	5.3	-4.5	-1.1	6.8	2.1
35.	-0.5	-0.1	-2.9	6.7	3.6	1.2	13.0	6.3	-4.5	-1.0	8.2	0.2
32.	-1.8	-1.0	-3.8	6.1	3.5	0.2	12.7	6.7	-4.4	-1.3	9.4	-1.1
29.	-2.3	-1.9	-4.1	5.7	3.2	-0.5	11.9	6.3	-3.8	-1.8	9.8	-1.3
26.	-2.3	-2.8	-4.0	5.5	2.9	-1.2	10.7	5.8	-3.2	-2.3	9.6	-0.9
23.	-2.1	-3.3	-3.7	5.2	2.6	-1.5	9.2	5.2	-2.8	-3.0	9.1	0.1
20.	-1.9	-2.5	-3.3	5.2	2.0	-1.4	7.6	4.3	-2.8	-3.8	8.5	0.7
17.	-1.2	-1.2	-2.4	5.1	1.9	-1.0	6.5	2.9	-3.2	-5.0	7.1	1.1
14.	-0.6	-0.7	-1.6	4.3	2.2	0.3	5.8	1.9	-3.7	-5.7	4.5	1.8
11.	-0.1	-0.9	-1.7	3.2	2.0	1.6	4.9	1.9	-3.9	-5.3	2.6	2.2
8.	0.1	-1.0	-1.3	2.1	0.9	1.7	3.6	2.0	-3.4	-4.2	1.7	1.8

Pressure profile deviations [%] for the models M37-M46

Z,km	M37	M38	M39	M40	M41	M42	M43	M44	M45	M46
80.	3.5	-32.5	-9.6	16.3	-12.4	-1.2	35.2	41.3	34.5	-35.4
77.	4.5	-30.0	-12.3	16.4	-13.6	-2.0	29.5	37.0	34.3	-36.1
74.	4.7	-27.9	-14.4	15.2	-13.4	-2.5	26.2	35.8	33.0	-36.5
71.	5.3	-26.1	-15.5	13.7	-11.4	-1.9	25.0	35.2	30.2	-36.2
68.	6.4	-24.4	-15.2	12.2	-9.0	-0.3	24.7	33.5	26.7	-35.3
65.	7.2	-23.2	-13.6	10.5	-6.5	1.5	23.5	31.1	22.9	-34.0
62.	7.4	-22.5	-11.3	8.6	-3.7	2.7	21.1	28.3	19.5	-32.4
59.	7.4	-22.1	-9.3	6.9	-1.1	3.3	19.0	25.7	16.6	-30.8
56.	7.4	-21.7	-7.7	5.5	0.8	3.6	17.1	23.5	14.3	-29.2
53.	7.3	-21.4	-6.5	4.3	2.1	3.5	15.5	21.5	12.4	-27.6
50.	7.1	-20.9	-5.7	3.1	3.0	3.3	13.9	19.6	10.6	-26.2
47.	6.7	-20.0	-5.1	2.1	3.5	2.8	12.6	17.9	9.2	-24.9
44.	5.8	-18.8	-4.5	1.7	3.8	2.1	11.7	16.8	8.6	-23.5
41.	4.5	-17.3	-4.0	1.8	3.7	1.3	11.4	16.3	9.0	-21.7
38.	2.9	-15.6	-3.8	2.4	3.4	0.5	11.3	16.0	10.3	-19.9
35.	1.3	-13.6	-3.7	3.1	2.9	-0.2	11.0	15.6	11.5	-18.1
32.	-0.1	-11.4	-3.5	3.8	2.2	-0.4	10.5	14.8	11.8	-16.4
29.	-1.3	-9.2	-3.0	4.3	1.4	-0.4	9.6	13.7	11.4	-14.5
26.	-2.1	-7.0	-2.7	4.6	1.0	-0.2	8.7	12.1	10.5	-12.4
23.	-2.7	-5.3	-2.8	4.4	1.3	-0.2	7.7	10.4	9.4	-10.6
20.	-3.1	-4.5	-3.3	3.3	1.9	-0.8	6.5	8.6	7.9	-9.1
17.	-2.7	-4.3	-4.7	1.3	1.8	-1.9	5.2	5.7	6.0	-8.1
14.	-1.3	-4.2	-5.9	0.2	0.8	-2.4	3.7	2.8	4.6	-6.6
11.	-0.3	-3.1	-6.0	0.9	0.0	-2.3	2.2	1.9	3.7	-4.3
8.	0.0	-1.5	-5.3	1.3	-0.1	-2.0	1.7	1.5	2.3	-2.0

Temperature profile deviations [K] for the models M1-M12

Z,km	M 1	M 2	M 3	M 4	M 5	M 6	M 7	M 8	M 9	M10	M11	M12
80.	15.1	1.7	22.4	-7.9	-8.9	-1.3	4.5	8.0	-12.3	-14.9	-12.3	0.9
77.	3.3	3.9	10.3	-5.0	-6.3	-3.3	3.0	4.3	-11.2	-11.6	-7.6	0.5
74.	-0.7	7.6	7.1	-1.6	-3.5	2.8	-1.3	0.6	-8.1	-7.1	-5.6	-3.2
71.	1.3	9.8	11.1	2.8	-0.6	5.6	-6.6	-1.4	-1.9	-0.3	-4.5	-3.7
68.	8.5	16.9	28.3	5.4	5.2	11.9	-2.0	1.9	-2.6	1.5	-5.2	0.2
65.	16.8	19.9	25.6	1.8	4.1	12.8	2.6	-1.1	0.9	5.6	-2.5	8.9
62.	15.3	18.0	23.0	-2.1	6.1	11.6	-5.7	-4.8	2.3	8.8	1.3	8.9
59.	12.6	14.7	18.9	-1.7	3.8	9.6	-4.6	-4.2	1.3	7.0	1.0	7.7
56.	10.2	11.8	15.4	-1.2	1.9	7.7	-3.5	-3.4	0.5	5.5	0.9	6.5
53.	8.5	9.9	13.3	-1.2	0.7	5.7	-3.2	-2.8	0.2	4.0	0.7	5.4
50.	7.4	8.8	12.6	-2.1	-0.2	3.5	-4.1	-2.7	0.0	2.1	0.0	4.3
47.	5.1	5.5	10.4	-3.5	-3.3	1.4	-4.4	-3.8	-1.8	-0.6	-2.0	1.9
44.	1.1	0.3	7.1	-4.2	-9.2	-0.5	-3.0	-5.6	-5.2	-3.4	-4.9	-1.6
41.	-3.3	-4.7	3.3	-4.6	-13.4	-2.8	-1.5	-6.3	-7.6	-6.4	-7.2	-4.9
38.	-4.0	-7.6	1.0	-4.0	-13.8	-4.3	-0.4	-5.2	-7.9	-8.0	-7.4	-5.9
35.	-0.6	-8.2	0.7	-3.2	-10.5	-5.2	-1.6	-3.4	-6.8	-7.7	-5.9	-4.1
32.	2.9	-4.7	2.4	-2.6	-6.1	-4.7	-5.2	-2.8	-6.1	-7.0	-3.7	-0.9
29.	4.8	0.0	3.7	-3.2	-3.2	-2.2	-10.5	-4.2	-6.0	-7.5	-2.0	2.3
26.	4.1	1.5	1.7	-3.9	-1.0	-2.2	-6.8	-1.4	-3.9	-6.9	-2.2	3.4
23.	1.7	1.6	-1.0	-5.6	2.5	-3.7	-3.1	-0.6	-1.4	-5.8	-0.7	2.0
20.	-2.7	1.8	-4.3	-8.2	4.1	-6.6	-3.4	-0.5	1.1	-5.3	0.5	-2.6
17.	-4.0	1.2	-8.3	-7.2	6.1	-11.8	-5.4	0.9	4.2	-6.0	-5.1	-1.3
14.	-1.6	-2.3	-1.8	-2.3	4.4	-4.3	-0.2	6.8	5.2	-2.1	-2.5	0.1
11.	0.2	-4.2	6.0	2.6	5.4	1.2	-4.0	4.5	-4.4	1.5	1.8	4.1
8.	3.7	1.3	8.6	7.1	-5.6	6.9	0.7	-12.2	-6.8	2.8	4.3	-2.9

Temperature profile deviations [K] for the models M13-M24

Z,km	M13	M14	M15	M16	M17	M18	M19	M20	M21	M22	M23	M24
80.	-13.4	4.3	-6.3	-9.5	-13.9	5.9	-11.9	7.1	4.6	16.4	2.4	3.0
77.	-12.0	0.4	-3.1	-4.2	-9.1	4.2	-11.5	4.2	3.1	10.0	3.7	4.8
74.	-1.6	-4.3	-5.7	-2.3	-2.4	1.7	-9.8	4.5	6.2	2.2	3.2	6.9
71.	0.3	-5.7	-5.6	0.7	0.5	1.8	-7.2	10.9	13.2	2.2	1.1	7.1
68.	3.1	-5.6	-1.9	0.1	3.4	-0.2	-3.3	13.8	16.4	0.2	-2.3	-6.6
65.	2.4	-5.8	-4.9	0.7	4.9	1.7	-5.9	18.7	17.5	-4.8	-4.8	-12.1
62.	2.2	-4.2	-1.3	2.2	4.1	3.2	-4.3	18.6	17.2	-12.8	-2.6	-10.0
59.	1.4	-3.1	-1.0	2.2	2.6	3.2	-3.2	16.9	15.4	-10.9	-1.9	-8.8
56.	0.6	-2.1	-0.8	2.4	1.0	3.2	-2.0	15.3	13.4	-9.2	-1.3	-8.0
53.	-0.8	-1.8	-0.7	3.3	-1.2	3.4	-0.2	14.3	11.3	-8.0	-0.6	-8.1
50.	-2.6	-1.9	-1.2	4.6	-3.4	4.3	2.0	13.9	9.7	-6.8	0.9	-7.4
47.	-2.3	-0.5	-2.4	4.2	-2.8	5.0	3.0	12.3	7.8	-4.0	3.6	-2.3
44.	-0.2	2.4	-4.0	2.3	-0.1	5.3	2.9	10.0	5.2	-0.4	6.8	4.7
41.	1.6	5.3	-5.2	1.1	1.9	5.5	2.9	7.6	2.0	3.3	9.4	10.8
38.	2.3	6.3	-4.8	0.4	1.8	4.8	2.7	6.7	0.5	5.7	9.0	11.3
35.	0.9	4.0	-3.1	-0.3	-0.7	3.9	1.5	7.8	1.2	6.9	6.1	8.2
32.	-0.4	-0.3	-1.0	-1.6	-3.1	1.9	-3.6	9.8	3.3	6.9	4.2	5.9
29.	-1.0	-3.5	0.3	-1.7	-3.2	1.8	-4.8	10.4	3.3	5.8	1.3	4.4
26.	-1.4	-2.6	-0.9	-1.0	-2.5	1.4	-1.2	6.5	3.0	4.0	-0.1	-1.3
23.	-2.6	-3.3	-0.9	-0.5	-3.5	0.0	0.6	5.7	0.5	2.1	0.6	-2.8
20.	-0.8	-5.2	-0.7	0.9	-5.5	-1.4	1.1	0.5	1.3	1.1	0.4	-0.7
17.	-9.8	-2.2	0.9	1.7	-4.0	-1.1	0.3	-9.2	-1.9	3.3	0.1	3.0
14.	-7.0	2.3	0.6	-5.0	3.5	-0.4	-5.2	-9.2	-3.1	1.5	4.8	7.1
11.	-3.1	-4.6	-2.7	0.3	5.1	2.5	-7.3	-2.3	4.8	-7.0	-5.2	7.5
8.	3.7	-4.8	-1.9	-5.1	7.3	6.0	-2.8	4.0	7.8	-6.1	-4.4	-6.4

Temperature profile deviations [K] for the models M25-M36

Z,km	M25	M26	M27	M28	M29	M30	M31	M32	M33	M34	M35	M36
80.	-1.9	7.8	0.8	-3.9	-6.2	-13.2	-7.0	-9.6	4.1	0.3	-1.0	3.2
77.	-1.9	9.7	-4.1	-1.2	-6.6	-9.5	-5.2	-2.2	3.1	2.3	3.0	3.9
74.	-2.7	6.7	-7.4	4.0	-2.8	-7.6	-3.9	-1.2	0.5	9.0	6.6	-0.6
71.	-8.5	-3.9	-11.7	3.1	0.8	-6.2	2.3	1.2	-6.4	1.4	7.1	-6.5
68.	-17.5	-8.4	-14.7	-2.9	-0.9	-9.6	-1.6	1.2	-11.9	-9.6	8.9	-6.9
65.	-15.4	-7.6	-19.5	-5.4	-2.1	-11.0	-7.6	-1.7	-13.5	-17.4	12.9	-14.4
62.	-21.4	-5.9	-24.1	-2.5	0.1	-8.0	-4.7	-0.3	-15.3	-14.8	11.6	-14.5
59.	-18.3	-5.5	-20.4	-1.0	1.0	-6.0	-3.1	-0.3	-12.5	-13.6	8.6	-13.1
56.	-15.5	-5.3	-16.8	0.0	1.6	-4.4	-2.2	-0.4	-9.8	-12.2	6.2	-12.1
53.	-14.6	-5.8	-15.2	0.5	1.9	-3.7	-2.4	-0.4	-7.5	-10.7	5.6	-12.4
50.	-14.2	-6.5	-15.5	1.3	2.1	-2.9	-2.5	-0.7	-5.9	-9.4	6.2	-12.2
47.	-7.9	-4.7	-10.9	2.5	1.9	0.2	-1.1	-2.5	-4.8	-8.8	3.7	-4.5
44.	2.0	-1.1	-1.7	3.9	1.7	4.5	0.5	-5.4	-3.3	-8.2	-0.5	6.2
41.	11.2	2.5	7.4	5.0	1.7	8.7	1.5	-7.6	-1.3	-6.5	-4.6	11.7
38.	13.7	4.5	11.0	4.2	1.0	9.5	0.5	-7.3	0.3	-2.9	-7.0	12.9
35.	9.8	4.8	7.2	3.0	-0.1	7.4	0.4	-4.5	0.3	1.6	-8.0	11.5
32.	5.4	5.5	3.2	2.7	0.9	4.3	2.5	0.8	-2.4	2.1	-3.8	3.7
29.	1.0	5.3	0.3	1.7	2.1	3.6	5.3	2.8	-3.8	2.7	-0.5	-0.8
26.	-1.2	4.2	-0.9	0.6	1.1	3.4	6.0	2.5	-1.9	2.9	2.3	-3.7
23.	-0.6	0.3	-1.5	1.7	2.0	-0.2	7.0	2.7	-1.4	3.5	2.6	-5.2
20.	-1.4	-6.4	-1.8	-0.9	2.6	-1.1	6.3	5.1	0.7	4.6	1.9	0.2
17.	-4.1	-4.4	-5.6	1.5	-1.0	-2.1	2.4	6.2	2.6	5.2	9.4	-3.1
14.	-1.3	-0.2	-1.5	4.6	-1.9	-8.4	2.8	1.4	1.5	0.6	11.9	-3.5
11.	-3.2	3.0	2.7	6.1	4.5	-3.7	5.5	-1.8	0.0	-4.5	5.3	0.3
8.	1.3	-2.2	-8.3	5.7	7.5	3.0	8.9	0.8	-6.0	-7.9	4.9	4.3

Temperature profile deviations [K] for the models M37-M46

Z,km	M37	M38	M39	M40	M41	M42	M43	M44	M45	M46
80.	-5.4	-13.8	12.2	-2.4	5.1	2.8	19.6	18.3	1.4	4.8
77.	-0.7	-10.1	11.5	2.7	5.5	3.7	14.9	6.2	0.3	3.8
74.	-0.3	-10.4	8.8	5.8	-6.5	0.6	6.4	0.9	7.8	1.0
71.	-3.6	-9.2	3.3	6.5	-11.3	-4.4	2.5	4.2	12.1	-3.6
68.	-4.8	-8.7	-5.4	7.7	-11.1	-9.1	1.0	9.0	16.7	-8.4
65.	-1.3	-6.3	-12.2	9.9	-13.5	-7.2	11.0	12.2	17.7	-10.8
62.	0.3	-2.0	-13.3	10.2	-15.6	-4.0	11.7	13.0	16.6	-12.0
59.	0.5	-2.7	-11.0	9.0	-12.2	-2.1	10.7	12.1	13.8	-13.1
56.	0.6	-2.6	-8.6	8.0	-9.1	-0.5	9.7	11.2	11.6	-13.4
53.	0.7	-2.9	-6.5	7.8	-6.6	1.0	9.4	11.1	11.3	-12.7
50.	1.7	-5.0	-4.8	8.1	-4.4	2.7	9.3	10.9	11.3	-11.1
47.	4.2	-8.5	-4.0	5.5	-2.4	4.0	7.0	8.4	7.0	-10.9
44.	7.3	-10.6	-3.5	1.0	-0.5	5.1	3.9	5.1	0.8	-13.3
41.	10.4	-12.4	-2.3	-2.6	1.5	6.1	0.9	1.9	-5.7	-14.6
38.	10.7	-13.3	-0.9	-4.2	2.8	5.4	0.3	1.3	-8.4	-13.5
35.	8.6	-13.8	-0.3	-3.8	3.5	2.7	2.3	3.3	-4.3	-11.5
32.	7.8	-12.1	-2.4	-3.8	4.2	0.4	3.5	4.8	0.6	-11.3
29.	5.5	-12.1	-2.7	-1.5	4.1	-0.8	4.7	5.6	3.9	-11.2
26.	3.0	-10.1	-0.3	-0.9	0.4	-1.0	4.1	8.8	4.6	-10.6
23.	3.1	-6.3	1.5	2.9	-3.1	1.6	4.8	6.2	5.0	-8.5
20.	1.0	-1.7	3.0	6.4	-2.4	3.7	5.2	8.3	7.3	-5.4
17.	-4.6	0.3	9.0	9.8	3.6	5.5	5.2	15.2	7.9	-3.8
14.	-7.4	-1.3	1.9	-0.9	4.7	-1.4	7.1	8.6	2.6	-9.2
11.	-1.1	-10.2	-1.8	-5.3	2.1	0.0	6.4	0.0	6.3	-13.0
8.	-2.0	-7.0	-5.8	0.7	-1.1	-3.5	-0.9	4.4	9.1	-11.2

Water vapor profile deviations [%] for the models M1-M12

Z,km	M 1	M 2	M 3	M 4	M 5	M 6	M 7	M 8	M 9	M10	M11	M12
80.	6.4	-8.3	-23.1	6.1	46.7	26.5	-43.9	-69.2	29.4	40.9	24.7	-0.4
77.	48.7	10.7	28.5	12.3	26.2	-1.5	-50.3	-26.1	37.4	28.1	12.6	37.2
74.	40.7	45.2	6.7	11.2	2.1	23.8	-9.1	-3.0	14.7	4.5	-0.2	-3.4
71.	8.7	14.7	1.1	11.1	13.6	13.0	1.4	-8.1	13.2	5.3	-11.6	-16.5
68.	10.1	-0.9	10.7	-2.5	13.5	16.9	-20.3	3.6	0.9	16.7	-7.9	-7.4
65.	-11.5	0.0	0.4	8.9	5.1	28.3	3.0	-14.5	3.0	21.3	7.7	7.3
62.	-5.8	15.6	-12.3	1.1	7.4	-1.7	-21.9	-8.9	-3.0	-6.1	12.3	11.0
59.	15.6	-1.2	-1.9	2.4	-11.9	15.3	6.5	0.3	0.4	-6.3	1.2	16.7
56.	7.3	2.2	1.4	4.6	2.8	-1.2	4.8	4.0	0.0	5.7	-2.2	16.5
53.	0.9	4.4	-10.1	1.4	-0.2	1.7	-3.0	-4.4	10.4	2.5	1.2	11.5
50.	-1.9	4.2	-2.4	-2.9	0.3	1.3	-5.0	-4.6	0.6	2.4	14.7	7.3
47.	4.8	-0.1	3.8	5.1	-3.3	4.3	3.7	-6.6	-1.9	0.7	-4.1	-4.8
44.	2.8	-3.8	-13.2	8.8	-1.2	-4.6	3.3	-6.1	6.5	12.5	-8.4	-0.6
41.	-3.4	-3.6	-14.9	9.4	4.1	0.0	3.5	-13.5	5.0	0.3	-3.1	2.8
38.	-6.0	-1.2	2.2	2.2	6.4	1.4	14.3	-9.2	3.7	-0.1	12.0	3.6
35.	-3.4	6.9	-3.0	0.6	9.7	9.7	-4.6	-21.6	19.4	-0.6	10.2	1.7
32.	6.8	7.4	-14.6	-3.6	4.7	5.4	-8.0	-17.3	17.9	-4.6	8.4	2.9
29.	0.0	-1.3	-14.9	-8.5	-12.0	6.4	-4.9	-16.2	11.1	-11.3	29.0	-2.8
26.	-8.6	-8.8	2.5	-5.2	-14.6	14.3	-0.9	-5.9	18.5	-9.0	14.8	-15.9
23.	-5.6	-9.7	-11.4	3.6	-9.1	25.2	-7.4	-20.2	18.3	-5.4	24.0	-8.5
20.	4.0	18.5	-5.7	15.0	10.8	22.7	-8.4	-8.4	-21.4	-5.3	-30.5	5.3
17.	8.8	-17.1	34.0	-26.0	10.1	-23.0	-10.8	-13.0	-35.9	2.0	-36.2	3.5
14.	39.6	14.8	95.7	75.1	-17.4	-36.0	16.0	-45.9	-82.7	0.8	19.8	-79.0
11.	31.4	11.1	80.5	76.3	-20.8	-35.0	18.6	-48.7	-82.1	2.3	20.7	-79.3
8.	52.2	38.5	110.6	22.0	-65.5	-24.7	3.0	-72.7	-62.2	-20.9	-20.5	-81.6

Water vapor profile deviations [%] for the models M13-M24

Z,km	M13	M14	M15	M16	M17	M18	M19	M20	M21	M22	M23	M24
80.	38.0	-3.7	4.3	19.7	15.0	-61.9	48.1	43.4	60.7	-28.8	-67.4	-68.3
77.	28.1	13.5	2.5	12.3	33.5	-62.5	31.6	26.4	38.9	-0.8	-65.5	-7.4
74.	14.1	12.6	3.5	25.5	6.5	-46.9	10.6	22.8	20.0	6.1	-56.7	-17.5
71.	2.0	18.8	7.6	21.2	8.1	-36.2	8.1	24.2	14.1	-2.1	-45.2	-13.3
68.	-5.6	4.1	-15.9	2.3	3.1	-35.8	21.7	12.5	25.6	-23.4	-39.2	4.4
65.	1.2	22.3	33.4	1.6	19.0	-33.1	1.2	-9.8	28.6	-12.1	-26.4	-6.0
62.	1.5	4.4	20.5	2.9	-1.7	-10.3	30.7	18.4	10.8	-15.2	-13.6	-16.3
59.	6.1	-7.3	-15.9	-6.4	-1.6	-8.3	14.4	26.6	6.4	-10.9	-20.4	2.7
56.	1.9	-2.5	4.6	3.0	1.4	-14.7	6.1	0.8	0.3	7.1	-17.2	-6.7
53.	-2.4	-1.7	2.5	3.4	4.6	-18.2	-10.1	7.2	3.0	3.4	-8.2	3.0
50.	5.7	-5.5	0.3	3.9	4.4	-9.4	-2.3	-0.7	8.0	0.6	-5.0	-9.1
47.	-3.3	-13.1	2.3	8.1	1.7	-3.3	9.4	7.1	4.3	3.1	-2.0	-3.8
44.	-1.6	-11.8	12.9	1.4	3.1	5.2	-4.1	-6.4	3.9	6.1	2.2	-13.0
41.	-2.5	-19.6	0.2	1.1	7.5	2.5	-0.9	5.6	4.1	11.9	-4.9	-6.1
38.	13.4	-15.8	3.9	3.1	1.1	-3.7	-1.2	3.4	-0.2	3.4	3.7	-10.8
35.	3.8	-12.7	-3.0	10.0	4.8	5.5	13.0	11.9	1.9	-6.7	4.6	-9.4
32.	3.8	-19.3	-11.2	21.9	0.4	17.2	-4.6	5.2	-9.1	-2.3	3.6	-6.1
29.	19.0	-28.6	-4.9	22.8	-3.0	19.6	-3.4	-11.7	0.2	2.7	4.5	-2.0
26.	22.3	-48.6	-12.7	32.9	-8.8	20.2	-6.3	-8.4	-9.4	1.2	12.9	-5.7
23.	26.9	-61.7	-8.3	27.5	-12.1	23.5	-4.7	-2.4	8.9	-13.7	16.0	-12.5
20.	-5.5	48.6	-5.7	0.7	3.8	33.3	-0.4	6.8	21.0	-10.6	23.6	0.2
17.	-41.5	115.9	15.4	-38.7	12.4	-1.1	4.8	11.6	-43.0	-7.2	-36.2	-20.9
14.	99.9	-60.0	31.3	-69.9	31.3	49.1	-35.2	-91.0	-41.8	-16.2	-61.7	-63.1
11.	109.4	-57.6	34.6	-68.7	27.1	48.5	-31.5	-91.8	-41.4	-13.9	-59.7	-62.8
8.	151.6	-9.5	39.5	-71.5	-35.3	7.6	-46.3	-81.1	-1.7	-5.5	14.8	0.6

Water vapor profile deviations [%] for the models M25-M36

Z,km	M25	M26	M27	M28	M29	M30	M31	M32	M33	M34	M35	M36
80.	3.9	25.5	-45.4	17.6	7.9	42.4	-6.9	26.2	26.2	-15.5	18.3	-56.5
77.	-7.1	-46.1	-0.3	12.6	32.3	-15.1	-20.5	-7.4	-7.4	-36.7	6.3	-50.5
74.	-0.8	-23.1	-17.0	-7.9	19.1	-15.2	-14.0	17.5	-7.9	-26.2	-5.7	-24.6
71.	4.6	-2.5	-16.5	-4.3	-2.1	-1.9	-6.0	16.2	-4.3	-8.1	12.1	-11.8
68.	-10.0	8.0	-2.9	25.9	1.2	-7.9	-10.0	6.0	-3.5	-6.9	17.5	-23.4
65.	-14.5	15.5	-15.0	10.0	33.4	-18.5	-16.3	-5.4	4.7	-8.4	-6.3	-19.1
62.	0.9	-6.4	-8.6	2.2	9.0	-4.1	-16.8	-8.3	4.9	-0.5	-5.0	-10.3
59.	6.8	-2.1	9.8	0.9	-18.5	1.3	-6.7	5.6	-13.6	2.5	3.1	0.9
56.	-0.9	-1.9	-2.2	-1.0	1.9	1.6	-5.5	-1.0	-0.6	-14.7	13.7	-18.1
53.	-4.4	11.8	1.8	7.3	9.2	10.2	-7.9	8.9	0.8	-0.9	1.8	1.1
50.	4.2	-1.1	-5.8	2.5	9.0	4.2	-5.2	4.7	-3.9	-7.9	5.4	-0.5
47.	6.3	14.2	-1.7	-0.4	4.7	-2.9	-6.8	0.0	-4.3	-11.3	-1.1	-2.3
44.	8.5	11.0	0.8	6.7	9.9	3.7	-8.0	4.8	-0.4	0.8	-1.8	-11.5
41.	4.6	8.0	-4.2	8.5	3.8	4.7	-4.9	-2.3	4.7	-2.7	6.9	0.9
38.	4.9	-1.6	-16.1	6.7	1.1	8.5	-4.9	9.2	-0.1	-4.0	8.5	-2.6
35.	10.7	-8.2	-16.6	-2.7	3.2	17.9	-9.4	18.2	-5.3	-11.7	11.6	-10.5
32.	6.1	-10.4	-6.8	7.4	-12.3	20.1	-10.0	19.2	-4.6	-12.3	12.7	-9.8
29.	6.2	-4.9	-18.4	11.1	-15.6	29.4	-12.8	29.0	-7.9	-8.6	23.9	-12.2
26.	-3.8	-8.6	-13.8	1.2	-10.0	25.2	-8.6	28.1	-4.2	-7.3	32.4	-4.8
23.	-8.3	-7.9	-7.9	20.6	-10.0	18.1	-9.8	27.7	-13.3	-3.5	29.6	-14.4
20.	-9.9	-4.4	-4.4	15.7	9.3	-1.8	-9.1	-5.3	-15.0	-13.9	-5.5	-1.1
17.	6.5	5.3	5.3	-35.2	-2.1	-32.9	-8.5	-32.4	-28.8	-28.8	-28.8	-2.6
14.	28.8	-17.0	-77.3	156.0	47.4	25.5	3.7	99.9	36.7	-40.9	-88.2	-10.8
11.	32.5	-17.9	-76.2	147.8	47.4	32.5	1.8	97.6	37.8	-39.3	-89.1	-9.1
8.	36.2	-46.1	-45.9	115.7	34.3	32.8	113.5	1.3	4.2	-47.4	-87.6	-3.4

Water vapor profile deviations [%] for the models M37-M46

Z,km	M37	M38	M39	M40	M41	M42	M43	M44	M45	M46
80.	32.7	27.6	-28.5	-9.4	-56.9	-70.2	-38.9	-3.3	70.0	-1.9
77.	-13.7	18.0	-32.9	17.0	-1.0	-63.4	23.1	-5.0	7.0	-23.8
74.	34.2	16.9	-25.0	-10.3	-3.6	-43.7	-1.2	19.1	12.0	-26.6
71.	10.8	12.6	-26.2	23.8	7.2	-26.5	-9.9	2.2	-4.9	-17.4
68.	1.8	4.1	-20.6	18.8	3.5	-32.3	33.4	9.1	11.9	-10.9
65.	17.0	6.7	-13.4	-9.2	-2.6	-30.2	-4.6	7.1	-2.8	-7.2
62.	11.0	38.0	-19.4	10.7	8.2	-27.3	33.8	-4.1	-18.6	-8.9
59.	10.6	-1.1	-6.4	10.9	-9.8	-10.7	-16.7	2.2	8.0	0.4
56.	11.8	-0.9	0.0	0.0	-6.1	-13.8	1.1	-5.2	8.0	3.7
53.	4.3	-3.3	-7.3	-4.4	-1.4	-23.6	-11.8	0.9	3.7	0.2
50.	4.7	-1.3	-5.9	-1.3	7.1	-3.7	-10.0	-0.7	3.2	-2.7
47.	-0.7	10.1	-1.6	3.1	-6.7	-6.4	-6.0	2.8	6.3	-7.6
44.	-7.7	-5.6	15.9	-3.1	-5.8	0.3	-15.4	9.1	-1.3	-4.7
41.	13.3	-7.4	0.0	-3.4	-3.0	7.1	-23.8	10.0	1.7	-8.1
38.	10.9	-5.5	-12.7	9.9	-10.7	-4.5	-23.4	-4.5	3.4	-2.1
35.	17.7	2.9	-15.9	10.9	-15.5	1.7	-24.7	-15.9	1.0	-8.2
32.	31.2	2.9	-13.6	8.1	-10.9	8.1	-32.2	10.8	-2.1	-6.1
29.	29.8	-12.6	-4.1	21.7	-12.6	6.2	-25.8	-3.0	-5.2	-3.9
26.	27.7	-12.1	-14.8	30.2	-12.9	18.7	-22.1	-4.0	-2.9	-4.6
23.	21.0	-6.2	-14.6	27.5	-20.9	23.5	-3.5	-5.4	-3.5	-19.6
20.	-6.8	-6.8	-2.9	-2.6	-15.7	36.6	4.4	-11.0	4.4	-66.4
17.	-10.5	10.1	14.9	-16.6	8.8	26.6	220.4	10.6	8.3	42.4
14.	-60.1	-76.0	-22.8	-3.0	82.1	-12.0	-5.0	60.6	142.0	-43.4
11.	-57.3	-73.6	-22.7	1.9	79.5	-11.4	-9.6	61.3	137.2	-38.3
8.	-5.5	-30.9	-55.4	1.9	34.3	-42.9	-44.6	130.5	122.0	-58.6

Ozone profile deviations [%] for the models M1-M12

Z,km	M 1	M 2	M 3	M 4	M 5	M 6	M 7	M 8	M 9	M10	M11	M12
80.	36.7	65.9	65.9	-48.1	-54.5	-2.9	-2.9	122.5	4.7	-41.7	3.5	-12.5
77.	69.6	91.1	91.1	-40.7	65.7	-21.3	-21.3	72.8	18.2	-44.8	-1.0	-36.4
74.	122.4	56.2	56.2	-30.4	91.9	-44.0	-44.0	-11.1	36.3	10.2	-10.3	-60.7
71.	83.3	1.1	1.1	-19.3	73.5	-26.9	-59.8	-12.0	31.5	-9.6	-23.0	-59.1
68.	59.2	11.7	11.7	-21.6	80.6	-26.8	-64.2	-9.7	35.9	-0.2	14.5	-53.6
65.	-85.1	-15.6	-5.0	-3.5	105.2	-26.5	-59.8	4.0	37.3	6.8	34.5	-41.8
62.	-76.8	6.7	-28.2	-8.2	105.5	-43.1	-44.6	52.1	19.1	-13.1	30.1	-50.2
59.	-59.9	15.5	-30.1	2.0	74.8	-40.1	-18.5	41.8	19.5	-2.0	26.5	-42.5
56.	-35.5	10.2	-24.4	0.1	43.9	-29.4	-10.8	24.6	10.2	-3.2	15.3	-27.5
53.	-15.5	2.1	-16.6	-6.2	20.2	-18.1	-13.0	10.4	1.0	-9.3	3.6	-13.5
50.	-9.1	-0.1	-10.5	-6.7	9.9	-12.3	-11.2	4.4	-1.8	-9.8	-0.8	-8.4
47.	-11.6	0.5	-11.9	-3.5	9.2	-10.6	-6.6	5.6	-0.2	-6.6	1.0	-9.1
44.	-12.7	-1.4	-13.4	-4.4	8.5	-10.2	-7.6	4.8	-1.2	-7.6	0.1	-9.3
41.	-9.5	-1.8	-11.8	-7.5	5.8	-4.1	-8.6	0.8	-2.1	-9.9	-3.1	-4.9
38.	-3.9	-2.0	-8.2	-12.0	1.5	-0.1	-11.0	-4.8	-4.4	-13.0	-7.8	-0.7
35.	2.6	-1.4	-3.1	-16.0	-2.8	6.1	-11.9	-9.7	-5.9	-15.8	-12.1	3.8
32.	10.0	-2.5	3.5	-18.4	-6.1	8.8	-13.7	-12.9	-7.9	-18.0	-15.1	5.1
29.	11.5	-2.6	5.7	-17.3	-5.4	9.0	-13.0	-12.3	-6.8	-16.6	-14.3	4.8
26.	6.7	-1.4	2.2	-12.9	-0.7	1.9	-11.0	-8.0	-2.8	-12.4	-9.8	3.1
23.	-5.1	-2.9	-9.9	-3.5	9.2	-9.1	-4.6	1.3	5.8	-3.5	-0.1	-0.4
20.	-25.9	-6.5	-30.4	6.6	24.3	-31.6	3.8	13.5	18.0	7.8	12.3	-8.2
17.	-58.7	-15.1	-63.1	20.0	49.7	-63.8	13.3	31.8	37.7	22.9	30.0	-20.5
14.	-64.3	-24.9	-68.2	19.6	59.6	-72.1	11.5	39.3	44.7	22.7	31.2	-24.0
11.	-55.8	-32.5	-57.8	15.4	47.1	-66.8	6.9	29.1	35.5	20.7	22.8	-18.3
8.	-45.6	-23.7	-47.5	7.6	41.7	-56.6	-2.0	21.9	25.4	10.2	15.9	-9.9

Ozone profile deviations [%] for the models M13-M24

Z,km	M13	M14	M15	M16	M17	M18	M19	M20	M21	M22	M23	M24
80.	-57.7	-80.2	-72.8	4.7	4.7	28.0	1.5	1.5	-61.5	-71.6	1.5	-64.1
77.	-53.6	-77.8	-24.5	18.2	18.2	-18.7	81.4	81.4	-87.4	-19.3	81.4	-79.4
74.	-59.2	-74.5	-46.7	36.3	36.3	-9.2	33.7	33.7	-85.6	-59.8	33.7	-95.8
71.	-48.9	-71.2	-33.2	31.5	-94.6	6.9	52.1	52.1	-86.4	-84.7	52.1	-92.0
68.	-58.5	-60.4	-33.5	-53.2	-53.2	62.5	94.8	-0.2	-87.6	-84.3	-0.2	-92.9
65.	-51.1	-45.8	-9.4	-76.0	-62.9	-50.5	91.8	-48.9	-88.1	-59.2	-25.9	-75.5
62.	-59.5	-59.7	-23.3	-74.4	-65.7	-51.9	84.6	-22.7	-75.9	-53.4	-52.1	-72.7
59.	-52.2	-52.0	-27.2	-63.0	-55.5	-38.2	65.2	-11.2	-53.7	-45.9	-50.7	-58.0
56.	-36.3	-35.3	-20.9	-42.9	-36.9	-17.4	41.4	-12.5	-26.1	-28.4	-38.3	-32.8
53.	-19.7	-18.1	-13.0	-22.8	-18.1	-3.1	21.8	-12.4	-8.3	-11.4	-23.3	-10.9
50.	-11.6	-11.2	-9.1	-14.3	-10.5	-1.2	12.4	-6.4	-5.3	-5.7	-14.0	-5.0
47.	-10.6	-9.4	-6.6	-12.9	-10.1	-3.8	12.5	-8.6	-8.3	-4.8	-12.2	-5.0
44.	-9.1	-9.9	-6.3	-14.0	-8.0	-3.7	12.5	-9.5	-8.2	-3.7	-12.9	-4.6
41.	-2.6	-11.1	-6.7	-14.3	-2.6	-3.6	10.9	-8.0	-6.7	-4.0	-14.3	-6.9
38.	2.9	-13.5	-9.4	-15.7	2.1	-1.9	7.3	-3.7	-3.3	-5.3	-15.6	-8.7
35.	10.8	-14.7	-11.8	-16.0	8.1	-0.9	4.9	1.0	-0.2	-6.5	-16.5	-10.5
32.	13.7	-16.4	-14.8	-17.3	10.8	-0.3	1.7	7.7	5.8	-8.2	-17.4	-11.5
29.	13.3	-16.1	-15.5	-16.6	8.5	-1.4	1.5	9.8	6.1	-8.5	-17.8	-12.2
26.	4.1	-14.6	-13.8	-14.1	-1.3	-3.3	4.0	5.9	2.1	-7.0	-17.2	-11.7
23.	-8.2	-7.4	-6.3	-5.7	-16.1	-10.2	10.3	-3.5	-13.3	0.5	-12.4	-7.4
20.	-30.4	2.1	4.9	6.6	-36.1	-18.5	15.8	-24.2	-32.7	11.8	-3.6	0.9
17.	-59.4	16.4	23.5	27.8	-66.0	-33.1	22.8	-56.4	-65.8	32.4	10.0	16.2
14.	-69.3	22.2	30.8	34.8	-71.5	-40.7	16.4	-65.8	-72.2	45.2	19.6	26.3
11.	-65.4	19.6	27.0	28.1	-65.0	-33.7	-2.8	-59.1	-63.0	44.0	24.9	35.5
8.	-55.6	8.0	16.4	18.6	-54.9	-24.6	-2.7	-48.9	-50.6	32.9	11.6	23.6

Ozone profile deviations [%] for the models M25-M36

Z,km	M25	M26	M27	M28	M29	M30	M31	M32	M33	M34	M35	M36
80.	-64.1	-87.3	-91.3	15.8	15.8	15.8	28.0	28.0	9.6	28.0	28.0	-82.9
77.	-79.4	-94.0	-93.4	-45.9	-45.9	-45.9	22.3	22.3	-13.7	22.3	22.3	-98.8
74.	-95.8	-94.0	-95.3	15.1	-24.6	15.1	4.0	4.0	-59.5	-13.2	-13.2	-67.0
71.	-92.0	-92.6	-96.2	7.7	-17.0	7.7	72.6	72.6	-75.5	-9.6	-9.6	-69.3
68.	-92.9	-93.8	-95.4	-21.1	-35.4	-54.1	-32.5	62.5	-63.6	15.0	15.0	-78.2
65.	-92.2	-93.1	-95.6	-30.6	5.6	-81.3	-57.7	-15.6	-59.2	59.4	-18.7	-67.0
62.	-87.5	-90.0	-93.6	-39.3	-16.9	-76.4	-15.4	7.3	-49.5	101.0	-29.7	-56.1
59.	-73.0	-72.2	-78.9	-29.0	-15.2	-61.2	12.2	17.6	-19.5	73.5	-22.4	-33.6
56.	-47.8	-46.1	-53.9	-11.6	-5.7	-36.2	14.5	13.6	-9.1	45.6	-9.1	-27.3
53.	-21.8	-23.8	-29.5	0.0	0.5	-13.5	8.8	6.2	-11.4	24.4	-1.6	-24.9
50.	-11.2	-14.0	-16.4	1.3	1.6	-7.0	8.9	4.4	-9.1	14.8	-0.5	-14.0
47.	-9.4	-11.9	-12.9	-0.2	-0.7	-8.6	8.7	5.4	-4.5	14.8	-0.5	-9.1
44.	-8.4	-11.0	-11.9	0.1	0.5	-7.2	9.1	5.7	-5.0	12.8	0.5	-6.5
41.	-9.1	-10.5	-11.2	-1.0	4.1	-4.6	6.0	5.5	-5.3	7.4	-0.1	-4.0
38.	-10.6	-11.3	-12.0	-0.7	9.3	-0.7	5.2	5.8	-7.3	2.2	-0.5	-3.0
35.	-11.1	-11.6	-11.6	-1.9	15.2	4.3	0.4	4.3	-8.3	-1.8	-3.2	-1.6
32.	-12.4	-13.0	-12.5	-3.0	20.7	10.7	-1.8	2.7	-10.2	-3.9	-6.1	-2.4
29.	-12.7	-12.8	-11.9	-4.8	19.6	13.8	-5.1	1.1	-9.9	-2.6	-9.4	-3.1
26.	-12.6	-11.3	-10.5	-6.5	12.1	11.1	-6.5	1.2	-7.5	1.7	-11.0	-4.2
23.	-7.1	-3.5	-2.9	-13.6	-3.5	1.9	-13.3	-3.5	1.0	9.7	-17.8	-1.8
20.	1.5	6.1	7.2	-20.2	-23.6	-19.6	-15.6	-6.5	14.0	18.0	-21.3	3.2
17.	15.5	20.8	24.8	-33.8	-56.4	-52.5	-23.8	-13.6	37.5	32.8	-29.3	12.4
14.	21.3	28.1	31.7	-42.5	-62.1	-59.4	-35.7	-22.7	48.3	32.1	-36.6	17.3
11.	24.9	33.4	34.4	-38.9	-52.7	-50.5	-32.0	-26.2	41.8	9.0	-35.4	29.1
8.	14.2	22.9	23.5	-28.4	-40.9	-39.6	-23.9	-17.5	32.4	9.5	-27.3	19.8

Ozone profile deviations [%] for the models M37-M46

Z,km	M37	M38	M39	M40	M41	M42	M43	M44	M45	M46
80.	28.0	-24.5	-21.6	16.3	16.3	9.6	178.7	4.7	16.3	162.4
77.	22.3	17.1	-81.7	-15.9	-15.9	-13.7	268.9	21.7	-15.9	77.3
74.	-13.2	-5.2	-23.1	-13.7	-13.7	-59.5	318.2	348.7	-13.7	-16.2
71.	-9.6	-8.7	-34.3	-43.8	-43.8	-75.5	371.1	284.8	215.7	-19.1
68.	15.0	-15.9	-28.3	3.6	-43.9	-63.6	384.6	277.7	274.4	0.3
65.	5.6	10.5	-5.0	48.2	-18.1	-77.0	404.4	345.3	342.1	41.0
62.	24.8	33.5	0.1	52.5	1.6	-73.2	302.5	264.2	257.8	159.8
59.	30.4	23.1	9.4	47.3	14.8	-58.4	213.9	191.9	183.6	101.0
56.	22.9	8.6	6.9	32.1	12.8	-34.6	138.2	126.4	118.0	54.9
53.	14.5	-4.1	0.0	16.6	7.3	-13.5	85.0	79.8	72.0	23.3
50.	11.0	-8.8	-1.2	9.9	5.8	-8.1	58.2	55.4	48.8	8.6
47.	7.9	-6.3	1.6	11.2	6.4	-8.6	48.3	47.0	39.9	5.4
44.	8.2	-4.4	1.6	5.5	5.1	-5.7	48.7	48.5	41.2	4.8
41.	9.9	-0.8	0.8	-6.2	2.6	-2.3	47.2	44.4	41.8	12.0
38.	13.3	0.4	-2.5	-17.7	1.0	-0.3	50.2	45.4	45.4	19.3
35.	18.5	1.4	-5.2	-28.8	-0.4	1.8	48.1	39.3	43.7	27.3
32.	24.1	0.0	-8.4	-37.6	-1.6	0.8	50.3	40.1	44.7	32.1
29.	26.4	0.9	-9.1	-36.4	-1.5	-0.3	47.5	37.0	40.9	38.3
26.	21.2	3.1	-7.5	-24.9	-0.4	-1.4	44.6	37.7	40.3	43.3
23.	10.6	9.5	0.8	-11.3	-2.9	1.9	32.5	28.0	28.5	58.9
20.	-13.9	13.5	14.0	9.5	-8.2	8.9	24.9	26.0	24.3	77.3
17.	-49.1	20.0	38.4	39.8	-17.1	22.9	8.9	19.8	14.7	114.6
14.	-59.8	15.5	52.4	34.4	-24.9	33.5	7.0	28.1	16.0	127.4
11.	-52.5	-4.9	40.8	12.2	-31.4	38.7	22.8	48.2	36.6	115.9
8.	-39.7	-4.9	34.0	11.9	-21.7	32.6	34.0	56.4	45.2	96.3

Appendix 2: Probability density function values for profiles in the statistical ensemble

Model	Pressure	Temp.	H_2O	O_3
M 1	0.78E-04	0.34E-05	0.62E-04	0.29E-05
M 2	0.16E-04	0.33E-05	0.72E-05	0.18E-04
M 3	0.14E-06	0.69E-07	0.50E-07	0.37E-05
M 4	0.14E-03	0.18E-04	0.76E-04	0.48E-03
M 5	0.19E-04	0.26E-05	0.50E-05	0.95E-06
M 6	0.26E-03	0.68E-04	0.42E-04	0.67E-04
M 7	0.14E-05	0.63E-06	0.87E-05	0.74E-05
M 8	0.48E-04	0.17E-04	0.20E-05	0.41E-07
M 9	0.58E-03	0.28E-03	0.17E-04	0.32E-02
M10	0.31E-02	0.19E-03	0.93E-03	0.34E-03
M11	0.48E-04	0.15E-04	0.10E-05	0.39E-04
M12	0.14E-03	0.27E-04	0.31E-06	0.21E-05
M13	0.12E-03	0.13E-04	0.15E-05	0.24E-05
M14	0.34E-02	0.32E-03	0.46E-08	0.26E-02
M15	0.27E-02	0.50E-03	0.63E-05	0.18E-02
M16	0.17E-02	0.36E-03	0.27E-05	0.23E-05
M17	0.37E-04	0.18E-04	0.36E-03	0.42E-06
M18	0.28E-02	0.87E-03	0.30E-05	0.12E-05
M19	0.37E-04	0.91E-05	0.11E-05	0.36E-05
M20	0.81E-05	0.49E-06	0.54E-06	0.23E-05
M21	0.20E-03	0.74E-05	0.21E-05	0.30E-06
M22	0.75E-04	0.62E-05	0.24E-05	0.73E-04
M23	0.23E-04	0.61E-05	0.27E-05	0.68E-05
M24	0.15E-05	0.31E-06	0.41E-06	0.14E-04
M25	0.86E-05	0.11E-06	0.16E-04	0.17E-03
M26	0.72E-05	0.24E-05	0.49E-05	0.15E-03
M27	0.15E-05	0.13E-06	0.11E-04	0.51E-05
M28	0.10E-03	0.13E-04	0.27E-05	0.66E-04
M29	0.29E-02	0.30E-03	0.15E-05	0.18E-06
M30	0.23E-03	0.26E-04	0.93E-04	0.49E-06
M31	0.19E-06	0.67E-07	0.18E-04	0.10E-06
M32	0.47E-04	0.96E-04	0.27E-05	0.76E-05
M33	0.74E-02	0.16E-02	0.53E-03	0.18E-05
M34	0.27E-05	0.30E-06	0.22E-04	0.75E-05
M35	0.32E-05	0.76E-08	0.19E-04	0.19E-04
M36	0.48E-08	0.47E-09	0.11E-04	0.30E-07
M37	0.79E-04	0.25E-04	0.58E-06	0.86E-06
M38	0.23E-05	0.73E-09	0.26E-04	0.26E-05
M39	0.76E-04	0.82E-04	0.63E-04	0.45E-05
M40	0.57E-04	0.56E-05	0.21E-05	0.18E-06
M41	0.48E-06	0.23E-06	0.20E-05	0.31E-03
M42	0.51E-03	0.80E-04	0.31E-05	0.79E-05
M43	0.21E-05	0.16E-05	0.46E-09	0.38E-07
M44	0.60E-06	0.30E-06	0.69E-08	0.15E-08
M45	0.20E-05	0.34E-08	0.13E-05	0.48E-08
M46	0.15E-06	0.74E-08	0.72E-05	0.10E-08